Development of Adhesive Bonding and Functional Testing Systems for In-Process Inspection of Hot Embossed Microfluidic Devices

by

Caitlin J. Reyda

Sc. B. Mechanical Engineering
Massachusetts Institute of Technology, 2011

Submitted to the Department of Mechanical Engineering
in partial fulfillment of the requirements for the degree of

Master of Science

at the

MASSACHUSETTS INSTITUTE OF TECHNOLOGY

February 2014

Author……
Department of Mechanical Engineering
January 15, 2014

Certified by……
David E. Hardt
Ralph E. and Eloise F. Cross Professor of Mechanical Engineering
Thesis Supervisor

Accepted by……...
David E. Hardt
Ralph E. and Eloise F. Cross Professor of Mechanical Engineering
Graduate Officer

Development of Adhesive Bonding and Functional Testing Systems for In-Process Inspection of Hot Embossed Microfluidic Devices

by

Caitlin J. Reyda

Submitted to the Department of Mechanical Engineering
on January 15, 2014, in partial fulfillment of the
requirements for the degree of
Master of Science

Abstract

Microfluidics has emerged as an increasingly popular field with a wide-variety of applications such as medical diagnostics, drug development, and DNA analysis. The transition of microfluidic devices from research to industry has stimulated interest in producing them at low costs and high volumes. Hot embossing has been of interest lately as a low-cost, high quality, and flexible manufacturing method that is ideal for medium-volume production. This project focuses on the continued development of a tabletop microfactory that can be used to study the control of a novel hot embossing machine. By incorporating an in-line measurement system, it would be possible to add feedback control to improve the process. This led to the design of an automated testing machine that uses an optical inspection of the microfluidic channel widths to determine embossing quality and a flow test to verify device functionality. The total cycle time of the testing machine is 85 seconds, which is well within the time of one embossing cycle (110 seconds). In order to produce complete devices for testing, an automated taping machine was also designed to seal the embossed channels. This machine took 15 seconds to complete its cycle. These two machines were integrated with the microfactory, which is currently capable of producing an embossed, sealed, and tested device every 170 seconds. The taping and width measurement processes have an error of 0.63 μm with a standard deviation of 0.82 μm. The mixing length test has an accuracy of 72.8 μm. A preliminary test demonstrated the ability to generate credible run data, and the effect of embossing temperature on width was detected to a resolution of 2 μm. The system is now able to characterize the embossing process and the effects of various embossing parameters on the final product. Closed-loop cycle-to-cycle process control can then be implemented, which will create a robust production cell that is capable of adapting to a variety of conditions.

Thesis Supervisor: David E. Hardt

Title: Ralph E. and Eloise F. Cross Professor of Mechanical Engineering

ACKNOWLEDGEMENTS

The work in this thesis would not have been possible without the invaluable advice, help, and support of several individuals:

I would first like to thank Prof. David Hardt for his incredible guidance and mentoring over the last few years. His enthusiasm for this project, endless quest for answers, and wealth of knowledge—whether in the laboratory or in colonial history—have truly been an inspiration.

I want to thank Maia Bageant for her company and wisdom inside the lab, during class, and out on the slopes. I want to thank Katharine Luginbuhl for working her robot magic and have the patience to deal with the occasional quirks of my machines. I want to thank Joseph Falvella for his enthusiasm while working late into the night and for keeping our work area tidy and organized.

I would also like to thank Melinda Hale and Joe Petrzelka for convincing me to join the lab in the first place and for their advice early on about research, classes, and life outside of grad school. I want to thank Monica Isava and Erin Bailie for their work in exploring early concepts of the taping machine. I want to thank Adam Libert, Scott Nill, and Larissa Nietner for the never-ending energy they bring to the lab.

I am especially grateful for the encouragement from my family and friends throughout the years and for Ben Peters who has always supported my endeavors.

Lastly, I have to thank the Singapore-MIT Alliance for generously funding this research and providing me with this amazing opportunity.

TABLE OF CONTENTS

LIST OF FIGURES

LIST OF TABLES

CHAPTER 1 INTRODUCTION

This thesis focuses on the scale up of microfluidic device manufacturing. With the use of quick in-line measurements, the fabrication process can be controlled from cycle to cycle to produce high quality parts.

1.1 Microfluidic Devices

Microfluidics, or the manipulation of fluids in channels with dimensions of tens to hundreds of micrometers, has gained popularity in the last few decades for enabling the development of low-cost, small-footprint bioanalytical devices. These devices can already perform a wide variety of laboratory tests including high-throughput screening for drug development, polymerase chain reaction (PCR), cell sorting, medical diagnostics, and fuel cell technologies [1]. Because the amount of samples and reagents used is extremely small (10^{-9} to 10^{-18} liters), the tests can be performed in short time periods with high resolution and sensitivity.

Despite the many current and potential applications for microfluidics, the technology is still not widely used. Many researchers have developed working designs and are ready to start producing them at a much larger scale. The transition of microfluidic technologies from research environments to industry has stimulated interest in the low-cost mass manufacturing of these devices from thermoplastic polymers. The manufacturing processes, however, are still under development as researchers try to investigate which of these processes are both feasible and economical.

1.2 Fabrication Methods

Many macro-scale polymer manufacturing processes have been adapted to form micro-scale features on microfluidic devices. Some of these are serial processes that use direct machining to remove material such as micromilling and laser ablation. These techniques are useful for

prototyping different microfluidic patterns, since they are extremely flexible and do not require the creation of a tool to make a new design. However, the processes themselves are extremely slow and do not scale well with larger area devices, making them poor options for mass production.

Replication techniques, on the other hand, are parallel manufacturing processes that replicate features through the use of a mold. Some examples include polydimethylsiloxane (PDMS) casting, hot embossing, injection molding, thermoforming, and ultraviolet (UV) imprinting. PDMS is not suitable as a material for mass production. It has poor dimensional stability, is not compatible with certain chemicals, and requires a two-part casting process that does not transfer well to automated production [2]. Thermoforming requires a very thin (on the order of 25 μm) film as a substrate [3]. UV imprinting uses the casting of a UV-curable resin into a mold [4]. The resin hardens after UV exposure. This process can be difficult and expensive to implement in manufacturing at a larger scale.

Injection molding is currently a common method for manufacturing microfluidic devices [3]. One of the difficulties associated with adapting this process for the micro-scale is that the injected polymer can often cool and thicken before it has a chance to fill all of the small features. This has been addressed by the use of heated molds. High quality feature replication can be achieved with carefully controlled cycle temperatures, and cycle times can be fairly short (on the order of minutes). Inserts can also be formed directly into the final parts. One of the greatest disadvantages of injection molding is the large capital cost associated with the tooling and production equipment. This is not an issue for applications that need millions of parts. However, for applications with smaller volumes (hundreds or thousands of parts) or applications with tool designs that might be revised over time, injection molding might not be the ideal option.

Hot embossing is a replication technique that addresses the low-cost, high-flexibility, medium-volume market. It is a parallel process that heats a patterned tool and a substrate to just above the glass transition temperature, $T_{g,}$ of the polymer and then applies pressure, allowing the plastic to flow into the features of the tool [4]. The two materials are then cooled and demolded. Since there is limited bulk flow of the substrate during embossing, residual stresses in the material are minimized. This makes hot embossing a suitable process for optical applications, which are sensitive to birefringence caused by residual stress. While cycle times are not quite as low as they are for injection molding, they have been improving gradually, and there might not

be much of a difference between their cycle times in the future [3]. Hot embossing machines are typically lower in cost than injection molding machines, and changing tooling or machine parameters is usually simpler. This is desirable for those who are looking for flexible, yet high rate manufacturing and medium volumes. An example of this would be a small company running clinical trials with a few thousand devices or researchers trying to translate their soft-polymer devices into hard-polymer designs [5].

The hot embossing process has shown great promise to be a feasible mass manufacturing technique for microfluidics, but there is still much left to be understood with regards to optimizing feature formation. This research studies parts made with hot embossing and seeks to improve the manufacturing process by implementing cycle-to-cycle process control.

1.3 Process Control

In order to improve the microfluidic manufacturing process, the system needs to be robust to disturbances. It needs to be able to adjust its parameters automatically when it detects a decrease in quality to continue producing high quality parts. To accomplish this, a measure of the device quality must be made. The results of this measurement can be used to adjust the initial forming parameters (temperature and pressure, in the case of hot embossing) until the device quality has been optimized. If a reliable measurement can be taken in a short enough period of time, the measurement can be integrated into the manufacturing process itself. If the measurement can be taken in an equal or shorter time period than the time it takes to form a part, then 100% device inspection can be achieved. This would allow real-time cycle-to-cycle process control to be implemented in the production system.

Most production systems only implement high bandwidth control of equipment parameters (such as displacement, force, temperature, and pressure) and low bandwidth control via occasional product sampling for statistical process control [6]. Systems rarely implement full in-line measurement because it is often too expensive or too complicated to achieve. However, if these measurements could be acquired, possible shifts in the mean would be detected early on, and closed-loop feedback control would allow the system to recover. Cycle-to-cycle process control would enable the system to be extremely robust and adaptive to disturbances—either in the material, the equipment, or in the environment—and product variation would be greatly reduced.

1.4 Project Motivation

As part of an ongoing project, a new hot embossing machine has been developed with a current cycle time of 110 seconds [7]. In order to study how cycle-to-cycle process control can be used to improve the system, a quick and reliable technique for measuring microfluidic device quality must first be developed. Current inspection techniques use high-end, metrology-grade equipment which provide extremely detailed information about feature geometry, but require a far longer measurement period than is desired.

One possibility for quickly measuring the embossing quality is with an optical inspection of the channels or other embossed features. Although transparent features can be difficult to image, it should be possible to take some sort of measurement of the feature geometries to compare between chips. Another possibility is to run a functional test of the chips. Even with a thorough visual inspection, it is difficult to know exactly how well a chip will perform as a final product. There might be slight constrictions near the inlets or variation in the surface roughness that somehow cause the device to behave better or worse. A functional test is a good method for averaging all of these variables over the distance of the entire chip instead of concentrating on discrete regions. The downside to a functional test is that the devices are typically ruined once they have been used. This is not a problem for this research because these chips are not being developed as products and 100% inspection is more desirable. In the future, functional tests could be performed much less frequently and can be coupled with a less destructive test.

In order to perform functional tests on the devices, the embossed channels first need to be sealed. This is accomplished by bonding a transparent cover plate to the embossed substrate. Significant research has been performed to study microfluidic feature formation, but sealing the devices is still a critical step in completing the manufacturing process, and an ideal bonding method has yet to be identified.

1.5 Overview of Thesis

The ultimate goal of this project is to be able to study process control on the microfluidic hot embossing process. To achieve this goal, a complete automated production cell must be developed. This thesis will focus on the development of quick, reliable bonding and testing methods that can be integrated with the current hot embossing machine to create a working factory for studying process control.

Chapter 2 discusses the background of hot embossing, various bonding methods, and the current microfluidic device measurement and testing methods. Chapter 3 reviews the history of the microfactory project, areas for improvement, and the current objectives that motivate this thesis. Chapter 4 covers the design of an automated taping machine that is used to seal the embossed chips before testing. Chapter 5 explains the different measurements that are being used to assess embossing quality. Chapter 6 covers the design of an automated testing machine that uses both optical inspection and functional testing to measure embossing quality. Chapter 7 reports the performance of these machines and the results of preliminary tests. Chapter 8 summarizes the accomplishments in this thesis and the next steps for the project.

CHAPTER 2 BACKGROUND

2.1 Hot Embossing

Hot embossing creates features by plastically deforming the surface of a heated polymer substrate with a heated precision stamp. A diagram of the process can be seen in Figure 2-1. In this research, polymethylmethacrylate (PMMA)—a glassy polymer with high optical clarity, good chemical compatibility, and well characterized molding parameters—is used as the substrate. For the plastic to flow, the substrate must be heated until it is at or above its glass transition temperature, T_g (85°C to 165°C for PMMA, depending on the molecular composition) [8]. This is done while the tool is in light contact with the substrate to reduce thermal losses and improve efficiency. The tool is then pressed into the substrate with a much higher force, allowing the viscoplastic flow of the substrate into the features of the tool. As the plastic flows in to fill the features, a front develops and gradually resembles the feature more and more with increasing pressure. This effect can be seen in Figure 2-2, which shows the cross-sectional profiles of a microfluidic channel at increasing forming forces for a constant temperature. The profile at the highest force exhibits a nearly-filled mold, whereas the profile at the lowest temperature exhibits an extremely under-formed shoulder. It should be noted that in all of these cases, the profile at the bottom of the channel remains the same.

Once the flow has been given enough time to replicate the features, the substrate and tool are cooled to below the substrate's T_g. This allows the features to solidify as the material returns to its glassy structure. The tool is then removed from the substrate. During cooling, the plastic exhibits shrinkage towards its center, causing the chip to adhere to the features of the tool [9]. This can cause problems if the substrate is allowed to cool for too long. Since the polymer has a higher coefficient of thermal expansion, it contracts with much larger stresses as the temperature is decreased, which can potential damage the features or the tool. On the other hand, if the substrate is demolded too quickly, adhesion forces cause the hot features to stick to sides of the

tool. This can also put stress on the tool and can even cause the channel edges to "smear" up slightly if the substrate has not been properly cooled. By optimize these two scenarios, the ideal demolding temperature for PMMA was calculated to be 60°C.

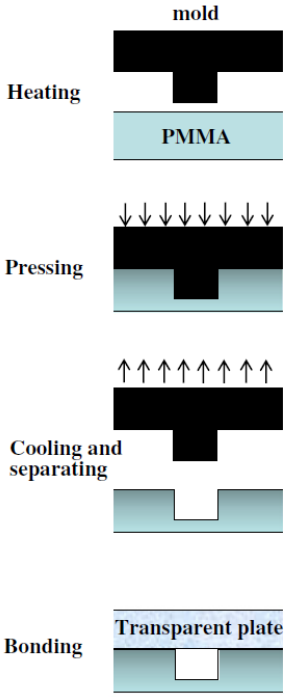

Figure 2-1: The steps in the hot embossing process. (1) The tool and substrate are heated to above the T_g of the polymer. (2) A high force is applied to press the tool into the substrate, and the plastic flows to fill the features. (3) The tool and substrate are cooled, and the part is demolded. (4) A transparent cover plate is applied to seal the channels, creating a complete device [10].

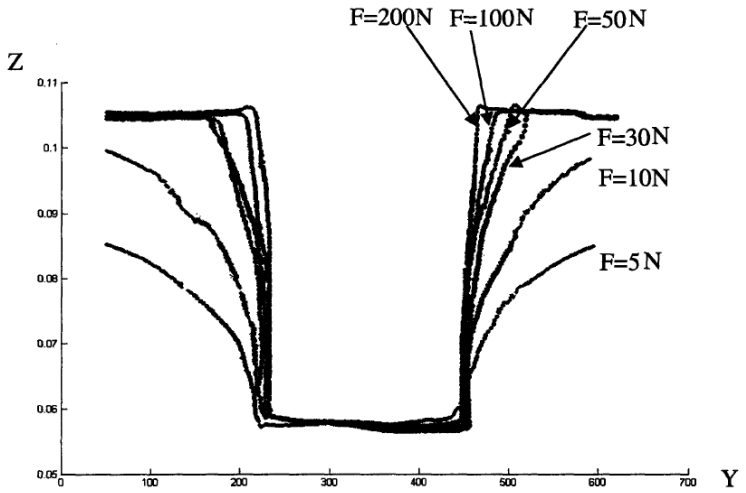

Figure 2-2: Cross-sectional profiles of a microfluidic channel for increasing forces. As the force is increased while the forming temperature is kept constant, the plastic flows to better fill the features of the tool [8].

2.2 Bonding

There has been a significant amount of research dedicated towards studying the formation of microfluidic features in a variety of thermoplastics, but the devices need to be sealed before they are functional. Macro-scale thermoplastic bonding methods have been adapted to address the challenges of sealing these chips at the micro-scale. When comparing the different bonding methods, there are several properties that must be considered, depending on the applications of the particular device [11]. Bond strength is one of the most important of these, to ensure that the devices can withstand the intended flow pressures. The channels must undergo minimal deformation during the bonding process to maintain their desired geometries. The resulting exposed surface material or bond interface must be chemically compatible for the intended purpose of the device. The bonding method must be easy to implement from a manufacturing standpoint, and in many instances, the bond cannot interfere with the optical properties of the device. The bonding method must also take into consideration the means with which the device will attach to a reservoir or other connection. The cover plate might need to be more rigid than a thin film to be able to support plastic connectors.

The bonding techniques for microfluidics can be divided into two categories: indirect and direct [11]. Indirect bonding includes methods in which an intermediate layer separates two layers—at least one of which has microfluidic features. These usually involve adhesives, either as laminate films or liquid glues. Direct bonding techniques merge the surfaces of two substrates without the addition of an extra substance. These include thermal bonding, solvent bonding, and ultrasonic welding. These result in channels with homogenous sidewalls, which can be desirable in certain applications.

2.2.1 Adhesive Film Bonding

One method for sealing microfluidic channels is by covering them with a laminate film. An example of a laminate film is pressure sensitive adhesive tape. These are adhesive films with a polymer layer that can flow at room temperature, which allows a bonding surface to effectively wet, encouraging a strong bond [12]. This method is attractive because it can be fast, reliable, and inexpensive in mass production. It also does not require any heating of the substrates, which prevents feature deformation. An image of a pressure sensitive adhesive film covering part of a micro-channel is shown in Figure 2-3.

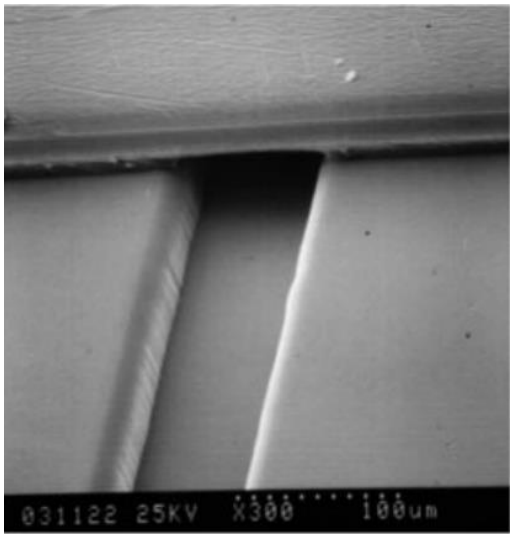

Figure 2-3: A pressure sensitive film covering a 70 μm wide by 40 μm deep channel [12].

Another form of laminate film uses a thermally-activated adhesive. These films can be found with an activation temperature less than the T_g of the substrate [11]. This allows the channels to be bonded without heating up the substrate enough to deform the micro-scale features. In both of these cases, however, it is possible for the film to fill the channels, depending on the adhesive thickness and backing thickness. Also, the channels are left with a non-homogenous fourth wall. While this is not always an issue, there are cases when the reagents in a microfluidic device are sensitive to the chemical composition of the channel walls.

2.2.2 Liquid Adhesive Bonding

Glues, such as liquid adhesives (which evaporate to set) and two-part epoxies (which cure with a catalyzing agent), can be used to bond cover plates to substrates. There are not very many examples of these methods working, however, due to channels becoming easily clogged by the adhesive [11]. A more popular approach is to use high viscosity UV-curable resins instead. These synthetic resins form a bond after being exposed to UV light. The greatest challenge is also preventing the resin from clogging the channels, so many strategies have been used to control the process. One example uses capillary action to wick adhesive resin into the 5-10 μm gap of interstitial space between substrates, shown in Figure 2-4 [13]. The resin stops flowing when it reaches the larger-dimension features due to the capillary pressure drop. As with laminate film bonding, this method also results in channel walls that are no longer homogenous.

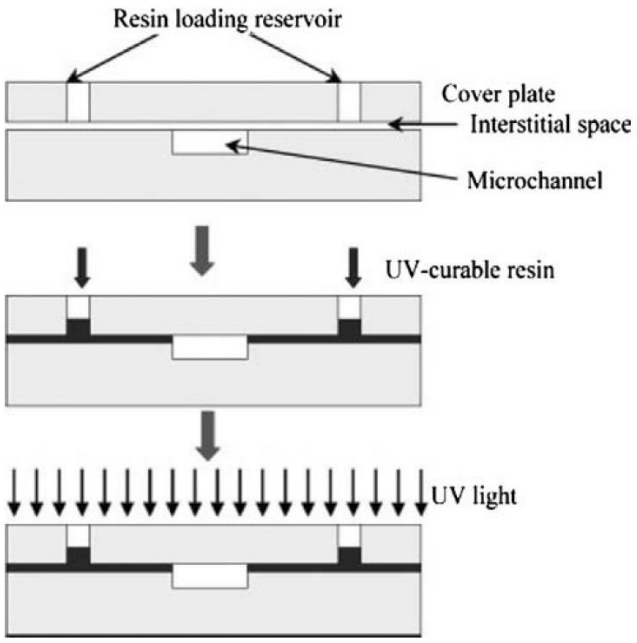

Figure 2-4: Application of a UV-curable adhesive resin using capillary action to prevent clogged channels [13].

2.2.3 Thermal Bonding

With thermal bonding, a substrate and a cover plate are heated to just above the T_g of one or both of the materials. Pressure is applied to improve the contact force between the materials. This causes polymer chains to diffuse across the surface, leading to a strong and homogenous, yet optically clear bond [11]. Because of this, thermal bonding is often viewed as a very attractive microfluidic sealing method, and there are many examples of this technique being used [14] [15] [16] [17] [18]. However, heating thermoplastics to their T_g frequently results in the collapse of formed features. The biggest challenge, therefore, is controlling the temperature, pressure, and bonding time to prevent bulk deformation of the substrate while still achieving a strong surface bond.

2.2.4 Solvent Bonding

A material will act as a good solvent for another material when their Hildebrandt parameters, δ, are nearly equal to one another [11] [1]. When a solvent is applied to a thermoplastic, the surface softens and polymer chains can diffuse across the layer and become entangled with those on the

[1] The Hildebrandt solubility parameter, δ, is an estimate of the degree of interaction between materials. Materials with similar values of δ are able to interact with each other, leading to solvation or mixing of the molecules.

other side. This leads to exceptionally strong bonds between the two materials. However, if the δ of two materials are too similar (ie. PMMA and acetone) then extended exposure can lead to the deformation of features at the micro-scale. This can be solved by shortening the exposure time or by using slightly less similar materials.

As with liquid adhesive bonding, there are challenges with preventing the solvent from flowing into features on a chip. In one study, water was frozen in the channels to preserve their dimensional stability while a layer of solvent was applied [19]. This technique can be attractive for applications that require much higher bond strengths than can be achieved with adhesive or thermal bonding.

2.2.5 Ultrasonic Welding

Another method of mating the surfaces of an embossed thermoplastic chip and a thermoplastic cover plate is to use ultrasonic energy, which locally heats and softens the interface. Ultrasonic welding is a well-established joining process for thermoplastics at the macroscopic scale [20]. Its advantages are a quick cycle time (in the range of seconds), homogenous sidewalls, and location-specific bonding. It does not result in the same feature deformation that is typically seen with thermal bonding. This method uses 20-40 kHz ultrasonic sound waves to cause the localized melting of "energy directors", shown in Figure 2-5, which are temporary structures to control the location of the joint.

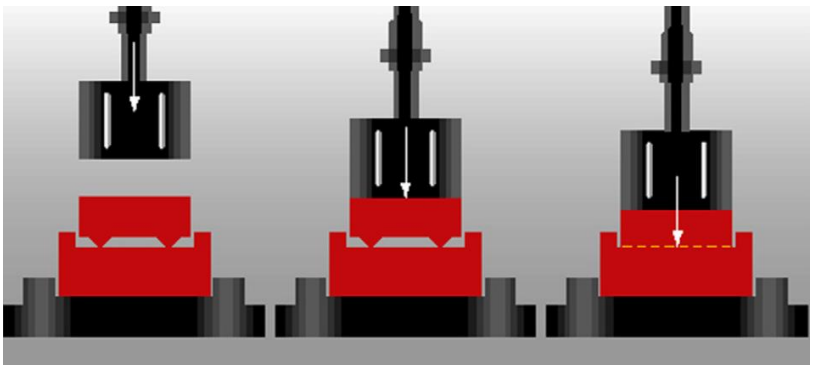

Figure 2-5: The steps in the ultrasonic welding process. (1) The chip and cover plate are placed on a stationary anvil. (2) A vibrating sonotrode, or "weld horn", contacts the parts. (3)The energy directors melt and seal the chip [20].

The geometry and placement of the energy directors need to be optimized for the process, and the forming method needs to account for these additional features, but preliminary tests have

shown that this method is feasible [21]. Channels with cross-sectional dimensions of 100 μm wide by 100 μm deep were successfully bonded with a leak-free seal and minimal channel deformation, as seen in Figure 2-6.

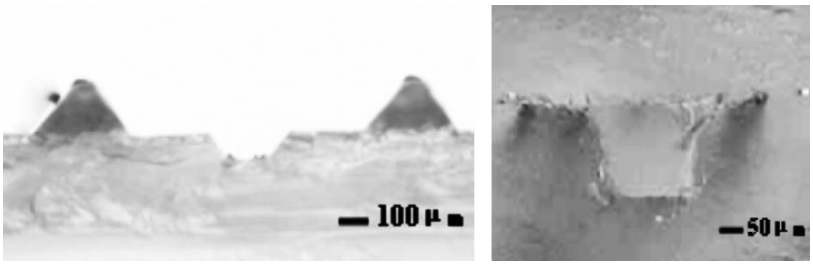

Figure 2-6: Ultrasonic welding of a 100 μm by 100 μm microfluidic channel. Left: Channel before bonding. The energy directors can be seen on either side of the channel. Right: Enclosed channel after bonding [21].

2.3 Measurement and Testing

The microfluidics manufacturing step with the least amount of documented research is the inspection or functional testing of devices for process control purposes. While there are currently businesses that provide large-volume production services for smaller microfluidics companies, there is very little information about the processes they use, particularly for inspecting their products. The businesses that *do* indicate some form of production control will only reveal enough to say that "each and every product is tested to ensure the quality"[2]. It is unclear what kind of test is performed—whether it is a simple feature inspection or a more thorough functional test—and it is unlikely that the results are being used to control the fabrication process with more than standard statistical process control.

For background on the use of in-line measurements for the control of fabrication processes, the semiconductor industry can be turned to as an example. As the fastest evolving major industry, the semiconductor industry has been at the leading edge for advanced process control technologies [22]. Historically, process parameters were left alone until a mean shift in the final output data triggered an alarm. The parameters would then be adjusted manually to correct for the change. However, this could result in many defective parts. Like microfluidic devices, semiconductor wafers require many processing steps to create functional devices. If a manufacturing defect occurs during an earlier step, there is a high probability that the resulting

[2] uFluidix.com/services

product will also be defective. This can end up being very costly. The form of process tuning that is currently being pursued by the industry instead is cycle-to-cycle control, which takes in-line measurements throughout the manufacturing process and can immediately identify changes. It can then automatically correct for these changes based on a process model. There are still some issues that hinder the adoption of this type of control. For example, there is a lack of commercial solutions and in-line metrology sensors available to implement this control.

While it is very difficult to find research on automated high-throughput microfluidic inspection systems, there are numerous examples of inspections that have been performed in smaller batches. These are often used to characterize the performance of a new device or to verify the resolution of a new manufacturing process. Optical inspection is one of the most widely performed test methods. It can take just seconds to capture images, and it is also possible to observe the chips while they are being functionally tested. The entire test set-up can be placed on a microscope stage, and a digital microscope camera can record the images, which are usually analyzed later. Unless there is a motorized vertical axis on the microscope, this method requires the stage to be adjusted by hand for each test to bring it into focus. It also limits the size of the test set-up to fit on the stage of the microscope and within the working distance of the lens. It is difficult to determine any 3D information from these images due to the limited depth of focus, so the images are limited to overhead views.

If identifying 3D features is desired, then higher grade metrology equipment such as a scanning electron microscope (SEM) is used. SEM images retain the object's original surface contours, which makes them an attractive option for observing 3D features at a micro-scale and studying the underlying physics of a manufacturing process. These machines can have extremely high resolutions (on the order of tens of nanometers and as low as 0.4 nm) [23]. However, polymer chips must be coated with an electrically conductive material prior to scanning, and most SEMs operate with a vacuum, which prevents the ability to run functional tests. It also takes minutes to run each inspection due to the time required to pump down the chamber to vacuum pressure.

Another common measurement method is to use a profilometer such as a white light interferometer to take 3D scans of chips. It is possible to image transparent polymers using this technique, so it is popular for identifying defects in microfluidic chip features. The vertical resolution is on the order of tens of nanometers and the lateral resolution is a few microns,

depending on the objective used [24]. Scans usually take 30 seconds to a minute to run. Unfortunately, the interferometer is not able to measure any surfaces that are not horizontal, which can make it difficult to measure side wall geometry. Also, functional tests do not work with this method because only the surface topography is measured.

CHAPTER 3 PROJECT HISTORY AND OBJECTIVES

3.1 History of the Microfactory Project

This thesis is part of a greater project—the "microfactory" or "μFac" project—whose initial objective was to create a fully-functional manufacturing cell for the production of microfluidic devices [25]. There has been a increasing flux of designs for new microfluidic devices, but there has been a lack of research on producing them at a larger scale. There are still many uncertainties in the microfluidic manufacturing processes and no single method has prevailed over the others. In addition to developing and improving upon some of these methods, this microfactory in its entirety could be used as a test bed for the emerging microfluidic device manufacturing field.

The microfactory would also be an opportunity to research novel process control methods on an entire production line. Currently, the most common forms of process control involve taking measurements at the equipment scale (ie. displacement, temperature, and pressure) or the infrequent sampling of process output for statistical process control [6]. Ideally, the product output can be measured for each cycle, and the input parameters can be modified accordingly. Initial research showed that cycle-to-cycle process control could be used to reduce the overall process variance. This microfactory would ultimately include stations for forming, sealing, and testing the devices. If the devices could be inspected and functionally tested in real-time, then the results of each cycle could be used to modify the forming parameters for the following cycle. This could then lead to a more thorough study on the practical implementation of cycle-to-cycle process control.

The microfactory project chose to focus on hot-embossing of polymers as the forming process for the devices. It is a popular method for medium-scale production because of the low capital costs associated with embossing machines. This also led to the need for a material

handling method to automate the process, a bonding method to seal the devices, and a functional testing method to be able to implement cycle-to-cycle process control. Several research projects covering all of these aspects have contributed towards the development of a fully integrated microfactory.

3.1.1 The Product

A custom microfluidic device was designed specifically as a test chip for the microfactory project [26]. The device is a simple micro-mixer with serpentine channels. Since flow at the micro-scale is laminar, mixing of two fluids depends primarily on diffusion. The longer the two fluids are next to each other, the more they will mix. The channel geometry for this design was chosen to be 50 μm wide and 40 μm deep and cover a 25 mm by 25 mm area. These are considered to be mid-sized channels for microfluidics, which made them a good starting point for this project. In addition to the main channels, the design includes a series of features that were designed to aid with registration, inspection, and testing the limitations of the embossing machine. The final pattern of the test chip can be seen in Figure 3-1. The project chose to focus on the embossing of PMMA. Future versions of the project will study the embossing of cyclic olefin copolymers (COCs), which are more widely used in the microfluidics industry. The tool is made out of a Zr-based bulk metallic glass, which is an amorphous metal. This allows for an extremely robust tool with a smooth embossing surface and precise features [27].

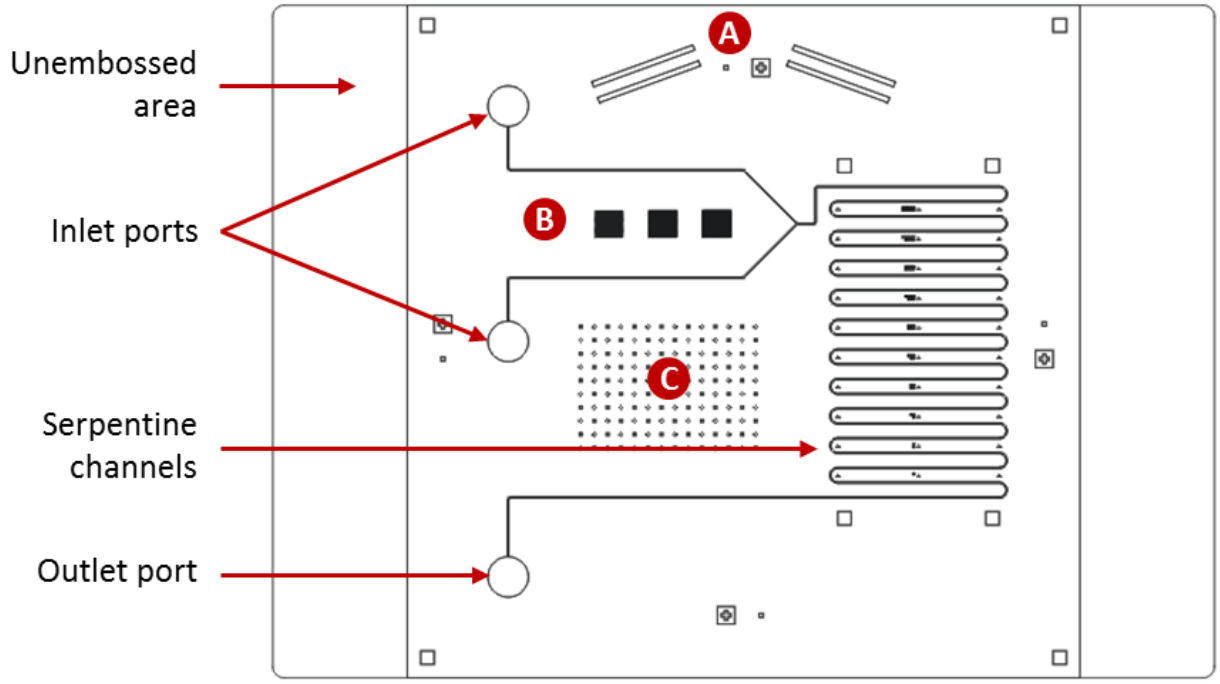

Figure 3-1: The final design of the micro-mixer device for the microfactory project. The two inlet ports take two different fluids and mix them together along the serpentine channels via diffusion. (A), (B), and (C) are additional features of varying dimensions that were initially designed to help assess the embossing limits.

3.1.2 Hot Embossing

Several generations of hot embossing machines were developed before the current design was chosen. The earlier designs focused on understanding and improving the embossing process rather than optimizing the embossing equipment [28] [29]. Using information gathered from these projects, a new machine was developed to have a faster cycle time, lower cost, and smaller footprint [30]. This was the first machine to be implemented in the microfactory. It can be seen in the back left corner of the table in Figure 3-2.

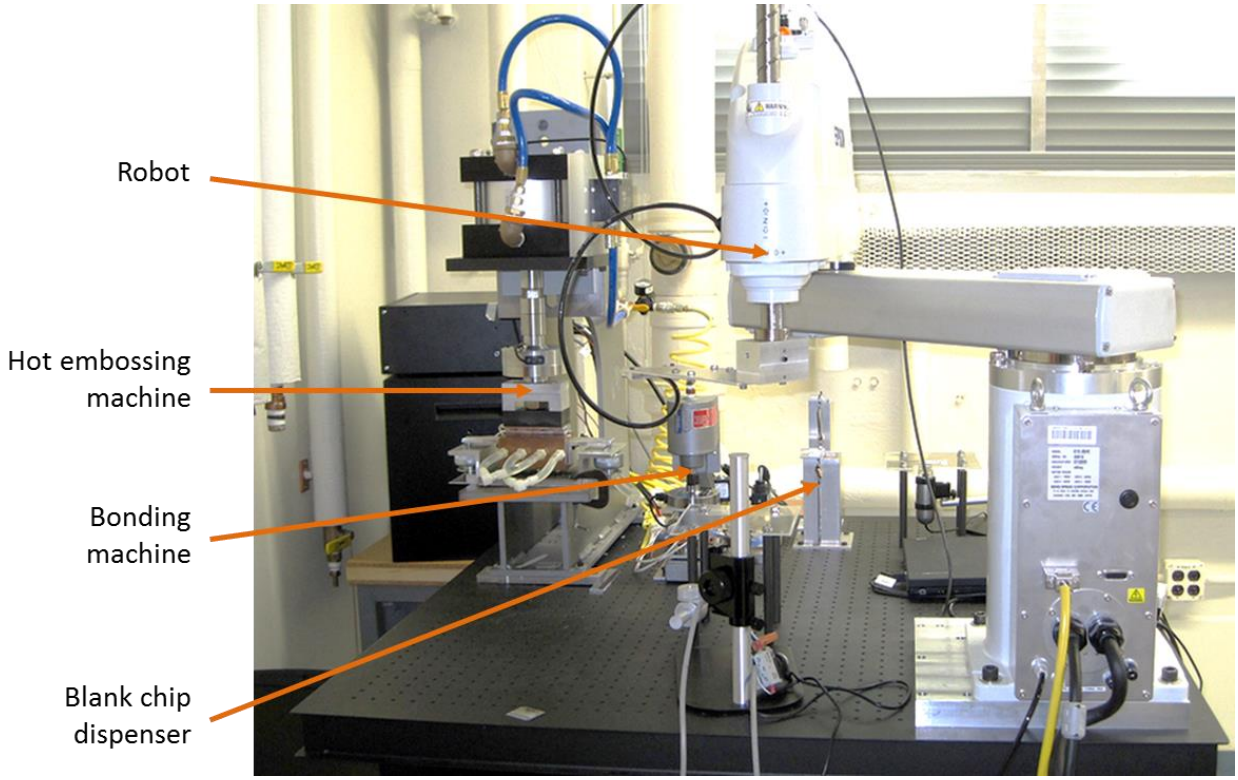

Figure 3-2: The first version of the microfactory. A previous version of the hot embossing machine is on the left. A robot arm for material handling is on the right. Previous versions of a bonding machine and dispenser for blank chips are located in the center [31].

The next and current hot embossing machine improved upon the previous version. In addition to being even smaller in size and having a faster cycle time (110 seconds), it also has several new alignment features for the tool as well as a linear variable differential transformer (LVDT) to measure displacement. A blank chip is placed on a platen between two thermal stacks that are embedded with ceramic heaters and cooling lines. The tool is mounted to the upper stack on a flexure that can be calibrated horizontally in the x-y plane to align with the pre-drilled inlet holes on the blank chips. The upper stack also has a thin sheet of rubber to account for small errors in parallelism between the tool and the chip. A pneumatic actuator at the bottom of the machine—combined with an air bearing—applies force directly upwards to push the plastic substrate against the stationary tool. The force is measured by a load cell and the displacement is measured by an LVDT. The plastic and the tool are brought into light contact while they are both heated to just above the glass transition temperature, $T_{g,}$ of the material. Then, the machine increases the pressure to fill the features of the tool. Next, the platens are cooled by pumping room temperature water through them. If the platens do not cool at similar rates (remaining

within approximately 10°C of each other) then significant warping of the chip can be observed. If the warping is too extreme, it can negatively affect the performance of other processes in the system. Finally, the pressure is released. During the cooling process, the plastic shrinks around the features of the tool. To release the chip from the tool, two thin tabs attached to the bottom platen hang over the un-embossed wings of the chip. When the platen lowers, the chip is demolded [7]. The final design is showed in Figure 3-3.

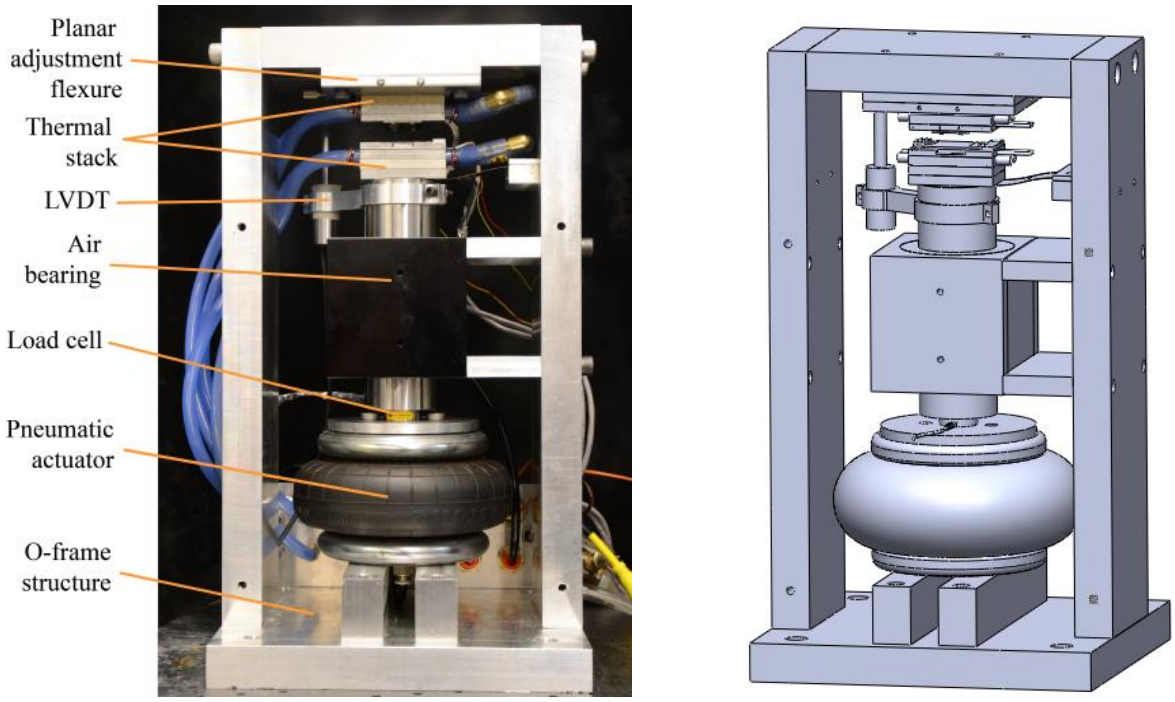

Figure 3-3: The current hot embossing machine design. Left: Photograph of machine with key parts labeled. Right: Solid model of the machine [7].

The input parameters for this embossing machine are forming temperature, forming pressure, heating time, forming time, and cooling time. Cooling time is held constant, since the substrate needs to reach a certain temperature before it can demold successfully [9]. Heating time is also held constant because the material needs to reach its T_g. Currently, the forming time is also held constant, but should be varied in the future to find the minimum cycle time. This leaves the forming temperature and forming pressure as the two main input variables for the machine. There are other variables that also need to be taken into account. Extruded PMMA sheets with a T_g of 105°C were originally used to create the blank chips. The nominal thickness for the

material was 1.5 mm, but the chips could range anywhere from 1.1 mm to 1.8 mm (±20% variation). This affected the extent of heating through the plastic substrate, which would then affect the quality of embossing [7]. To avoid this problem, a new batch of PMMA blanks were injection molded. The variation in material thickness for the new blanks was reduced to ±1%. It was also found that the new material, despite still being PMMA, had a significantly higher T_g of 115°C.

3.1.3 Material Handling

Another important component of the microfactory is the material handling system. In order to have a fully automated factory, a method was needed for transporting the chips between the different stations. This positioning method also needed to be very precise, since the channels are only 50 μm wide. An Epson G10-85 robotic arm with 4 degrees of freedom was chosen to transport the chips. It has 25 μm repeatability in the horizontal plane and 10 μm repeatability in the vertical direction [32]. A custom end effector, shown in Figure 3-4, was designed to pick up the chips. The end effector needed a low profile to fit in between the hot embossing platens. Internal channels were added to draw a vacuum of 80 kPa (absolute pressure). Compliant rubber was added to the bottom surface to help improve the seal of the chips against the vacuum holes [33].

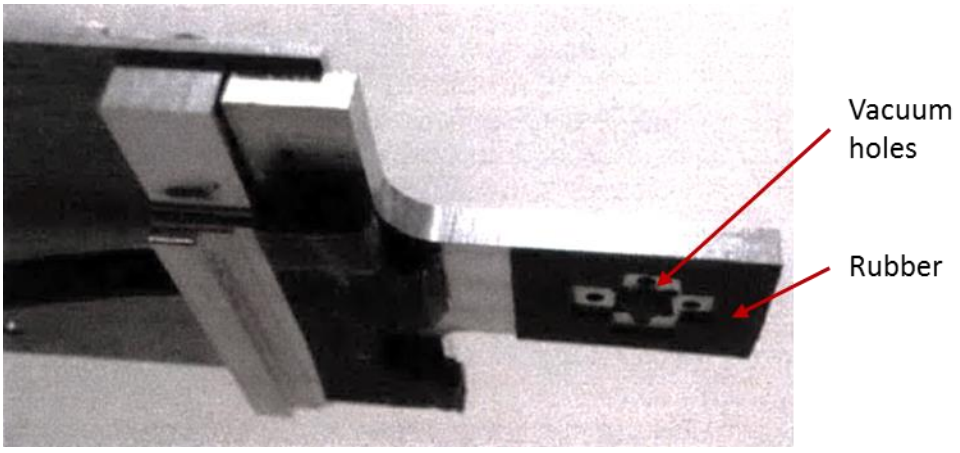

Figure 3-4: The underside of the original end effector [33].

The repeatability of the robot in the horizontal direction was improved from 25 μm to 11.3 μm by using a 3-pin alignment system [33]. These pins, shown in Figure 3-5, were mounted to

the lower platen of the hot embossing machine where the blanks are placed by the robot. The robot first placed the chip close to the pins. It then moved forward until the chip contacted the back pins and then moved to the right until the chip contacted the side pin.

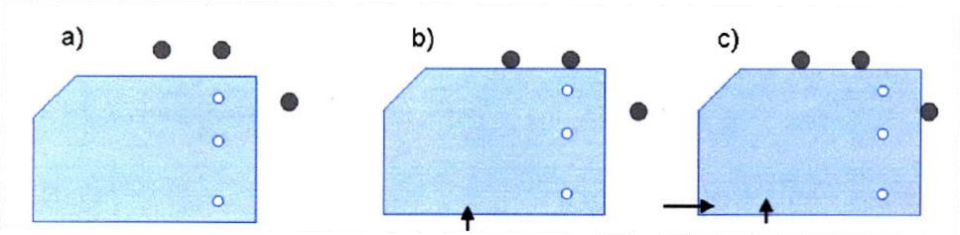

Figure 3-5: The 3-pin alignment system reduced robot positioning variation from 25 μm to 11.3 μm [33].

The current robot end effector is based off this design but includes a few improvements. It now has two ports instead of one, which can be seen in Figure 3-6. This symmetrical design allows the robot to carry two chips at once. It can carry a blank chip in one port, remove an embossed chip from the hot embossing machine with the other port, and then immediately replace it with the blank chip. This significantly reduces the amount intermediate time between embossing cycles and improves the overall takt time of the microfactory. The current design also has a different vacuum hole pattern. The holes are located outside the embossed channel region on the edges of the chip. The region above the channels is milled away slightly. This prevents dust or dirt from accidentally transferring into the channels.

It was also noticed that the compliant rubber coating was causing the chips to occasionally stick to the end effector. To prevent this, the rubber was removed and a PMMA layer was used instead. The holes are still sealed well enough without the rubber. Lastly, a short “hook” was added to the front of each end effector. The robot picks up blank chips from a spring-loaded dispenser before it brings them to the hot embossing machine, and the vacuum pressure is not enough to overcome the pre-load of the dispenser. By adding the extra hook, the robot can pull the top chip free before turning on the vacuum to remove it from the dispenser. This hook is also useful in aligning chips later on in the system. If the robot pulls back on the chip before turning on the vacuum, the chip automatically straightens itself against the edge of the hook.

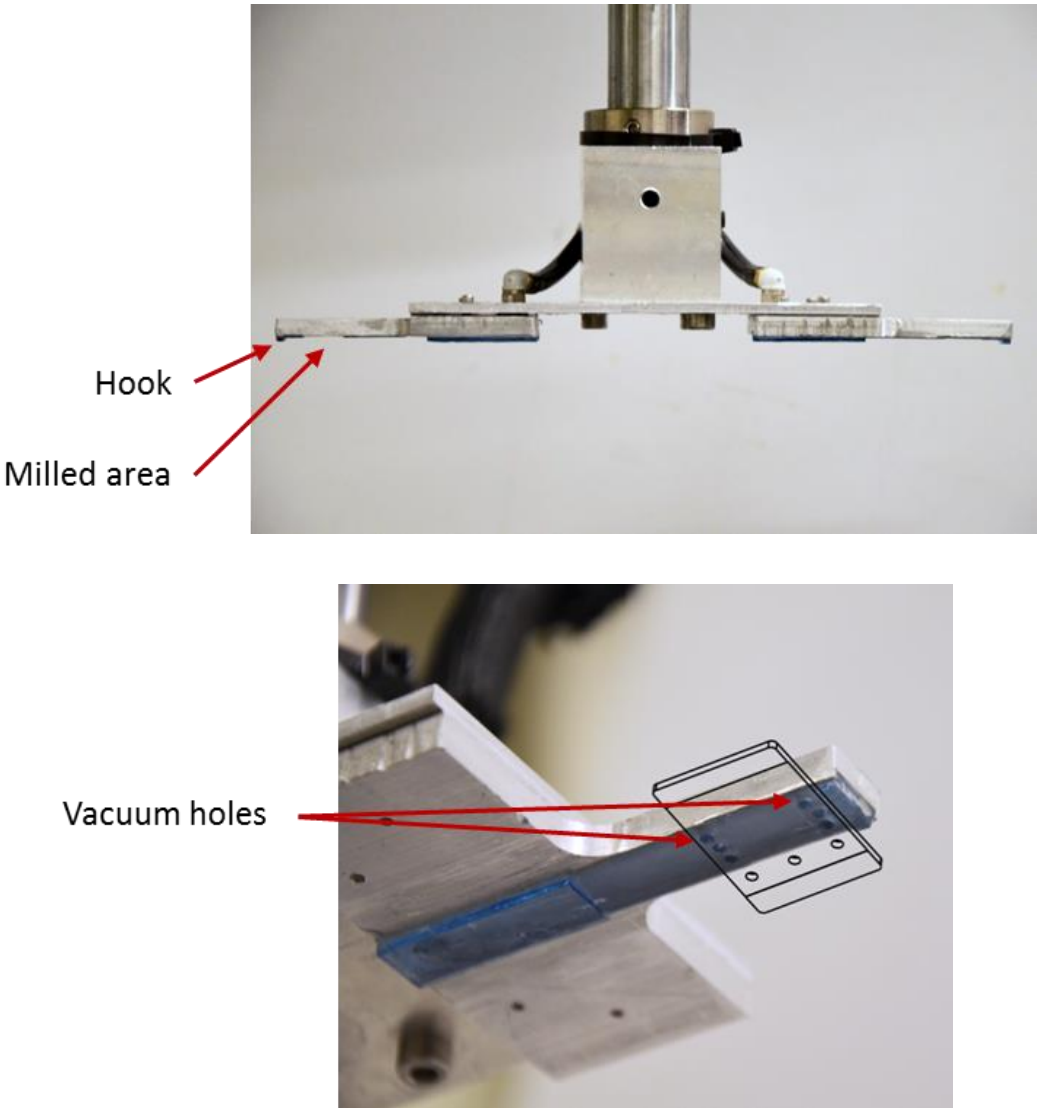

Figure 3-6: The current robot end effectors. Top: There are two symmetrical ports. Each port has a short hook for manipulating the chips. Bottom: The vacuum holes were repositioned to avoid contacting the embossed channel region on the chip. The area between the holes is milled away. A simulated chip is added for clarity.

3.1.4 Bonding

After the microfluidic channels have been embossed, they need to be sealed before the chips are functional. This is currently one of the greatest difficulties in microfluidic device manufacturing. The first method that was attempted during the microfactory project was thermal bonding [34]. By heating up the embossed chip and a plastic cover plate and then applying pressure, the two pieces can be fused together for a strong seal. Unfortunately, reheating the channels often leads to deformation of the embossed features. One approach to minimizing feature deformation is to

use interfacial heating. Instead of heating the entire chip, only the surface is heated to just above the T_g. There is a temperature gradient throughout the rest of the chip, which helps prevent over-heating. The use of radiative heating also allows the temperature at the surface to be controlled more rapidly than a traditional conductive heating system, since there is no residual heat when the heat source is turned off.

The final set-up used three 50 W halogen bulbs combined with an integrating sphere to created uniform light. The chip and cover plate were sandwiched between two pieces of glass above the light source and placed on an Instron machine that applied uniform pressure. The bonds were homogenous and optically clear. Sample images of the bonding process can be seen in Figure 3-7. The bonding region begins in the center of the chip and expands outwards.

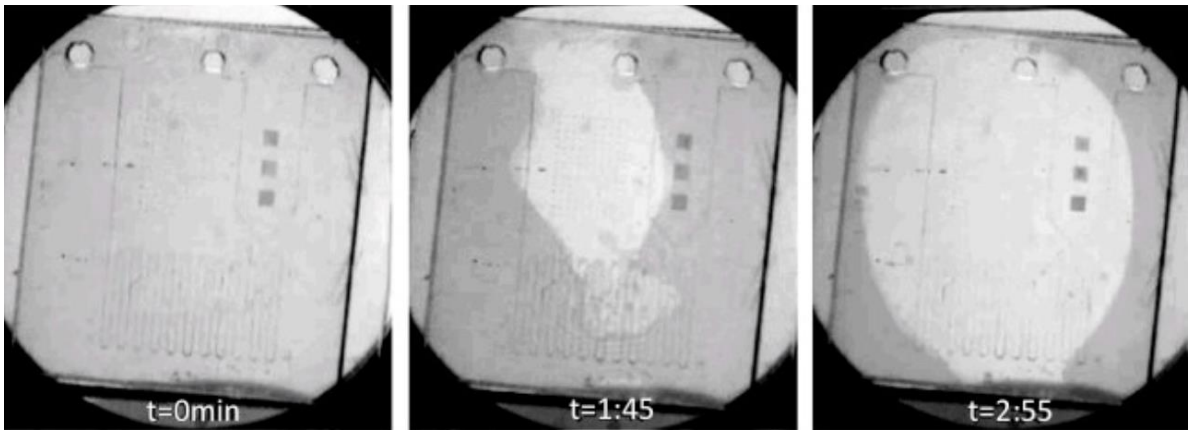

Figure 3-7: Images of the chip and cover plate taken at different times during the bonding process. The lighter areas indicate regions that have been bonded [34].

Unfortunately, there was still a significant amount of deformation in the channels. A variety of heating powers, pressures, and bonding times were tested. Out of the chips with all 10 channels fully bonded, most had final channel heights of less than 30 μm (compared to an initial 40 μm). The only sample with minimal deformation (final height of 37.7 μm) took 209 seconds to bond. This is nearly twice the desired cycle time of 110 seconds or less.

A new approach using adhesive tape as a cover plate to seal the channels was also explored briefly. While not all microfluidic designs are compatible with a non-homogenous fourth wall, it is still an accepted method. For the purposes of the microfactory project, this was an attractive solution because it would not alter the embossed channels and could be implemented quickly, which would enable the factory to start running earlier.

3.1.5 Inspection and Functional Testing

The final component of the microfactory project is a station for inspecting and functionally testing the microfluidic chips. The system needs to be able to detect if channels are under-formed so that it can signal the hot embosser to adjust its forming parameters accordingly. A high speed, high resolution inspection machine was developed to measure the chips [35]. It has comparable resolutions to a commercial interferometer with 0.5 μm horizontal and 1 μm vertical resolution, but is capable of processing a much higher rate of data points per second. It uses a high speed (500 fps) camera combined with motorized precision x-y stages to collect the data rapidly. It measures features by having the camera at an angle, as shown in Figure 3-8. Based on the depth of focus, it can determine the profiles of features in the image. Since the camera is at an angle, it is also able to image vertical side walls unlike other machines in its class. Commercial white light interferometers would take over 24 hours to image a 25 mm by 25 mm chip. This machine can measure the same area at a rate of 640,000 voxels per second. This corresponds to 65 minutes per chip at the highest resolution.

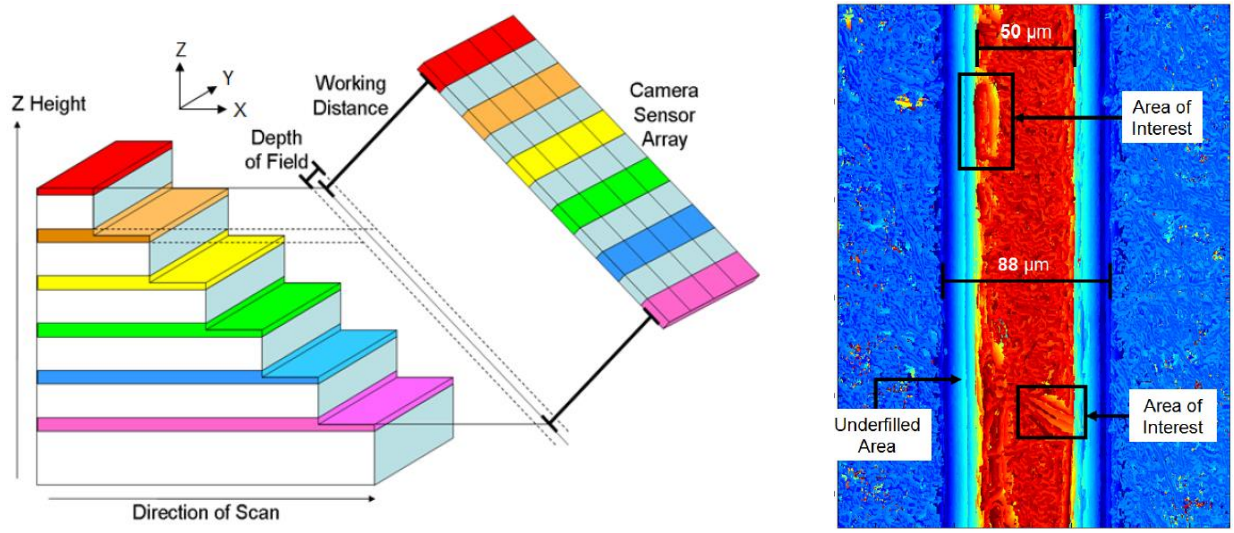

Figure 3-8: Left: Diagram of the high speed inspection with an angled camera. The different rows of sensors in the camera focus on independent Z-heights. The camera moves horizontally, so multiple line scans can be taken in parallel. Right: Sample image of a channel compiled from the data taken with the inspection machine. It is able to detect the underfilled corners of the channels as well as defects in the features [35].

While this process produces very high quality and informative data which can be used to automatically detect small defects in the chips, it is not fast enough to be implemented in the microfactory system. It was decided that a simpler measurement within the given cycle time (110 seconds) would be more desirable from a process control standpoint. This led to the development of a series of functional testing machines that could use a quick test to measure whether or not the chips were functional.

One of the advantages to performing a functional test on the chips is that a bulk measure can be made to assess the overall geometry of the channels instead of relying on isolated measurements. Although functional tests for microfluidic devices are typically destructive, since the chip can no longer be used again, this is not important for the research factory. In an industrial application, the functional test could be performed once every hundred or so chips, while a less destructive inspection is performed every cycle.

The first generation of a functional testing system for the microfactory project used a constant-flow test designed to measure variations in pressure [36]. This test used a chip design different than the current micro-mixer. It used a series of short, straight 8 mm long channels with a variety of widths and depths (50-800 μm wide and 20-100 μm deep). The chips were sealed using a silicone gasket layer and two support platforms that were clamped together manually. The top support platform had pipe fittings to connect to a constant-flow syringe pump and a pressure gauge to the inlet and a mass scale to the outlet. The mass scale was used to calibrate the flow rate of the syringe pump. Results of these tests showed that it was possible to detect variation in channel geometries caused by changes in the embossing parameters. However, the testing process was very labor-intensive due to a complicated loading and unloading process, and there was too much fluid capacitance in the system. A long time was spent waiting for the tubing to expand and the air pockets in the pressure gauge to compress before fluid would start flowing, so testing times were on the order of 60 minutes. This was still too long for it to be implemented in the microfactory.

The next generation of the functional testing system, shown in Figure 3-9, was designed for the new micro-mixer chip pattern [37]. It used a constant-pressure driven test instead of a constant-flow rate driven test due to the difficulties with fluid capacitance in the previous system. This new system greatly reduced the amount of time required to test each chip (on the order of 2 minutes). To test the function of the micro-mixer chip, blue and yellow food dyes

were run through the channels where they would mix and turn green. This required sealing the chips first, so different adhesive tapes were tested using this system. Chips were placed by hand on a series of outlets connected to dye reservoirs with o-rings for a tighter seal. Two air cylinders on either side of the chip pulled down on an aluminum bar with a compliant rubber coating to clamp the chip in place. Two cylinders were chosen in this design because they were thought to be more symmetrical, but they were later found to be unnecessary. Once the chip was clamped, the flow was turned on. Both reservoirs were connected to the same line of pressurized air to ensure that the two fluids were at the same pressure. A Dino-Lite digital USB microscope was placed below the chip to capture images of the flow.

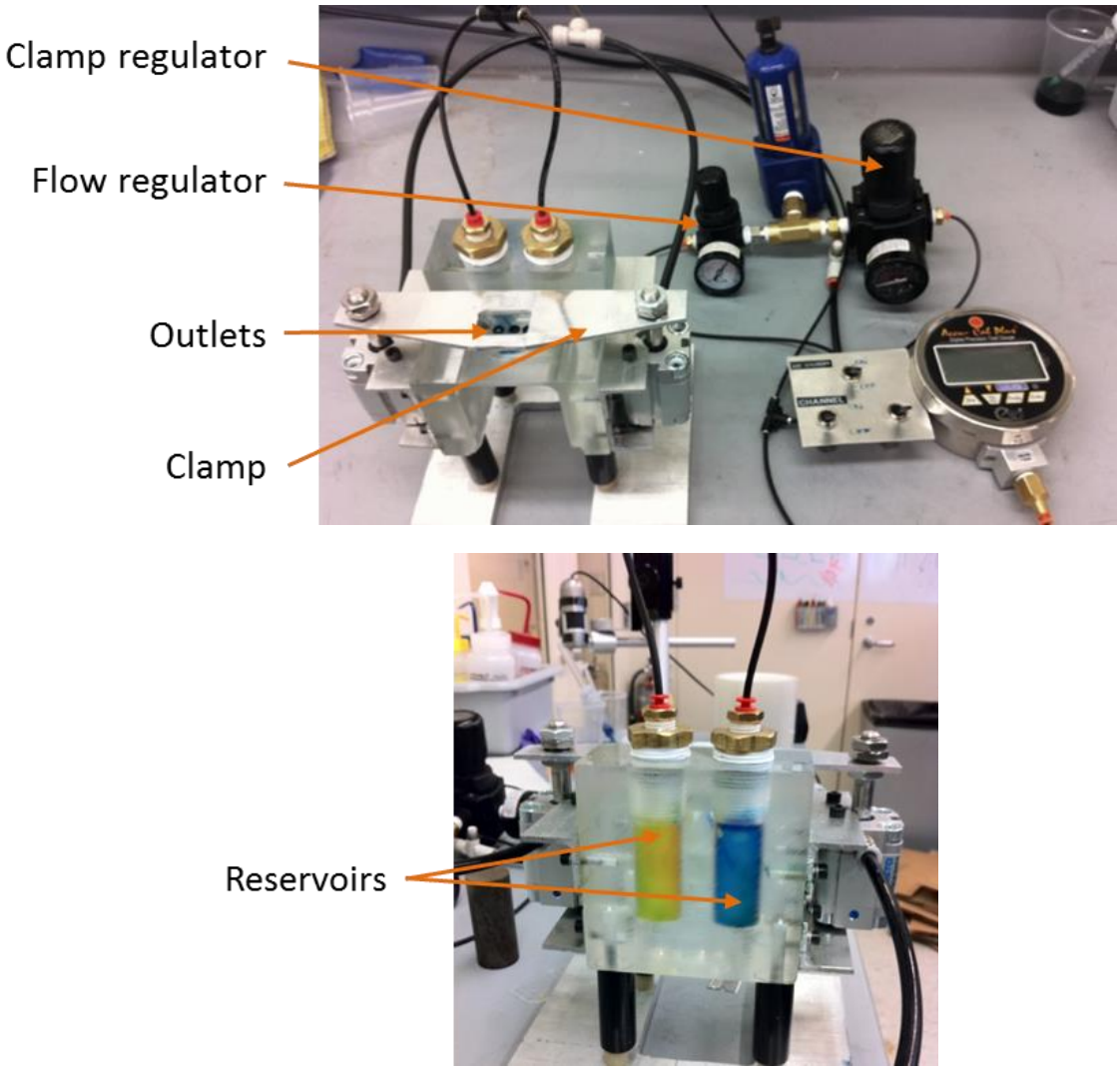

Figure 3-9: A pressure-driven functional test system for testing the micro-mixer chips. Blue and yellow dyes connected to outlets were run through the channels of a chip which was clamped by two air cylinders. The clamp and flow pressures could be controlled by regulators [37].

This testing apparatus was a successful proof-of-concept for a functional test that could be integrated with the microfactory. It could successfully flow fluid through the channels within the desired cycle time, and it was small enough in size to fit on the table with the other equipment within reach of the robot arm. A variety of potential adhesive tapes for sealing the chips were also identified during the design of this system.

3.2 Areas of Improvement

The microfactory project had finally reached a point where it was feasible to integrate all of the different subsystems and create a working factory. The two biggest obstacles were in bonding and functional testing. A faster and more reliable method needed to be developed for bonding the chips. Without this, the chips could not be sealed and tested. Some initial tests with pressure sensitive adhesive tape had been promising, but the ideal tape still needed to be chosen. This also required the development of a fully automated machine that could apply the tape to the chips if the factory was to run autonomously. Since there were no commercially available machines for this specific purpose, a custom machine needed to be designed.

A proof-of-concept had been shown for the functional testing system, but the images recorded with this process were not a high enough quality. This required a redesign of the system to use higher quality optics and cameras to image the chips during the test. Also, the system needed to be automated in order to function with the rest of the microfactory. This included improving the alignment of the chips to allow for repeatable positioning.

Both the new bonding system and new functional testing system needed to be designed to be compatible with the rest of the microfactory. Previous generations had been designed to explore the processes, and they were not restrained by their size, control, or interface. These new systems needed to be able to fit on the tabletop factory with the hot embossing machine and robot arm. They needed to be accessible by the robot's end effectors, and they needed to be able to communicate their current states with the robot. This became the motivation for the project described in this thesis.

3.3 Current Microfactory Project Objectives

The microfactory project has been running for several years, and its objectives have evolved based on the results of each individual project. While it started out as a project to study the process control of microfluidic devices, it later turned into a series of smaller in-depth projects to study the different processes of microfluidic device manufacturing. The focus has now shifted back to integrating all of the individual systems into a final capstone project. The current goals for the microfactory are as follows:

1. A production rate of 20-25 devices per hour (2.5 to 3 minute cycle time of the system).
2. Produce a continuous run of over 100 sealed and tested devices.
3. Determine the relationship between the test measurements of devices and the input parameters of the hot embossing machine.
3. Develop a strategy for closed-loop cycle-to-cycle process control.

The following chapters will describe the design of two machines—a taping machine and a functional testing machine—that are used to complete the microfactory system.

CHAPTER 4 DESIGN OF A TAPING MACHINE

4.1 Design Specifications

The primary goal of this thesis project was to develop a reliable method to measure the quality of hot embossed chips in the microfactory. One of the possible methods for measuring quality was to perform functional tests of the microfluidic mixing devices. In order to perform tests, functional devices were required, so a sealing method for the embossed chips needed to be developed first. Previous work had investigated thermal bonding by applying a blank PMMA cover plate and heating it with the embossed chip to seal the channels. However, the channels started to melt back to their original state when enough heat was applied, causing the chips to no longer be functional. It was found that minimal channel deformation was possible, but not within the desired cycle time of less than 110 seconds (or the cycle time for the slowest machine in the system) [7]. Since the main purpose of the microfactory project as a whole was to study cycle-to-cycle process control in microfluidic device manufacturing rather than the mechanics of bonding methods, it was decided that a simpler, more reliable sealing method would be used instead. Laminate film bonding with adhesive tape seemed to be the most promising of the current microfluidic sealing methods for this project. While there are some devices which cannot function with non-homogenous walls, there are plenty of other applications that have been designed to work with adhesive tape [11]. It is inexpensive, quick to apply, and seals the micro-mixers well enough to be functionally tested.

Precisely handling and autonomously applying a non-rigid material, however, can be a challenging task. There are currently no off-the-shelf machines available for the needs of the project. This led to the development of a custom taping machine that could prepare embossed chips to be inspected and functionally tested by applying a layer of adhesive tape. The following design specifications were identified:

1. The tape must fully cover the channel and inlet region of the chip with at least a 2 mm border from the edge, to improve the seal and avoid leakage.

2. The tape must be strong enough to withstand 30 psi of fluid pressure for 2 minutes.

3. The adhesive must be thin enough that it does not clog the channels and obstruct the flow.

4. The adhesive's backing needs to be stiff enough to keep the tape rigid and prevent it from deforming into the channels.

5. The tape must be optically clear, so chip features can be measured.

6. The adhesive must be uniform, so fluid doesn't leak out into air bubbles between the adhesive.

7. Optional: The adhesive is biocompatible.

8. The chips do not require a manual processing step after taping to separate them from one another.

9. The taped chip can be picked up in a repeatable orientation to be placed precisely in the functional testing machine.

10. Full automation and compatibility with other machines in the microfactory project.

The following sections will describe the challenges and solutions that led to the final design of a taping machine for hot embossed microfluidic chips.

4.2 Design

4.2.1 Adhesive Tape Selection

First, a tape needed to be selected to seal the chips. There are a wide variety of tapes available to choose from. Some are heat-activated at a lower temperature than the glass transition temperature of PMMA, which would make thermal bonding more feasible. Others are UV curable. For this project, pressure-sensitive adhesive tapes were chosen because of their

availability and ease of application. Many tapes were sampled with a wide range of properties. From initial testing, it was found that adhesive strength, adhesive thickness, and plastic backing thickness were the most important parameters [37].

Several tapes did not have the strength to withstand flow pressures higher than 10 psi before leaks began to form around either the channel area or the inlet area. The more successful tapes could withstand over 35 psi, which is far higher than the maximum pressure required for testing chips (10-20 psi). Adhesive thickness also played a large role in tape selection. For example, 3M 600 tape has an adhesive thickness of 37.5 μm. Since the channel height is only 40 μm, the adhesive ended up filling most of the channel and blocking flow. It was found that tapes with adhesive thicknesses less than 20 μm were ideal. Adhesive backing thickness is also important. Tapes with very thin backings were able to deform into channels too easily. Therefore, a more rigid backing of 50 μm or higher is preferable.

Some other important factors include uniformity of the adhesive to keep the channels sealed without leakage and clarity to allow measurements of the features to be taken through the tape. One of the more successful tapes was 3M 810 Scotch Magic Tape, which was able to withstand up to 30 psi of flow pressure. Unfortunately, it has a slightly hazy appearance, shown below in Figure 4-1, making it difficult to take measurements within the channels. Another promising tape was product 92712 from Adhesives Research, Inc. This is a medical grade tape, which is an additional advantage, with a thin 17.5 μm adhesive thickness. Unfortunately, it is only available as a double-sided tape, which does not work for this project.

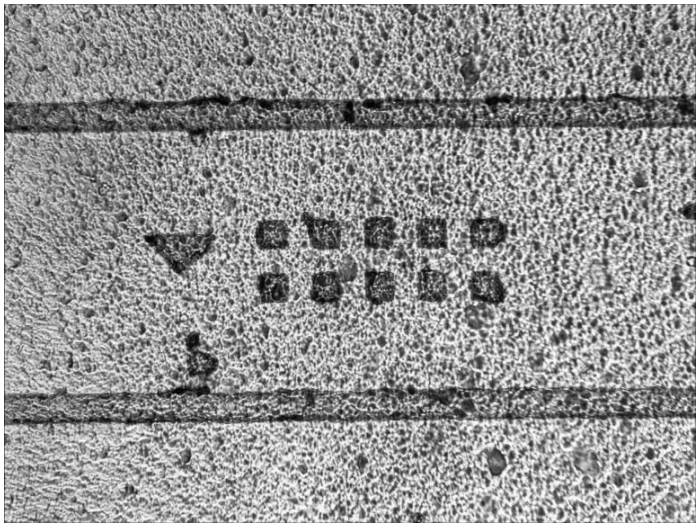

Figure 4-1: A micrograph of a chip sealed with 3M Scotch™ Magic Tape.

The most promising tape for sealing these devices was product 62551 from Tesa Tape, Inc. The tape is biocompatible and was originally designed for microfluidic applications with channels that were much wider at 200 μm. The adhesive is very thin to avoid filling channels and the backing layer is rigid enough to avoid collapsing into the channels.[3] This tape can easily withstand pressures up to 35 psi (higher pressures have not been tested) for extended periods of time, and it is also visually clear, as seen below in Figure 4-2.

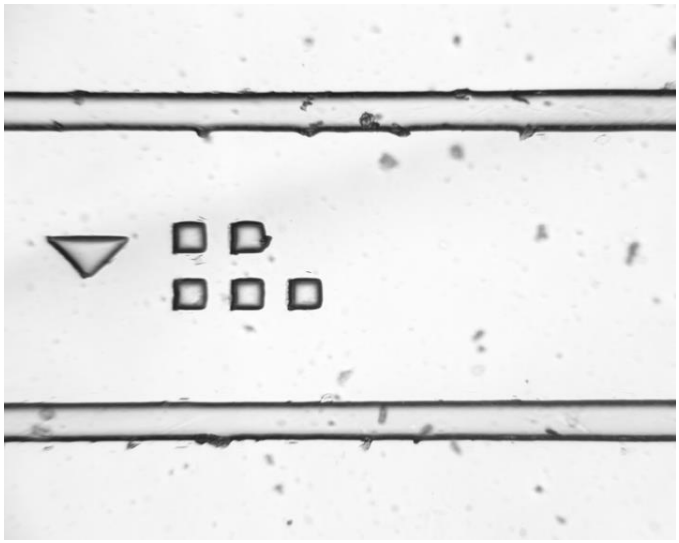

Figure 4-2: A micrograph of a chip sealed with Tesa Tape 62551.

The surfaces of channels sealed with Tesa Tape 62551 were measured using a Zygo white light interferometer to check for signs of tape sinking into channels[4]. The profile of tape covering a well-embossed channel is shown on the left of Figure 4-3. The channel is barely visible, but most of the height data varies over less than 0.4 μm. The profile of tape covering a poorly-embossed channel is shown on the right of Figure 4-3. The scale is exaggerated, since the height difference is only 1.6 μm, but there is still evidence that it is possible for the tape to sink into the channels if they are poorly formed enough.

[3] This tape is still under development, so further details will not be published, per their request.
[4] Zygo NewView 5000

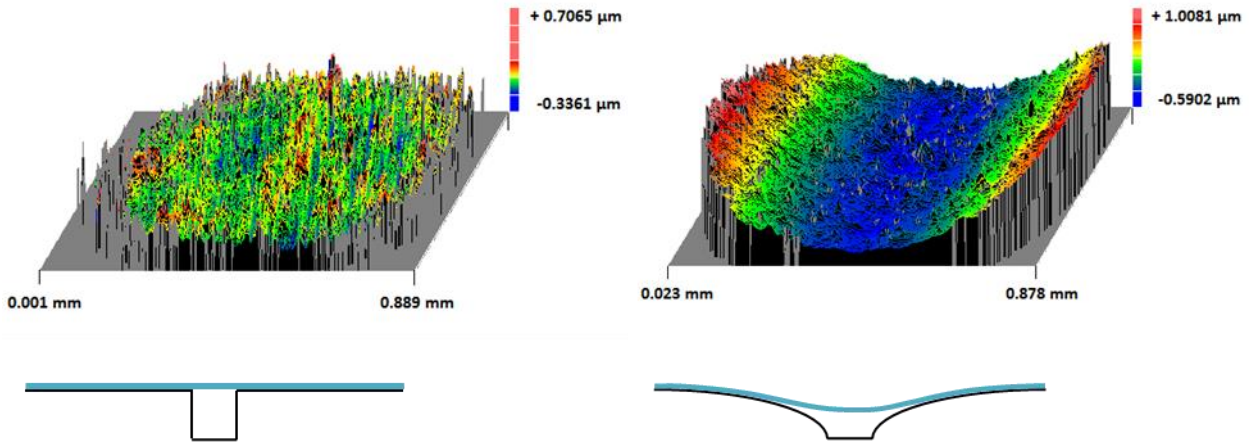

Figure 4-3: Scans of taped channels taken with a Zygo white light interferometer. Cross-sectional diagrams below illustrate how the tape behaves for well- and under-formed channels. Left: A well-formed channel. Most of the height data varies over 0.4 µm and doesn't appear to follow a trend. Right: A poorly-formed channel. There is a height difference of 1.6 µm and there is a clear trend of the tape sagging along the direction of the channel.

The tape was slit into reels that are 1 in. wide by 100 m long, which is enough to tape over two thousand chips per reel. The tape also has a protective plastic liner, which prevents the adhesive from picking up unwanted dust and dirt, but it needs to be removed during the taping process.

4.2.2 Force Application

After a tape was selected, a tape application method needed to be chosen. The tape could either be precut and individually aligned with the chips, which would avoid the need for separating the chips later on, or the chips could be taped together on the reel and separated afterwards. Tape handling made it too difficult to use precut pieces of tape. A group of colleagues in Singapore built a semi-automated taping machine. A chip was placed a moving linear stage, then taped and cut individually [38] [39]. This required a special mechanism to keep track of the end of the tape. For this project, a more continuous method was desired for the manufacturing cell.

Next, a variety of methods were explored to seal the tape onto the chips. The tape could be pressed directly downwards, but this made it very likely to trap air bubbles in the center of the chip. The tape could be applied gradually from one edge to the other with a rigid object, such as a plastic card, dragged across the surface, pushing out air bubbles. This method was difficult to control because the stiff card did not always contact the chip completely to remove air bubbles,

especially if there was slight warping from embossing. Using a compliant roller turned out to be the best choice since it could adapt to small variations in surface flatness. A roller, or series of rollers, would also work very well for taping multiple chips continuously in an assembly line. The concept for this approach is illustrated in Figure 4-4.

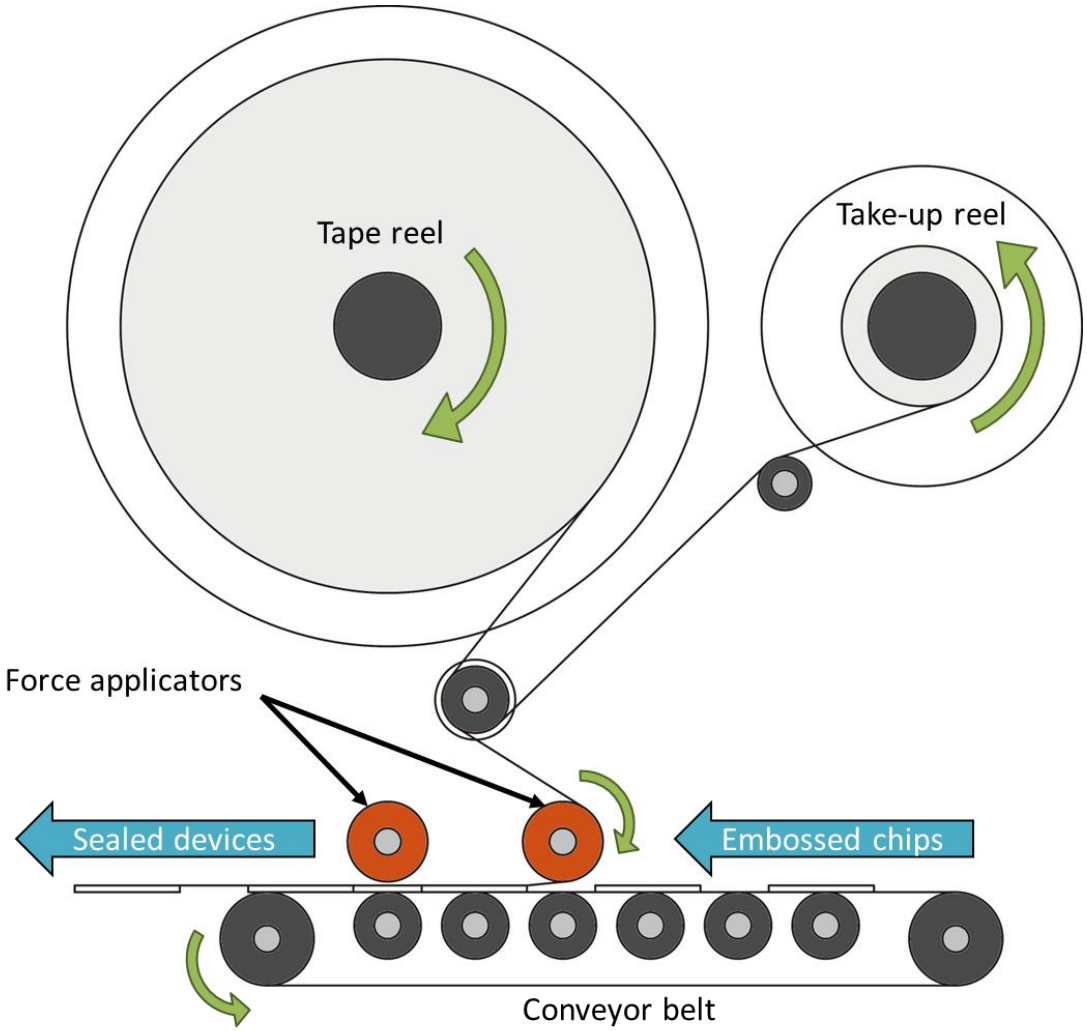

Figure 4-4: Concept for a taping machine. The chips from the embossing machine enter from the right. Compliant rubber rollers apply tape on the chips with a set amount of force as the chips pass underneath them on a conveyor belt. Sealed devices exit the machine on the left.

A range of rubbers with different hardness ratings were tested on the chips. The material needs to be stiff enough to apply enough force to seal the tape, but it also needs enough compliance to distribute the force evenly across the chip. Super-soft latex tubing with a durometer hardness of 35A was too soft. Neoprene tubing with a durometer hardness of 75A was

too stiff. Norprene rubber tubing with a durometer hardness of 60A worked well and was used in the initial prototypes[5]. However, a larger diameter of tubing was desired for the final prototype, since rollers with larger diameters apply less horizontal force for the same downward force when initially rolling over chips compared to rollers with smaller diameters (see Figure 4-5). Since the desired diameter tubing was not available in Norprene rubber, silicone rubber with the same durometer hardness was used instead[6].

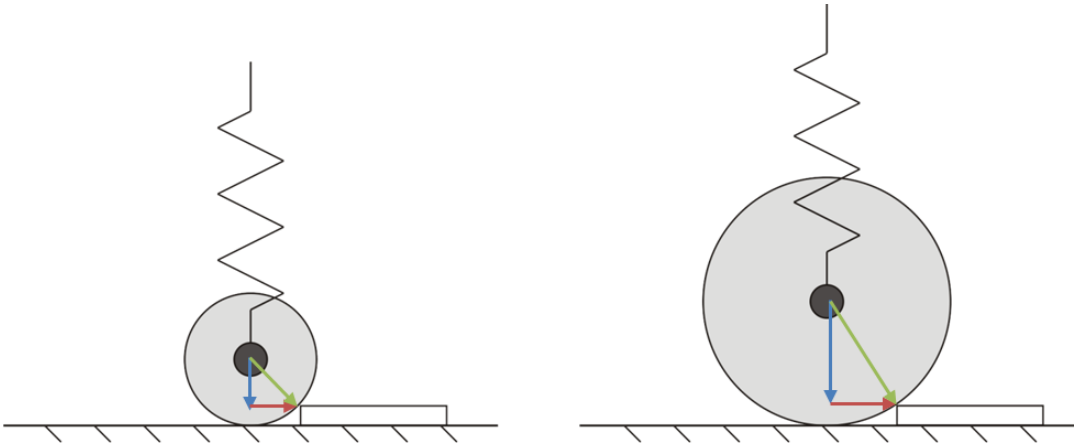

Figure 4-5: Reaction forces of rollers on chips. For the same downward force, the smaller roller applies a proportionally larger initial horizontal force compared to the larger roller.

To determine the ideal downward force for applying tape, a chip was placed on an Instron machine and tape was applied by hand using a rubber roller. Different rolling forces were measured, and the ideal force range was found to be 10-13 N. It is possible that the taping force could be a variable that will be changed while running the system in the future, so an adjustable force system was desirable. One idea was to use a range of weights to apply the force. However, there was not enough space to easily fit the necessary amount of weights for the required force. Extension springs between the rollers and a fixed lower point were also considered, but it was difficult to attach the springs to the roller shafts. For the first prototype, rubber bands were used to wrap around the bushings on the roller shafts as seen in Figure 4-6. It was thought that the force could be changed by using rubber bands with different thicknesses. Unfortunately, the rubber was found to creep over time and eventually crack.

[5] McMaster-Carr Part #51075K53: Durable Norprene rubber tubing, 0.25" ID, 0.625" OD

[6] McMaster-Carr Part #5546T51: Extreme-temperature silicone rubber tubing 0.25" ID, 0.75" OD

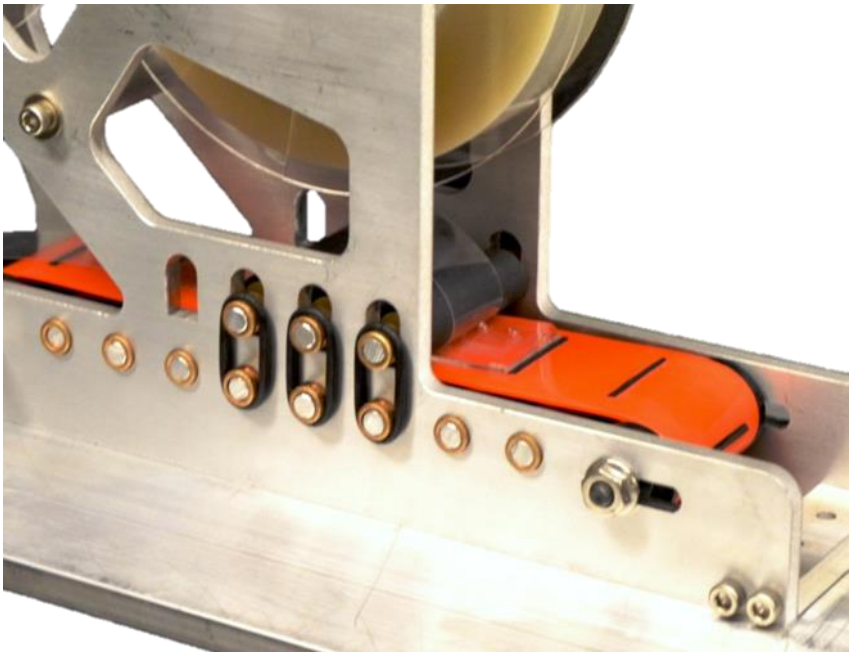

Figure 4-6: First prototype of the taping machine. Rubber bands were used to apply force on the rollers to tape the chips, but they were found to creep and crack over time.

A long term solution was needed, so a new mechanism using compression springs was designed. In the new design, compression springs apply force between the compliant rollers and fixed upper points. The spring compression can be changed by adjusting a screw, which changes the force accordingly (see Figure 4-7). With the selected springs, there is a range of 0-37 N of force[7]. The current set-up displaces the front springs by 0.1 in. for a total force of approximately 10.1 N. The rear springs are not currently being used, since they did not appear to affect the quality of taping. Occasionally, the chips rotate up after passing under the rollers due to an uneven force being applied at the very edge. To minimize this, a series of idle bars were placed after and between the rollers to keep the chips from rising too high and causing problems later down the line. The final assembled spring mechanism can be seen in Figure 4-8.

[7] McMaster-Carr Part #9657K273: Zinc-plated music wire compression spring, 0.500" L, 0.300" OD, 0.026" wire diameter, 4.23 lbs. max, 11.3 lbs./in.

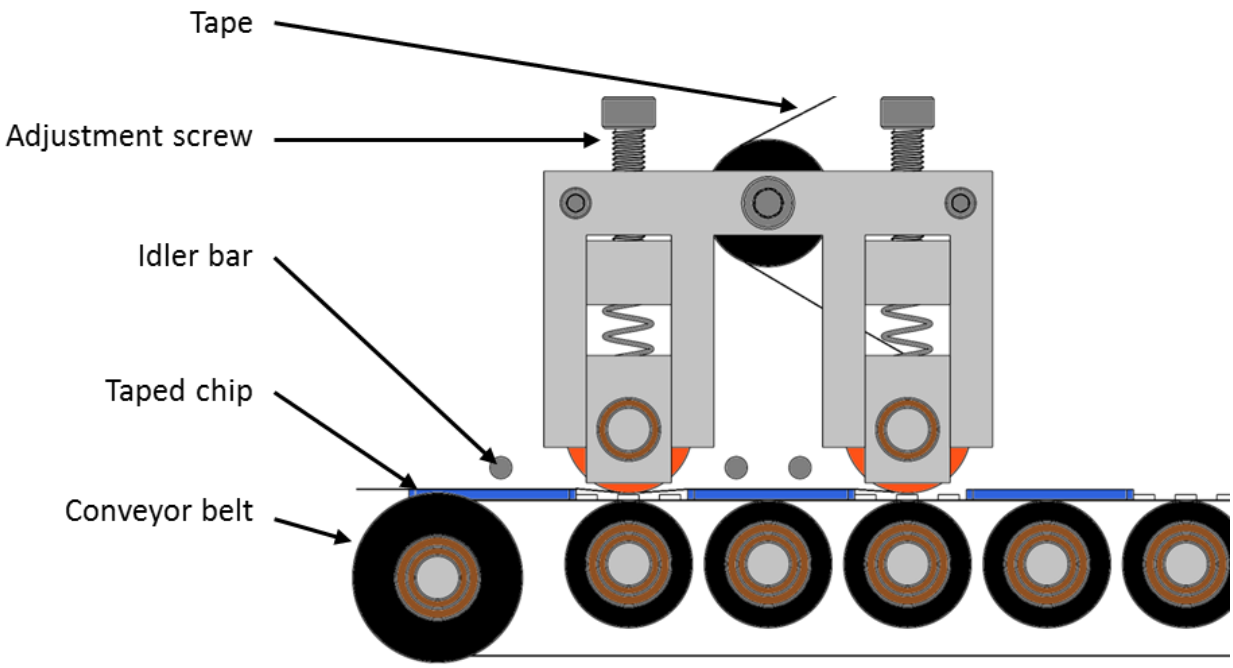

Figure 4-7: The new force application mechanism for the rollers of the taping machine. The spring force can be increased by tightening the screws above each upper roller. The chips are highlighted in blue and move on a conveyor belt from right to left in this diagram. Bars to prevent the chips from rotating up are shown between the two rollers and after the second roller.

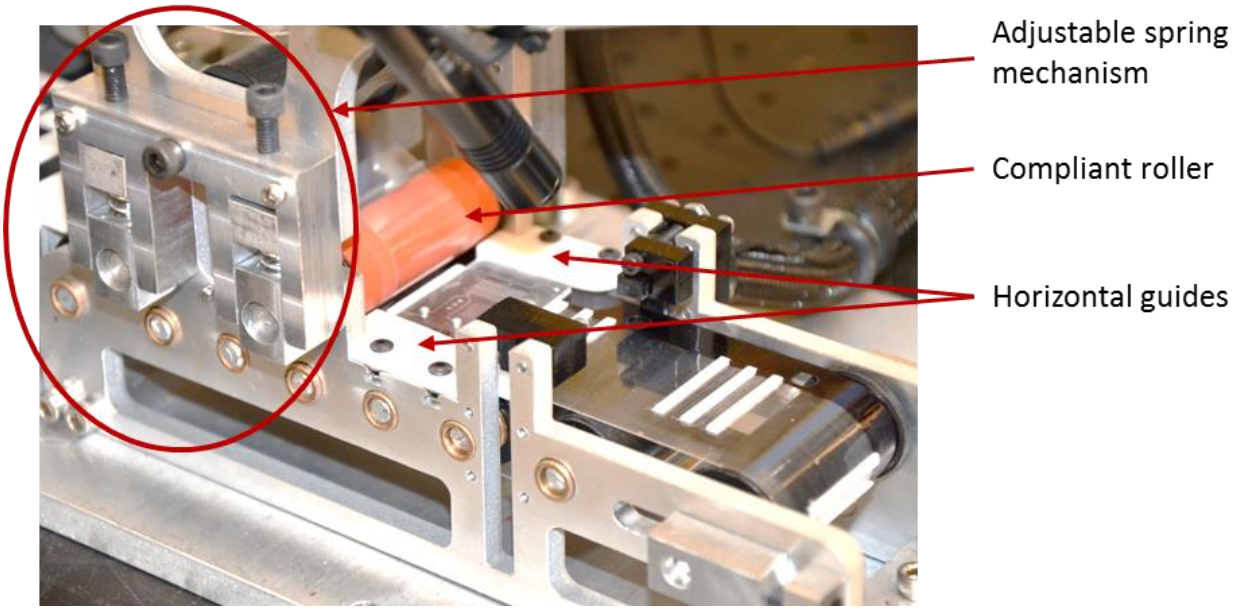

Figure 4-8: The final assembled spring mechanism. The belt transports chips from right to left. The first roller (in orange) applies tape to the chips. The force on the rollers can be adjusted by screws. Horizontal guides (in white) center chips on the belt before they are taped.

4.2.3 Belt Drive and Take-up Reel System

A conveyor belt system was chosen to move the chips through the machine. This allowed for a continuous taping process that could run autonomously in the factory cell. In order to keep track of the chip locations, the belt was segmented at even intervals. The spacers used to divide the belt were also used to push the chips forward, since friction is not enough to move the chips under the current spring-loaded rollers. These spacers needed to be shorter than the thinnest embossed chip (1.2 mm) to avoid interfering with the taping process. There were no off-the-shelf flat belts that fit this description, so a custom belt was constructed.

For the first prototype, a premade flat belt was used as a base[8]. 0.031 in. thin strips of rubber were laser cut and carefully attached to the belt using tweezers and superglue. The process was messy and time intensive, but it proved to be successful in transporting chips under the rollers. The belt was supported by passive plastic rollers and was tensioned by hand using a bolt and nut that clamped to the machine's frame as shown below in Figure 4-9. A motor was attached to the rear roller to drive the belt (more on motor selection can be found in Section 4.2.5).

Figure 4-9: First prototype of the belt. A bolt and nut were used on the front roller to apply tension.

In the first prototype, multiple upper taping rollers were placed in series immediately after each other. However, the chips take some time to advance through the machine rather than moving continuously because of the embossing step. To avoid having chips stopped directly

[8]McMaster-Carr Part #9485T18: High-performance urethane flat belt, 1.75 in. wide, 0.0625 in. thick

underneath a roller (and causing uneven force application), the new upper rollers were spaced apart by one chip length, as shown in Figure 4-7. This was done to keep the force application consistent and to avoid any problems with adhesive sinking into channels. However, this introduced a new problem. The gap of tape between the chips began sticking to the rubber that was used for the belt spacers. They were later made out of 0.031 in. adhesive-ready Teflon® instead to prevent sticking. These spacers needed to be cut into multiple thin strips to allow the stiff Teflon® to bend around the tight curvature of the end rollers.

It was also decided that the belt could be made out of a thinner material, which would require less tension and would decrease the amount of friction in the system and the amount of torque required from the motor. 0.005 in. thick clear polyester film was cut to size using a laser cutter. 0.25 in. diameter holes for each chip location were cut along the length of one side, which was also colored black. These were used to index the belt with a photodiode. Teflon® spacers were attached using superglue while the film was still flat. Lastly, the plastic film was bonded to itself using superglue to form a complete belt, shown in Figure 4-10. A new frame-mounted screw tensioning system was also added.

To keep the chips properly aligned with the tape, a series of guides were mounted above the belt. Two horizontal plastic guides funnel the chips to center them on the belt between the sides of the machine. They can be seen in Figure 4-8. Initial tests showed that the chips would occasionally be placed too far forward and would pass under the taping rollers before getting pushed back against the belt spacers. This amount of variation was not acceptable, so another guide with thin rubber fingers was added to lightly brush the chips back against the belt spacers before entering the taping roller. Small metal dowels prevent the chips from popping up over the spacer behind them in the chance that the rubber fingers apply too much force. This guide is magnetically attached for easy access during troubleshooting. It can be seen in Figure 4-10 and Figure 4-11.

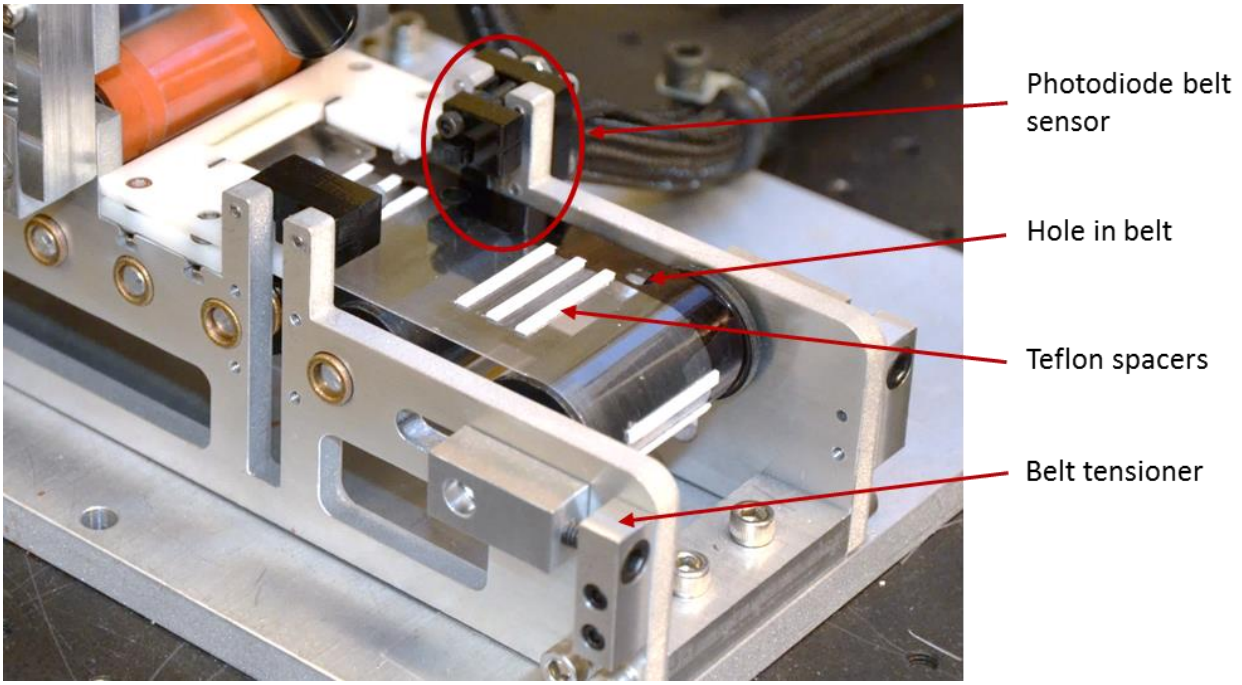

Figure 4-10: The new belt with Teflon® spacers, photodiode sensor, and tensioning system.

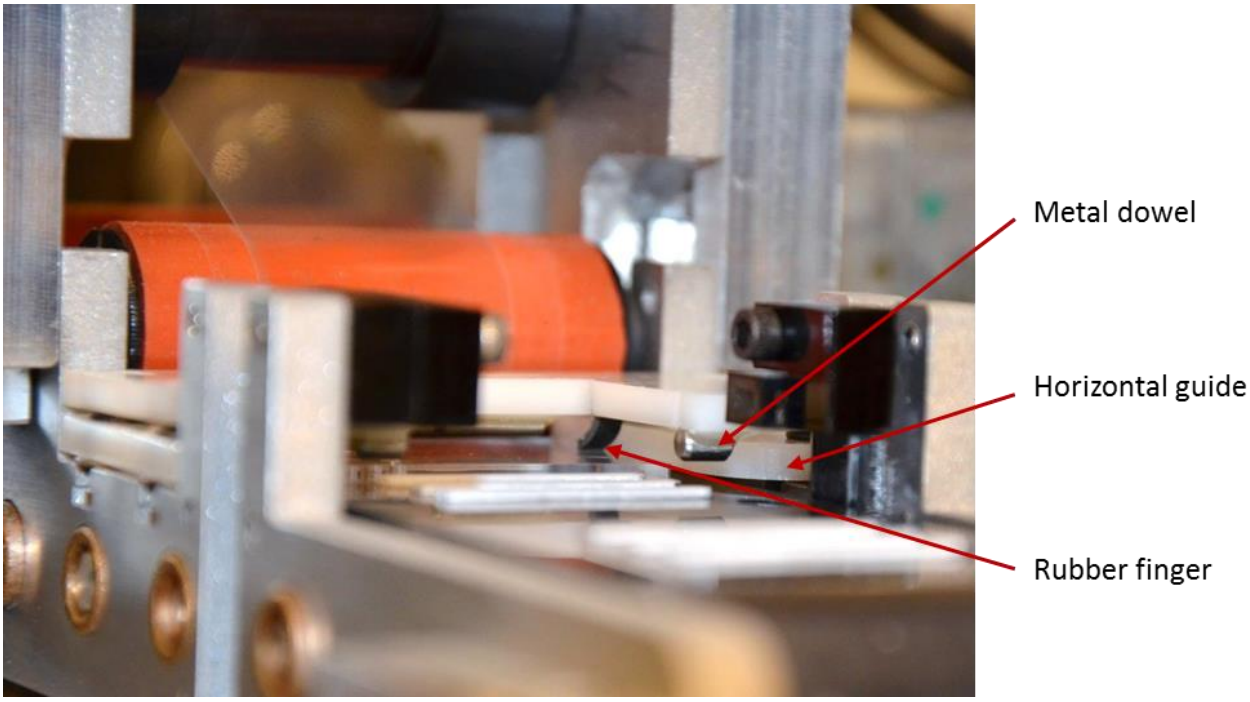

Figure 4-11: A close up of the positioning guides viewed from the front. Thin rubber fingers brush the chips back against the Teflon® belt spacers while small metal dowels on each side prevent the chips from getting pushed up and over the belt spacers.

Because the belt is driven, the motion of the chips moving under the compliant rollers causes them to roll and the tape to advance forward. There is no need for the taping rollers to have their own motors. The tape reel can also be passive. Attaching a motor to the tape reel was briefly considered since it could be used to adjust the tension in the tape. It was decided that the friction in the tape shaft would be enough tension for now. If the tension needs to be varied in the future, a motor could be mounted to this shaft. Since the Tesa tape comes with a protective liner on it, there needed to be a take-up reel to collect the liner. A small motor is attached to this reel to wind up the used liner. Idler rollers are placed between the reels and the taping roller to route the tape and keep it covered with the liner for as long as possible. A schematic of the reels is shown in Figure 4-12.

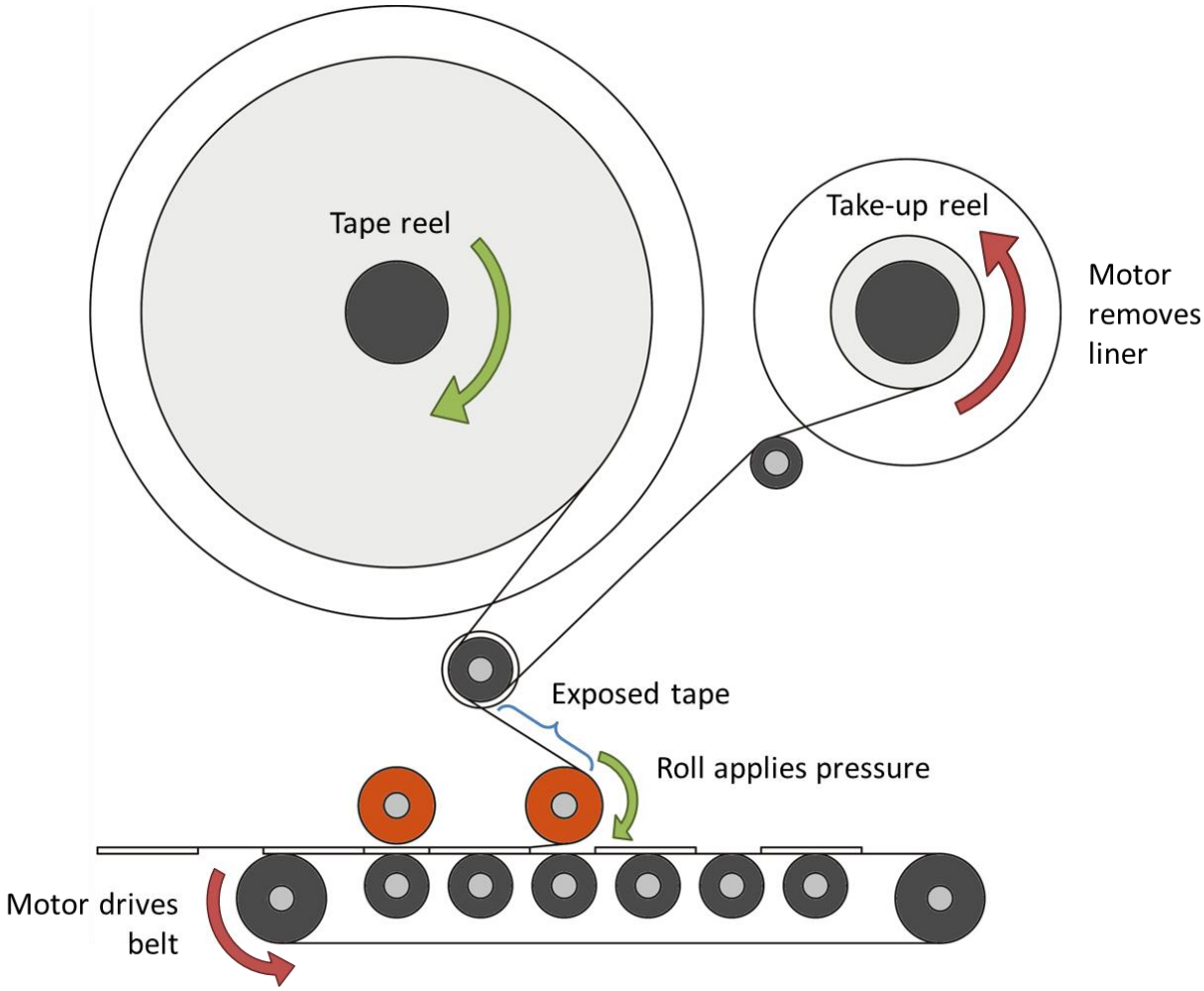

Figure 4-12: A schematic of the tape and liner reels, taping rollers, and conveyor belt. The chips enter the machine from the right and move left. The red arrows indicate rolls that are powered by motors. The rolls with green arrows (and no arrows) are passive. This design minimizes the amount of tape that is exposed before taping to prevent dust from gathering.

4.2.4 Tape Cutting

After the embossed chips have been sealed, they are still attached to each other by a length of tape. In order to be tested, they need to be separated into individual chips. Because the factory needs to be automated, this led to the development of a tape cutting mechanism. One idea was to use a vertical cutting motion. Blades were attached to an air cylinder to test the idea, but they had difficulty cutting all the way through the tape using this motion. Another idea was to use a chopping motion to slice the tape off the chips, but it was difficult to find an actuator to test this idea. The idea that was pursued instead was to use a pair of titanium-coated stainless steel rotary blades powered by an air cylinder[9]. These blades act like pizza cutter wheels and slice the tape just inside the edges of each chip. One blade cuts the back edge of the last chip and the other blade cuts the front edge of the penultimate chip, as shown in Figure 4-13.

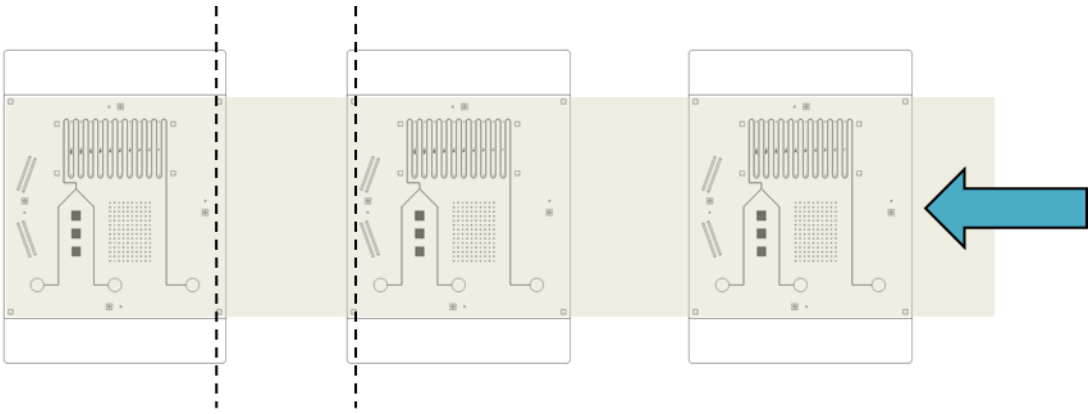

Figure 4-13: Path of the cutting blades over the taped chips. The chips feed in from the right in this diagram. The chip on the left is fully separated after the cut and can be removed for testing.

In order to cut the chips reliably in the same spot, a precision positioning system needed to be designed for both the chips and the blades. After leaving the taping conveyer belt, the chips move to a cutting block. They are still powered by the movement of the belt and rely on the stiffness of the tape to push them forward. Assuming the chips were properly positioned by the belt guides, they should be in approximately the same position each time. To account for any errors, an alignment fork is used to locate the chips, shown in Figure 4-14. This fork moves forward with the motion of the blade assembly. Each prong is tapered in the front, which helps to push the chips into position if they are slightly offset. The chips move into position between the

[9] Amazon.com Item #158290-1001: Fiskar 45mm titanium rotary cutter blades, 2-pack

prongs of the fork just in time for the blades to cut the tape. Two 0.5 in. thick foam rollers roll with the blade assembly and help keep the chips in position while the blades cut the tape. The cutting block is aligned so that the chips are always slightly too far forward when the fork moves forward. The tape can always buckle, allowing the chips to move backwards into position, but the tape cannot stretch, so the chips are unable to move forward if they are too far back.

The blade assembly and alignment fork are powered by an air cylinder (more on actuator selection can be found in Section 4.2.5). The air cylinder can be used to generate linear motion, but it should not be relied on for alignment. Instead, a pair of linear guides is mounted to the base below the cutting block, shown in Figure 4-15. Only one of the linear guides is tightened down while the other is free to float to prevent side-to-side torque without over-constraining the assembly. The air cylinder connects to the assembly via a rod clevis and pin joint, which also prevents over-constraining the system. The blade assembly connects at the same pin joint and gives the blades freedom to move up and down and adapt to different thicknesses of chips. To apply a downward force on the blades, two parallel spring-loaded rails, shown in Figure 4-16, are mounted to the cutting block. The rails press down on two bushings on the blade assembly. The spring compression can be modified by tightening or loosening the screws. This is helpful in case a different type of tape is used in the future.

Below the spring-loaded rails, a pair of fixed rails guides the blades to make up for any extra slack in the joints. This combined with the alignment fork for the chips enables the tape to be cut precisely just inside the edge of the chip. Once the chips are cut, the blade assembly and fork retract. The robot can then pick up the taped chip and use the edge of the cutting block to square the chip before bringing it to the functional testing machine.

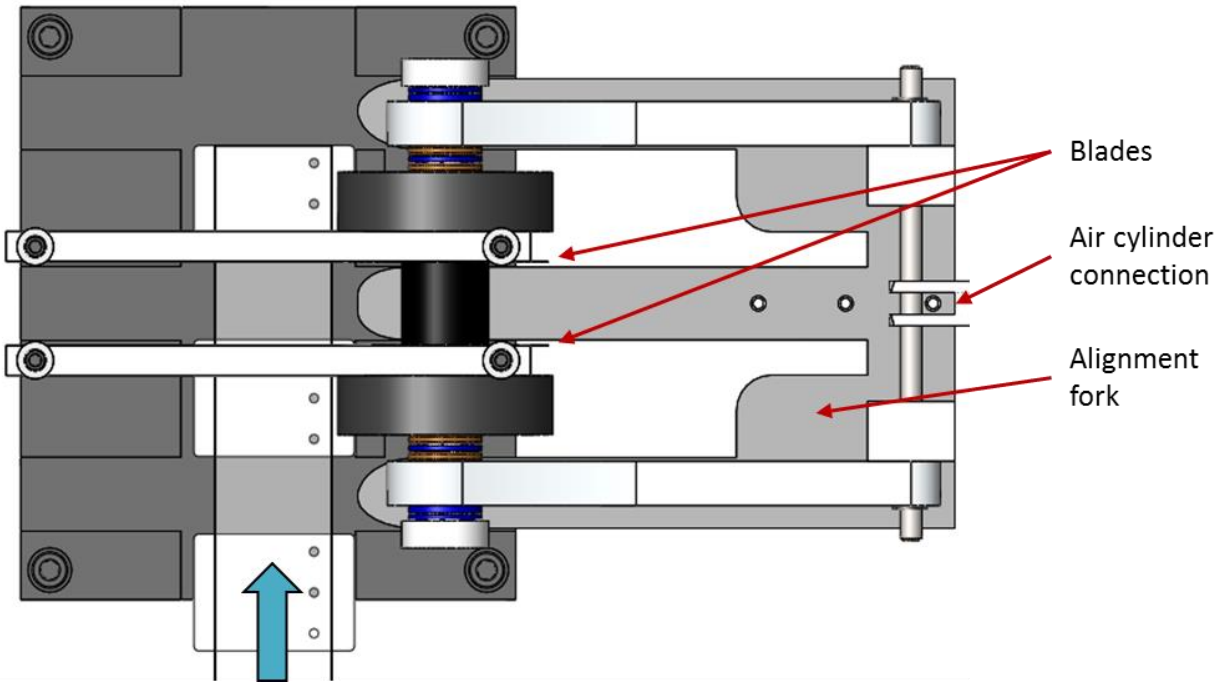

Figure 4-14: Top view of the tape cutting assembly. The chips move from bottom to top. An air cylinder moves the alignment fork from right to left to push the chips into position as the blade assembly rolls forward to cut the tape.

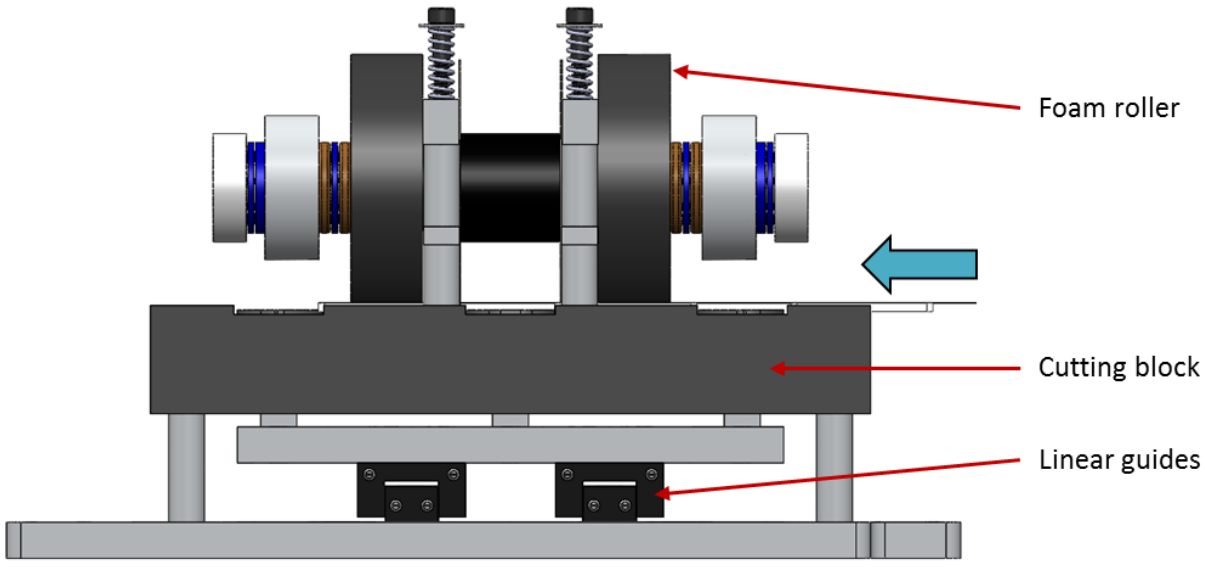

Figure 4-15: Front view of the tape cutting assembly. The chips move from right to left. The alignment fork and blade assembly are guided by linear rails mounted to the base below the cutting block and move forward out of the page. Foam rollers on the outside of the spring-loaded rails keep the chips in position as they are cut.

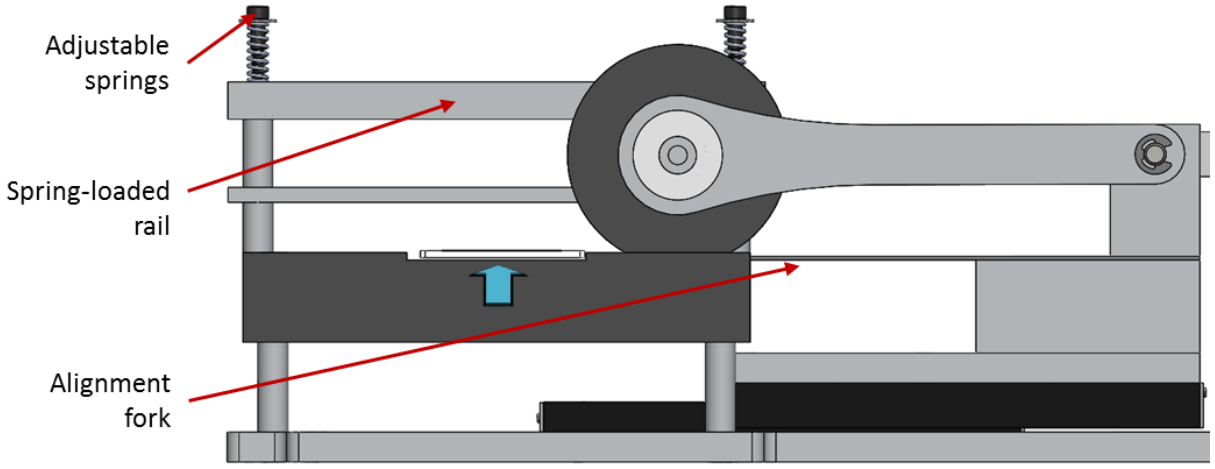

Figure 4-16: Side view of the tape cutting assembly. The chips move forward into the page. The alignment fork and blade assembly move right to left. The blades are pressed down by spring-loaded rails with adjustable force.

Since the chips are spaced apart on the belt, there is an extra gap of tape between each chip. While the rest of the cutting mechanism was being designed, there was no obvious solution for how to remove the tape, so it was set aside until the cutting process was proven to work. After the cutting assembly was built, it became apparent that the extra tape would get caught in between the blades after each cycle and would eventually jam the mechanism or leave undesirable tape fragments on the chips.

To remove the tape, a second smaller air cylinder was mounted to the middle prong of the alignment fork (more on actuator selection can be found in Section 4.2.5), and a curved "shovel" head was mounted to the rod end just between the rotary blades. The fork and blades slide forward as before, cutting the tape. However this time, the shovel helps peel up the tape as it trails the blades when the whole assembly moves forward. When the blades reach the end of their stroke, the second air cylinder actuates, ejecting the extra tape off the edge of the cutting block and into a waste collection container. This method works quite well. It can be seen in Figure 4-17 and Figure 4-18. Occasionally, a piece of tape will not eject completely, but will eventually get removed in one of the following cycles.

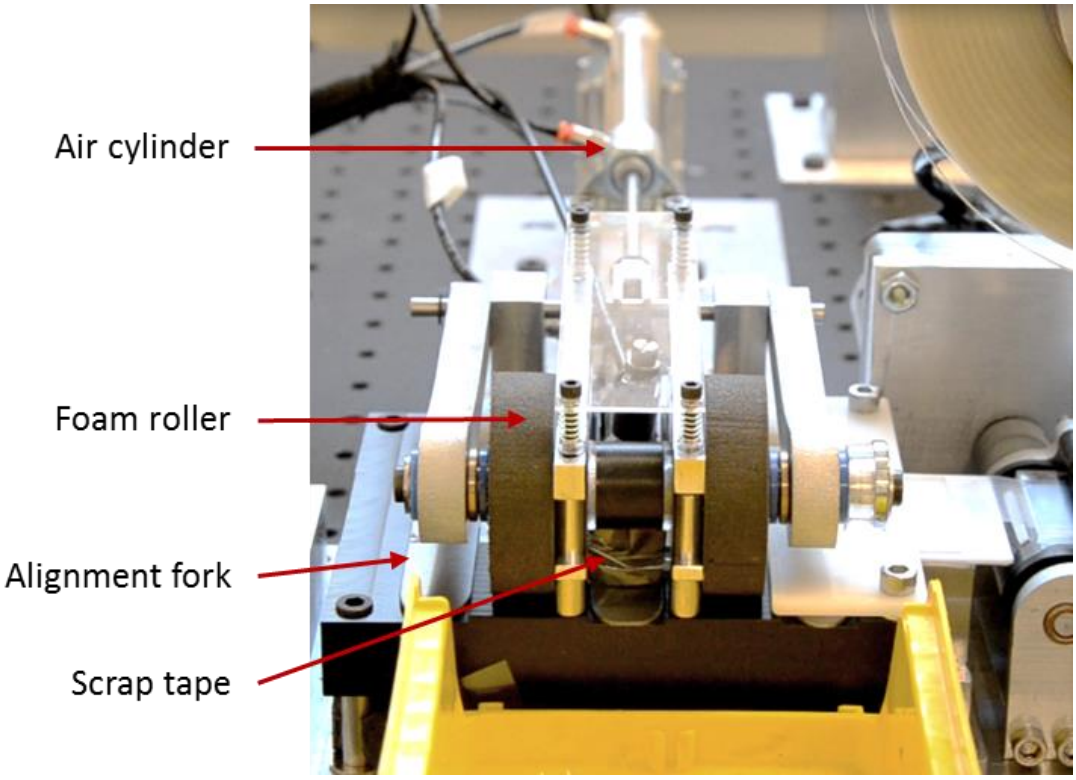

Figure 4-17: The completed cutting mechanism. The blade assembly, alignment fork, and attached shovel have moved forward, and the scrap tape has peeled up in front of the shovel head.

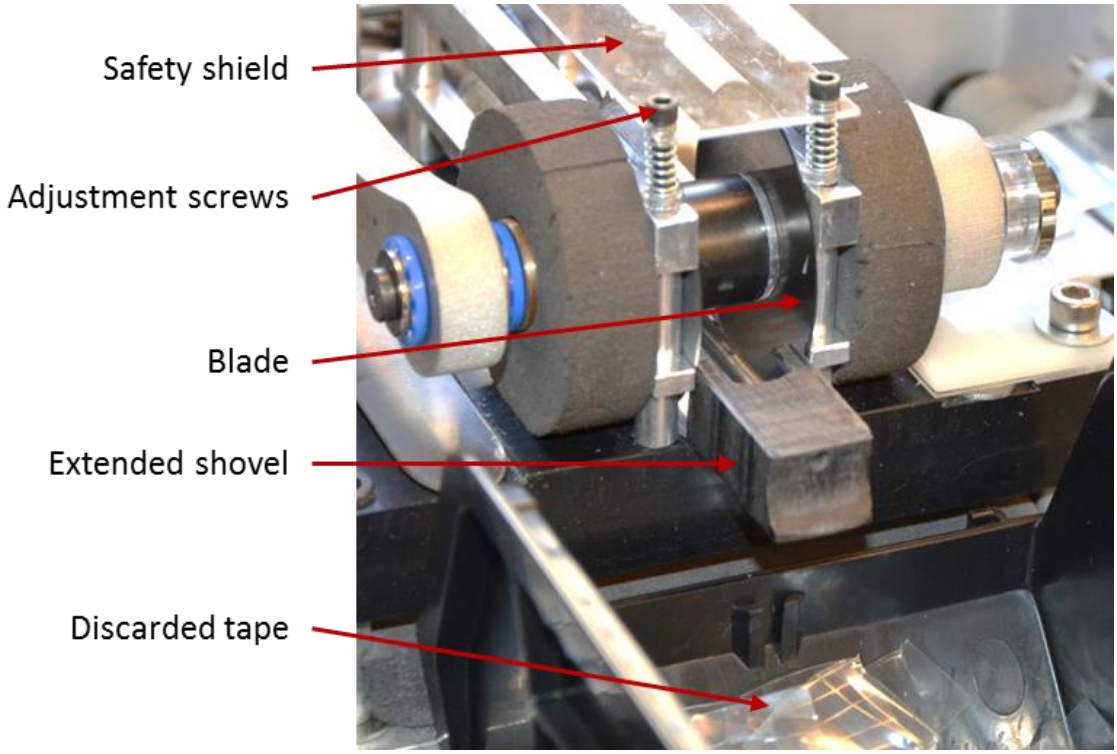

Figure 4-18: Tape removal. The smaller air cylinder activates and pushes the shovel head forward, ejecting the scrap piece of tape into the waste bin.

After cutting a few hundred chips, the blades tend to get dull. They sometimes do not cut through the tape completely, and the tape removal shovel ends up tearing off the tape instead. This leaves a ragged edge that sometimes protrudes over the chip profile and can interfere with chip pick up by the robot or chip placement on the functional test alignment pins. The whole cutting assembly does not need to be removed in order to replace the blades. The blade assembly can be unscrewed and the shaft can come partially out until the blades pull out. Alternatively, the spring-loaded rails can also be removed, but this requires calibrating the compression springs to control the blade force each time.

4.2.5 Actuators and Sensing

The taping machine uses two motors during its first half of operation to seal the chips. A larger motor drives the conveyer belt and a smaller motor drives the liner removal reel. A stepper motor was originally chosen for the large motor in order to easily control the position of the belt[10]. However, this particular model did not have enough torque to overcome the friction in the belt (the prototype with this motor had a thicker belt with higher tension and more friction). The belt tension was lowered and a new motor with a higher torque was chosen. It was speculated that a stepper motor might not be enough to control the location of the belt due to the potential for error accumulation. A better method for position control would be to use a sensor to index the belt along with a standard DC motor to run power it. A geared DC motor with over three times the torque of the stepper motor was used, which worked well for powering the new belt [11].

To control the liner reel, a low-power miniature geared DC motor was chosen with the intent of having it stall when there is no slack left in the liner[12]. The liner wheel ended up having more friction than expected, though, so a higher torque motor was needed. Another miniature geared DC motor with a higher gear ratio was chosen instead. It has the same no-load speed and five times the amount of torque[13]. This is more torque than is necessary, so the voltage can be lowered to prevent it from removing too much liner. Also, to prevent damage, the liner wheel motor is controlled to only run while the belt motor is moving instead of stalling continuously.

---

[10] Alltronics.com Model #5718M-15-09: Unipolar stepper motor, 0.92 N-m

[11] McMaster-Carr Part #6409K16: 12VDC Compact DC motor, 16 rpm, 2.82 N-m, 1.4 full load amps

[12] Pololu.com Item #2204: Miniature low-current brushed DC motor with 100.37:1 metal gearbox. 0.94" x 0.39" x 0.47". At 6 V: 120 rpm and 40 mA free-run, 0.085 N-m and 0.36 A stall.

[13] Pololu.com Item #995: Miniature high-powered brushed DC motor with 250:1 metal gearbox. 0.94" x 0.39" x 0.47". At 6 V: 120 rpm and 70 mA free-run, 0.42 (4.3 kg-cm) and 1.6 A stall

An infrared photo interrupter with an emitter and a detector was installed to sense the position of the belt[14]. It was placed on one wall of the taper near the entrance to read the holes cut into the custom conveyor belt. It can be seen on the right side of the belt in Figure 4-10 and Figure 4-11. The photo interrupter did not perform very well initially because the emitter was too weak. An extra flashlight was added to improve the contrast of lighting in that area. This worked well, except the flashlight only stayed at full brightness for the first few hours. Instead, a plug-in miniature spotlight was obtained. Ideally, the photo interrupter would be able to detect both the location of the belt as well as the presence of a chip, since the edges of the chips fall on top of the holes in the belt as they pass over the sensor. However, there is not enough difference in lighting between a hole with a transparent chip on it and an uncovered hole. If the sensor was sensitive enough or if the chips were translucent at the edges rather than transparent, then it might be possible to detect the chips. This would be beneficial for confirming that a chip is in place before beginning the taping cycle to prevent possible errors.

Two air cylinders are used to actuate the tape cutting process. The first controls the movement of the alignment fork and blade assembly, so a cylinder with a 3 in. stroke length was needed[15]. A spring-return version was initially used, but the spring was not always strong enough to retract completely. If the alignment fork sticks out even slightly, the chips can run into the tips of the prongs while they are advancing forward. The tape will then buckle, causing the chips to become jammed. The second air cylinder did not need to be quite as large. A cylinder with a 45 mm stroke length was enough to eject the tape from the cutting area[16]. Each of the cylinders are controlled with a 5-port solenoid valve, since they are both double-acting[17].

The taping machine was designed to run as a stand-alone system. The only information communicated with the rest of the system is a start trigger sent from the robot to the taping machine after it places a chip on the belt. The rest of the process is performed automatically after receiving the signal, and takes approximately 15 seconds each time. The robot knows this and can immediately begin moving to pick up the taped chip from the cutter assembly.

[14] Sparkfun.com Part #SEN-09299: Sharp transmissive photo interrupter GP1A57HRJ00F, 10 mm gap, 1.8 mm slit
[15] McMaster-Carr Part #6498K433: Stainless steel air cylinder, pivot-mount, double-acting, 0.625" bore, 3" stroke
[16] SMCpneumatics.com Part #CJ2D10-45: Stainless steel air cylinder, double clevis mount, double-acting, 10 mm bore, 45 mm stroke
[17] Automationdirect.com Part #AVS-05211-120A: Nitra single solenoid valve, 120VAC, 5-port, 2-position

An Arduino Uno microcontroller was chosen to control the taping machine[18]. This board controls the photo interrupter sensor, both motors, and the solenoid valves for both cylinders. Once the robot places a chip down, it sends a signal to one of the Arduino's pins. When the Arduino receives the signal, it starts powering the belt and liner motors. The photo interrupter is then covered by a solid section of the belt. As soon as the next hole in the belt appears, the photo interrupter detects this and the motors stop. The large air cylinder is triggered to push forward to cut the tape. Next, the small air cylinder moves forward to eject the tape and then retracts. Finally, the large cylinder retracts and the cycle ends.

In the future, it would be helpful to include more sensors in the machine to be able to detect its current state and to prevent any catastrophic errors. For example, if it is possible to detect the locations of the chips along the cutting block, then the machine could send an error signal if it detects that the chips are not aligned properly. Also, if there was a position sensor on the blade assembly, and if an irregular position was detect (ie. the blades are jammed on an incorrectly aligned chip), then the machine could send an error signal rather than continuing to run and potentially making the problem even worse.

[18] Arduino UNO R3 board with DIP ATmega328P

4.3 Completed Hardware Design

The final taping machine with labeled key components is shown below in Figure 4-19.

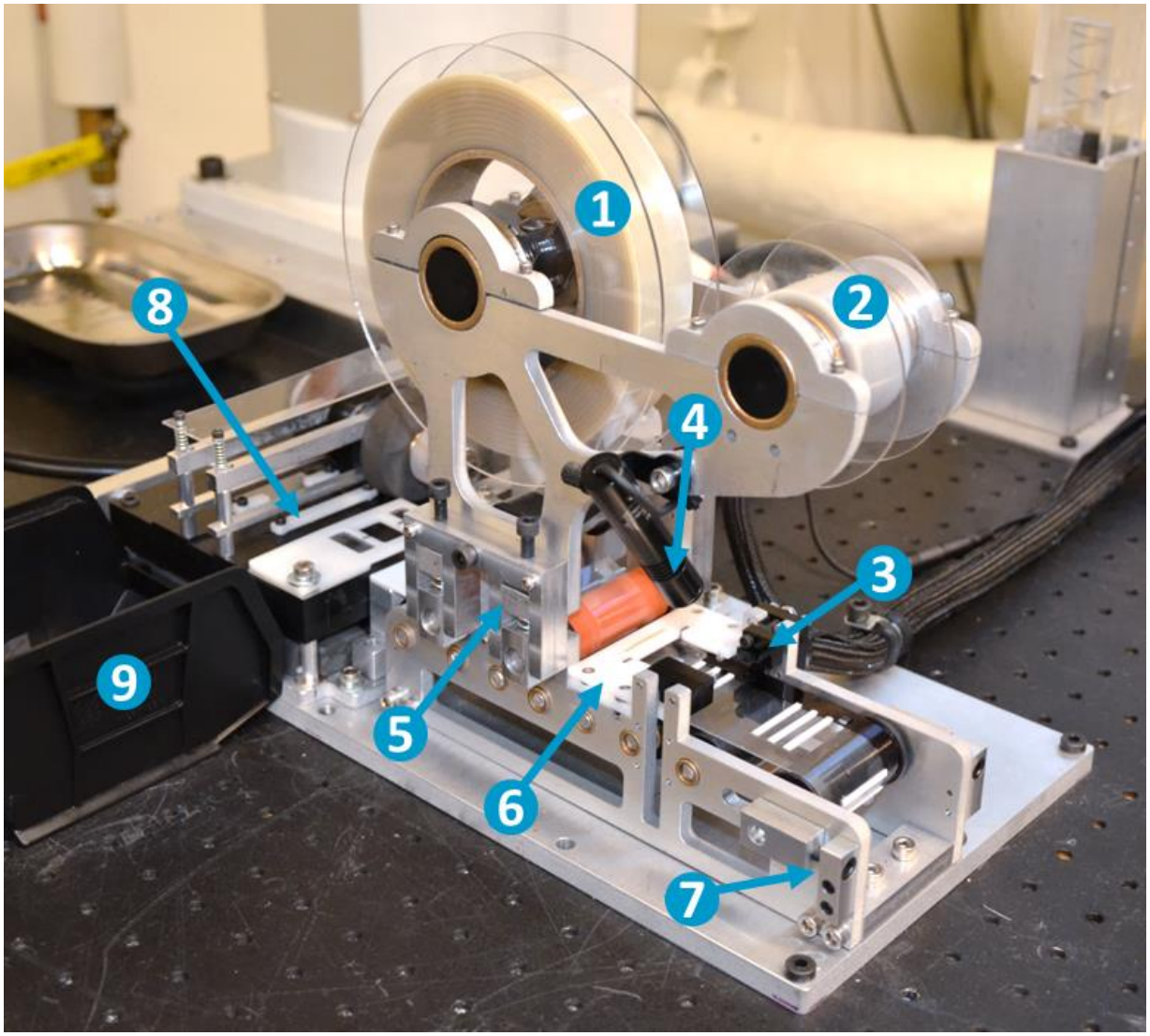

Figure 4-19: The final taping machine. (1) The tape reel, (2) The liner take-up reel, powered by a miniature geared DC motor, (3) A photo interrupter to index the belt, (4) A light to improve sensor readings, (5) The adjustable-force compliant roller system for applying tape, (6) Plastic guides to align chips before taping, (7) The belt tensioner, (8) The cutting block where chips are separated by air-powered rotary blades, and (9) The waste bin for collecting scraps of tape.

The frame of the taping machine consists of 0.25 in. waterjet aluminum. The tape is sandwiched between 2 acrylic disks to keep the tape properly aligned. The tape is fit over a 3-pronged flexure of spring steel mounted to an axle that resists motion in one direction (to prevent accidental unraveling of the tape) but allows the tape to be wound back up if it becomes loose for

any reason. The tape shaft is clamped between the 2 frames for easy access that does not require full disassembly to replace the tape. A liner reel is mounted similarly at the front of the machine. It is powered by a miniature geared DC motor that is designed to be strong enough to peel off the tape's lining yet weak enough that it will stall once it has taken up the slack in system.

A custom-made conveyor belt with 0.031 in. thin Teflon® spacers pushes chips through the taping machine. The spacers ensure that the chips are spaced far enough apart so they never get stuck directly underneath a roller between cycles. The belt rests on a series of plastic rollers mounted to the frame via bronze bushings. The belt is tensioned using a pair of screws attached to collars on the front belt roller. A larger geared DC motor drives the conveyer belt and is attached to the rear belt roller. The belt is colored black along one edge and has holes at every chip location, which a photo interrupter can detect to index the belt's location.

When a chip is placed, the belt advances forward. The chip passes between two plastic guides that position it horizontally and underneath hanging brushes that position it flush against the Teflon® spacer. This accounts for any error that may accumulate between removal of the chip from the hot embosser and placement into the taping machine by the robot. To apply tape, a series of 2 compliant rollers are used. These rollers have adjustable springs on the sides of the frame, which allow the tape application force to be adjusted.

Lastly, there is a separate cutting area for separating chips from the line of tape. After each taping cycle, a pair of air-actuated rotary blades rolls forward to cut the tape between the chips. An alignment fork moves forward simultaneously to ensure that the chips are positioned precisely relative to the blades. The fork and blade assembly ride on a pair of precision linear guides. The downward force on the blades can be adjusted by a pair of spring-loaded rails. Another air-cylinder ejects the cut piece of tape into a separate waste container, and the blades retract. The last chip is then ready for pick up by the robot. The sides of the cutting block can be used to reposition the chip before bringing it to the functional testing machine. If the machine is running at capacity, there will always be 5 chips in the buffer. If there is a sixth chip, then the last chip is waiting to be picked up for testing.

4.4 Final Taping Process

The taping process requires the following steps:

1. The robot places an embossed chip onto an open gap on the belt and triggers the taping cycle to begin.

2. The belt and previously placed chips advance forward and continue moving until the next position on the belt is detected by the infrared photo interrupter. The most recently placed chip is funneled into position by a series of plastic guides. The next chip in the line is pushed under a compliant rubber, which applies adhesive tape using a constant force. At the same time, a miniature geared DC motor removes and collects the protective liner from the tape.

3. The last chip in the line is pushed past the last blade on the cutting block. After the belt stops moving, two rotary blades roll forward between the last two chips. Then, a second air cylinder moves forward and ejects the extra tape into a container. The blades return to their original position.

4. The robot picks up the last chip from the cutting block, using the sides of the block to help realign the chip and takes it to be tested.

All of the initial design requirements were met. The Tesa tape is strong enough to withstand over 35 psi of pressure for longer than 2 minutes. Its adhesive layer is thin enough that it does not flow into the channels and it is uniformly distributed to avoid fluid from leaking. The adhesive's backing is sufficiently stiff to prevent the tape from collapsing into the channels and the tape is optically clear. The tape is also biocompatible and was originally designed for microfluidics. The tape covers a 25 mm by 25 mm area above the embossed area on each chip. There is approximately 3 mm between the features and the edge of the tape. The chips are separated automatically with a cutting step and are able to be picked up reliably by the robot. The machine runs autonomously and has been integrated with the rest of the system.

CHAPTER 5 MEASURES OF QUALITY

Before a method could be developed for measuring the quality of embossed chips, a metric needed to be developed to distinguish good chips from bad chips and everything in between. The ideal chip would have a profile that perfectly matched the shape of the tool. In this case, the channel would be rectangular (40 μm by 50 μm) and have sharp corners. If the embossing temperature and forming force are not high enough, then the corners of the tool will not fill properly, leaving a rounded or curved profile, shown on the left in Figure 5-1. This can be considered a poorly-formed chip. If the channels are under-formed enough, there will be no flow, and the chips will not function at all. As the temperature and pressure are increased, the plastic is able to fill the tool more completely. However, if the embossing temperature and forming force are too high, then it is possible for the chip to over-form, as seen on the right in Figure 5-1. This is also undesirable, as it ruins the overall aesthetics of the product and makes it more difficult to handle during the remaining steps in the manufacturing process.

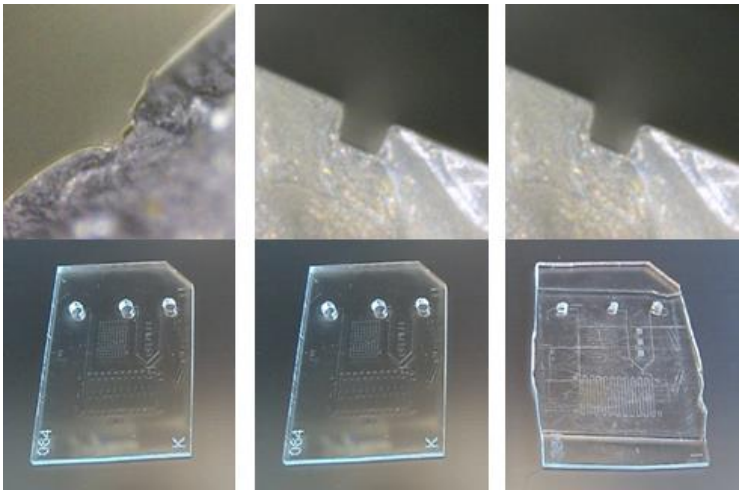

Figure 5-1: Examples of under-formed, well-formed, and over-formed devices. Left: Low temperature and pressure caused the channels not to fill completely, resulting in rounded edges. Middle: A well-formed chip has sharp channel edges. Right: High temperature and pressure lead to an over-formed chip, shown by the uneven perimeter [37].

Bulk deformation occurs in the chip as the tool compresses the plastic substrate, causing some of the material to flow out the open sides. This compression can be detected by the use of a linear variable differential transformer (LVDT) during the embossing process on the hot embossing machine itself [7]. If the LVDT detects a displacement larger than the acceptable threshold, then either the embossing process can be aborted, or the pressure could be reduced and the displacement held constant for the remainder of the cycle. However, a quick and low-cost method still needs to be developed to measure the shape of the channels.

In addition to channel geometry, the overall functionality of the devices can also be used as a measure of embossing quality. For this chip design, fluid should be able to flow from both inlets to the outlet, and there should be some degree of mixing in between. If there is no flow, then either the channels are too under-formed, or there is something blocking the inlets of the device. If a method can be developed to functionally test the chips using fluid, then a more general measure of the chip quality and variation can also be made.

5.1 Quality of Channel Formation

Pressure-sensitive adhesive tape was found to be useful as both a cover plate for the embossed chips and an aid in measuring channel geometry. Once the tape has been applied, it highlights the distinction between well-formed and poorly-formed chips. Since good channels have very sharp corners, there is only one edge of the channel wall when viewed from above, shown on the left of Figure 5-2. Under-formed channels have very rounded corners that are caused by the lack of flow into the corners of the tool during forming. This leads to the appearance of separate inner and outer widths, which appear where the tape contacts the top of the channel, as seen on the right of Figure 5-2. The inner width, or nominal channel width, is approximately 50 μm, and the outer width varies depending on how poorly formed the channels are. Figure 5-3 shows the same effect on sample well-formed and under-formed chips when viewed with an optical microscope. If this outer channel width can be measured reliably from a single image, then it is possible to determine the embossing quality without the use of complex and time intensive 3D scanning.

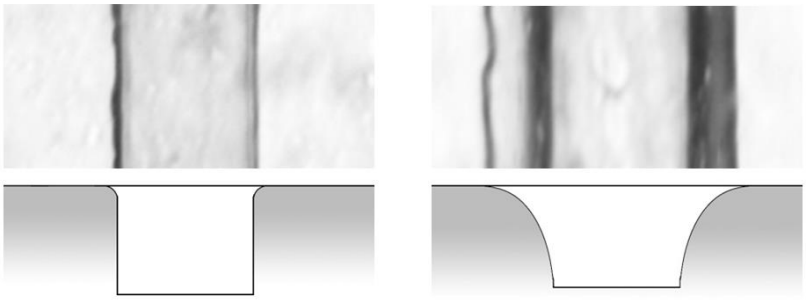

Figure 5-2: Top and cross-sectional views of the channels on well-formed (left) and under-formed (right) chips after adhesive tape has been applied.

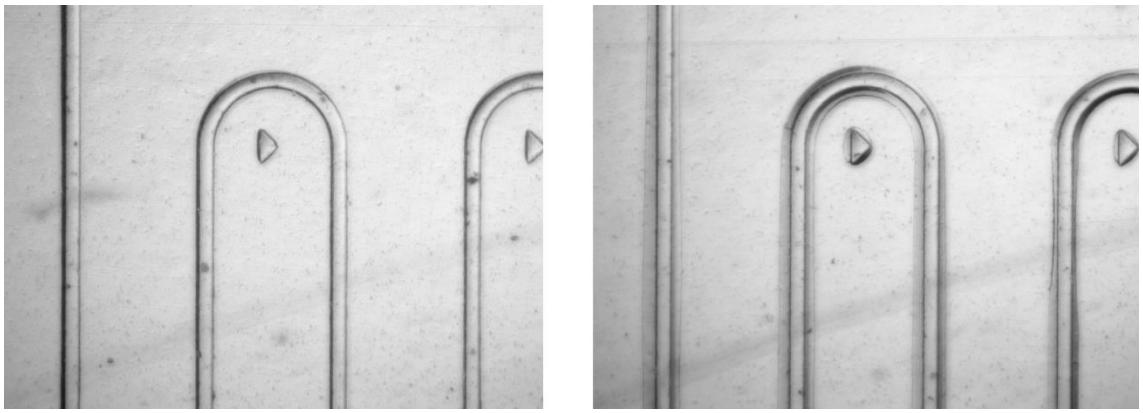

Figure 5-3: Sample images showing outer channel widths on well-formed (left) and under-formed (right) chips after adhesive tape has been applied.

5.2 Functional Test of Chips

It is also important to test that these devices are functioning properly. They are designed to take two fluids and mix them together via diffusion. There are several scenarios that would prevent both fluids from flowing properly in the first place. If the plastic substrates are not properly aligned with the tool during embossing, then the inlet channels might not intersect with the inlet holes, which are pre-molded into the blank chips and no flow would occur. Other scenarios that would prevent flow include under-formed channels that are too narrow and, in an extreme case, a tool that has been severely damaged. It is also possible for only one of the fluids to flow if the other inlet is blocked by an air bubble, dirt, or an under-formed channel. Alternatively, it is possible for the channels to be formed just well enough for there to be flow, but not well enough

to be functional. It is possible for the features' corners to be so rounded, that there ends up being "bridging" between channels as shown below in Figure 5-4.

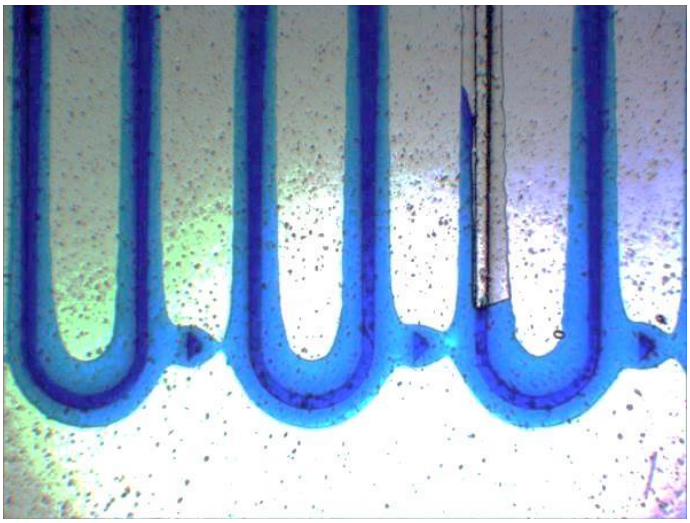

Figure 5-4: Sample under-formed chip with bridging between channels.

If the channels are well-formed, but something goes wrong during the taping process (ie. the adhesive is not strong enough or it is not making a good seal over the channels), then it is also possible for the devices to leak. By flowing dye through the chips, a functional test can be made by first confirming that there is flow, and then by checking for leaks or other flow irregularities. This functional test would be destructive, since the chips would be unusable once fluid has contaminated the channels. In a real factory, this type of test would only be performed on a small sampling of the chips. In this case, however, there can be 100% inspection, which will be more helpful for gathering data and analyzing how process control can be used for the embossing process.

5.3 Variation between Chips

Ideally, every chip of the same initial thickness and material that is embossed with the same forming parameters should have identical channel geometries. For the same fluid pressure, the flow rate should remain constant from chip to chip. In reality, there will be variations between each cycle that will cause the channel geometry to vary slightly. Measuring the variation in the flow rate can provide an approximation of the overall variation in chips. It can take multiple factors into account such as the quality of channel geometry, inlet formation, and bonding.

Since the flow rates are extremely low (on the order of 0.003 mL/min), it is very difficult to accurately measure the mass of the fluid output in a short period of time. Instead, the flow rate can be determined by measuring the mixing location of two fluids during a functional test. Since mixing at the micro-scale occurs by diffusion after a set amount of time, the mixing length will be shorter for slower flow rates and longer for faster flow rates. If the mixing location changes, it would indicate variations between the chips.

To measure the mixing location, two different colored dyes can be used. The average pixel intensities across channels can determine when a flow is considered "mixed". When the flow is still unmixed, there is a large gradient in the intensity from one edge to the other as seen on the left in Figure 5-5 below. The slope of this gradient will decrease along the length of the channels until it reaches a minimum when the flow has fully mixed. Alternatively, the standard deviation of the pixel intensity across the width of the channels can also be used to detect mixing.

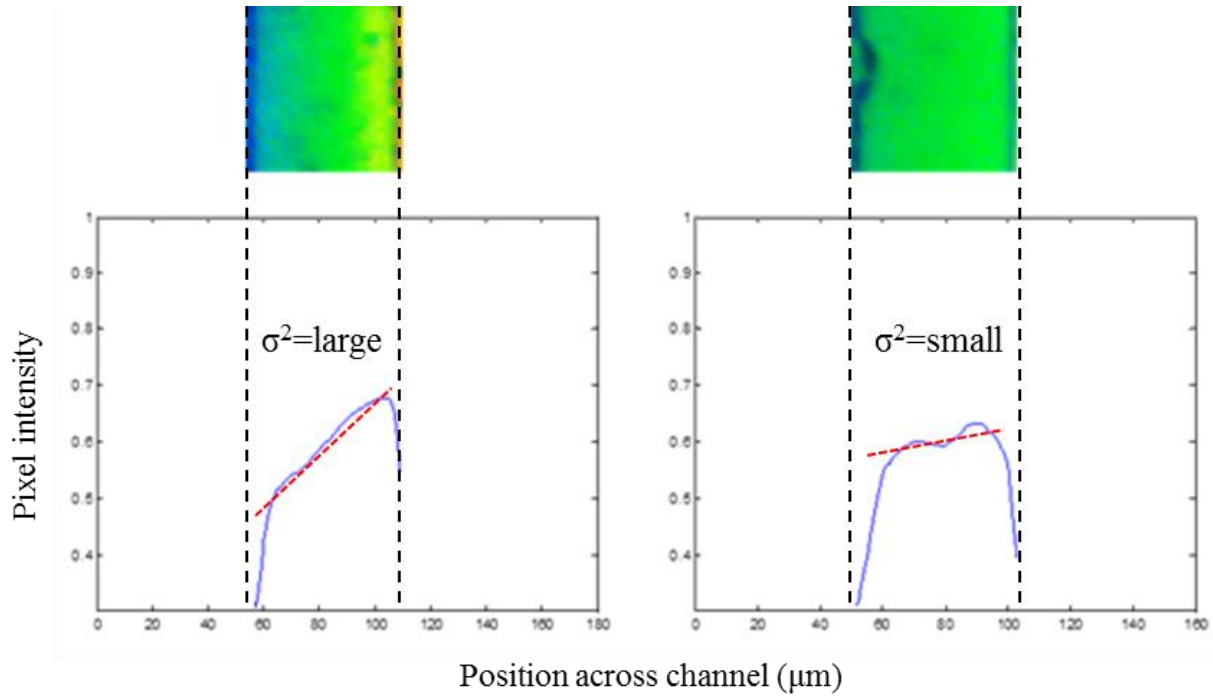

Figure 5-5: Locating the mixing point using pixel intensity across channels. Left: The variance in pixel intensity across the channel is high for unmixed dye. Right: The variance in pixel intensity across the channel reaches a minimum when the dyes have mixed.

The micro-mixer pattern for this project was originally designed by the previous researchers such that the flows were completely mixed by the end of the serpentine channels. For the channel

dimensions and a given flow pressure, the predicted mixing length could be calculated. For laminar flow below a critical Reynolds number of 80, mixing occurs entirely by molecular diffusion, so the mixing time, t_{mix}, can be approximated as

$$t_{mix} = \frac{w^2}{D} \tag{5.1}$$

where w is the characteristic length for mixing, which is the width of the channel in the case of the microfluidic mixer. D is the diffusion coefficient of the fluids [40].

The required mixing length can then be calculated using

$$L_{mix} = t_{mix}\bar{u} \tag{5.2}$$

where $\bar{u}$ is the average fluid velocity in the channels.

In a round channel with a circular cross-section, the pressure drop in a channel of total length, L, can be modeled as

$$\Delta P = f\frac{L}{d}\rho\frac{\bar{u}^2}{2} \tag{5.3}$$

where ρ is the fluid density, d is the channel diameter, and f is the Darcy friction factor, which is given by

$$f = \frac{64}{Re} \tag{5.4}$$

for laminar flow in a round capillary [41]. The Reynolds number is defined in terms of the characteristic length scale d, by

$$Re = \frac{\rho\bar{u}d}{\mu} \tag{5.5}$$

where μ is the dynamic viscosity of the fluid. This can be adapted to describe flows of arbitrary cross-sections by substituting d for the hydraulic diameter, d_h, which is a ratio of the cross-

sectional area of a channel to its wetted perimeter. For a rectangular channel of width, *w*, and height, *h*, it is defined as

$$d_h = \frac{4A}{P} = \frac{2wh}{(w+h)}. \tag{5.6}$$

The flow resistance, f Re, for fully developed flow in a micro-channel with a rectangular cross-section can be approximated as

$$f \text{ Re} = 96(1 - 1.3553\alpha + 1.9467\alpha^2 - 1.7012\alpha^3 + 0.9564\alpha^4 - 0.2537\alpha^5) \tag{5.7}$$

where α is the aspect ratio, h/w [42]. For an aspect ratio of 0.8, the friction factor is 57.53/Re. Combining this with (5.3), (5.5), and (5.6) gives

$$\Delta P = \frac{57.53}{\left(\frac{\rho \bar{u} d_h}{\mu}\right)} \frac{L}{d_h} \rho \frac{\bar{u}^2}{2} = \frac{7.19 \mu L \bar{u} (w+h)^2}{w^2 h^2}. \tag{5.8}$$

Solving for $\bar{u}$ and substituting into (5.2) along with (5.1) gives

$$L_{mix} = \frac{\Delta P w^4 h^2}{7.19 \mu L (w+h)^2 D}. \tag{5.9}$$

The diffusion coefficient of food dye was measured to be approximately 4×10^{-10} m^2/s [43]. The dynamic viscosity of the dye is estimated to be roughly the same as water, or 9.55×10^{-4} Pa-s at 22°C. For a channel length of 182 mm (including the inlet channel length) and channel dimensions of 50 μm wide by 40 μm deep, and a range of pressures, a table of mixing lengths is listed in Table 5-1.

	1 psi (6.90 kPa)	5 psi (34.48 kPa)	10 psi (68.95 kPa)	20 psi (137.9 kPa)
Mixing length [mm]	17	85	170	340

Table 5-1: Estimated dye mixing lengths for a range of flow pressures.

It can be noted that the mixing length increases linearly with pressure. The distance from the Y-junction—where the two dyes meet—after the inlets to the outlet of the device is 170 mm. Theoretically, the flow should be fully mixed by the time the flow reaches the outlet. However, possible variations in the input parameters could cause this length to vary. From (5.9), it can be seen that the mixing length is most sensitive to changes in the channel width. For example, a 1 μm decrease in channel width results in a 10 mm reduction in mixing length. Thus, if the mixing length can be accurately measured during a functional test, then it can be a good measure for the overall variation in feature geometries.

CHAPTER

6 DESIGN OF A FUNCTIONAL TESTING MACHINE

6.1 Design Specifications

The goal of this project and the microfactory project as a whole is to be able to perform cycle-to-cycle process control on the embossing process. In order to implement closed loop feedback control, the quality of embossing must be measured and fed back to the hot embossing machine automatically, which can update its parameters accordingly. Using the outer channel width and mixing location measurements detailed in Chapter 5, a reasonable measure of embossing quality can be made. This required the development of an inspection and functional testing machine that could operate within the manufacturing cell.

The following needs were identified in order for this to be successful:

1. An image of the channels with a resolution of 1.5 to 2 pixels per μm (the outer widths are generally around 60 μm, so each pixel would correspond to a difference of 1% in the width) for measures of the outer channel widths.

2. An image of the inlet channel region and the first 10 channels (observed locations of the mixing points on the current devices) with a resolution of at least 0.4 pixels per μm (or 20 pixels of measured across the width of a 50 μm channel).

3. A precise and repeatable chip alignment system.

4. The ability to flow dye through the chips.

5. A program to process the images and identify the quality of embossing.

6. A cycle time faster than the slowest machine in the system (currently the embosser at 110 seconds) to allow for 100% inspection during production.

7. Full automation and compatibility with the other machines in the microfactory project.

The following sections will describe the challenges and solutions that led to the final design of a functional testing machine for hot embossed microfluidic chips.

6.2 Design

6.2.1 Optics

An early version of the functional testing system was mounted to the stage of a compound laboratory microscope, shown in Figure 6-1. A digital USB microscope camera allowed the image to be transferred to a computer for observation and logging. The microscope's optics and linear stage worked very well, but it only allowed for one field of view (at its corresponding resolution) to be recorded at a time. It also had a very short working distance with very little clearance for a clamp, dye outlets, and robot access. This set-up worked well for manually running preliminary tests on the chips and verifying the feasibility of the measurements. However, it needed to be redesigned to improve and automate the process so that it could be used during production cycles.

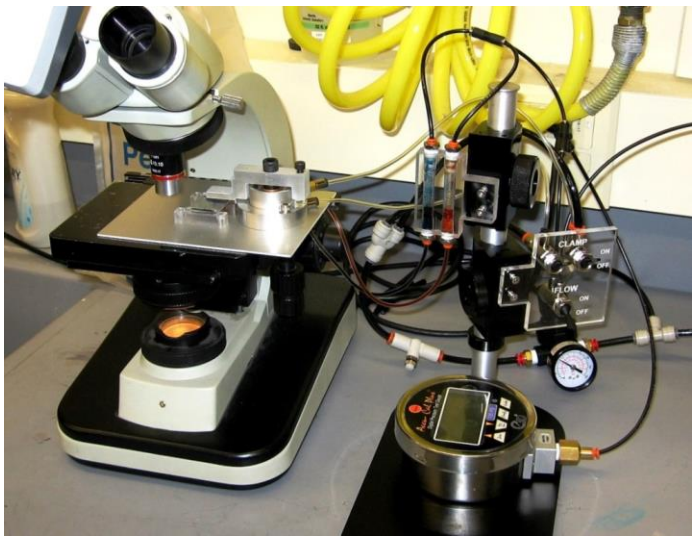

Figure 6-1: An early prototype of the functional testing system. It used the optics and stage of a compound microscope with an added digital USB microscope camera.

Instead, a custom microscope set-up was pursued to allow for a much greater working distance. In order to meet the minimum resolution for an accurate measure of the outer channel widths and still have a large enough field of view to measure the mixing locations, two different sets of optics with different magnifications were used. To provide flexibility for potential changes in the test set-up, two AmScope industrial inspection monocular microscopes with adjustable magnifications were chosen[19]. The channel width microscope was set to 5x for a 2.42 mm by 1.73 mm field of view. The mixing location microscope was set to 2x for an 8.22 mm by 5.88 mm field of view.

To record the images, a 9 MP CMOS color USB microscope camera from OMAX[20] and a 10 MP CMOS color USB microscope camera from AmScope[21] were used initially. USB cameras were chosen for their plug-and-play abilities and ease of access. They both claimed to be DirectShow compatible, which should allow them to be used with third party programs such as LabVIEW. Unfortunately, neither camera could communicate with LabVIEW or any other non-proprietary software. Instead, two 10.5 MP CMOS monochrome USB cameras were purchased from Edmund Optics[22]. This allowed the channel width microscope to have a resolution of 0.63 μm/pixel and the mixing location microscope to have a resolution of 2.14 μm/pixel.

Specification	
Sensor Format	1/2"
Sensing Area, H x V [mm]	6.41 x 4.59
Pixels, H x V	3840 x 2748
Pixel Size, H x V [μm]	1.67 x 1.67

Table 6-1: Specifications for the current 10.5 MP CMOS monochrome USB microscope camera.

[19] AmScope.com Item #H800: 11x-80x Industrial inspection zoom monocular microscope
[20] Amazon.com Item #B004OF0U8O: OMAX 9 MP microscope digital USB camera
[21] AmScope.com Item #MU1000-CK: 10 MP USB 2.0 microscope digital camera + calibration kit
[22] EdmundOptics.com Stock #86-746: EO-10012M 1/2" CMOS monochrome USB camera

Unfortunately, both microscopes could not fit next to each other and still view the correct regions on the chips. One option was to use an actuated stage that could move the chip from one camera to the other midway through the inspection. Another option was to turn one of the microscopes at an angle and have an actuated mirror that could flip to direct the image from one microscope to the other. Although both of these options would allow for an unobstructed view of the chip for both microscopes, a stationary method was preferred to avoid introducing unwanted error to the system. Instead, a small 5 mm right angle mirror was mounted above the stage to direct an image of the chip's outlet channels to a stationary camera mounted horizontally, shown in Figure 6-2 and Figure 6-3. A vertical camera was positioned over the inlets of the chip and the first half of the channels. Based on preliminary tests, mixing occurs within the first 6 channels—contrary to the predicted mixing length in Section 5.3. It isn't necessary for this camera to see the latter half of the channels, which can be assumed to be fully mixed.

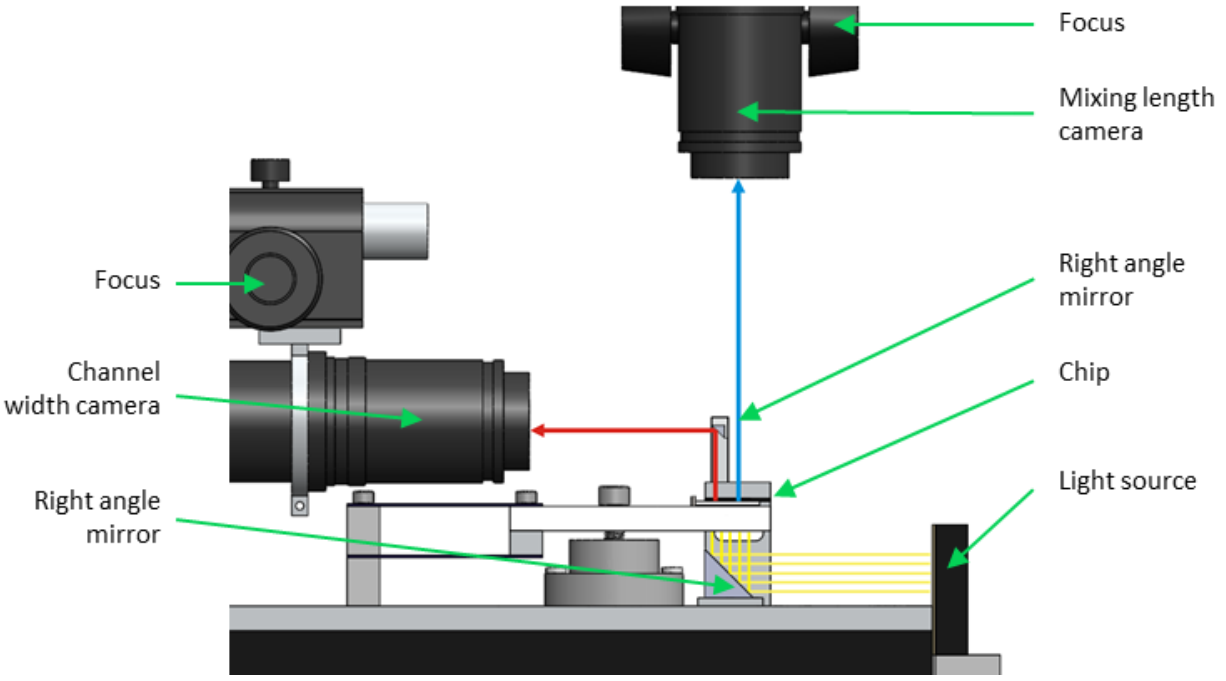

Figure 6-2: A diagram of the new optical arrangement. The two cameras were placed perpendicular to each other and a right angle mirror was added to split the image of the chip (red and blue arrows). A right angle mirror below the stage redirects light into the optics.

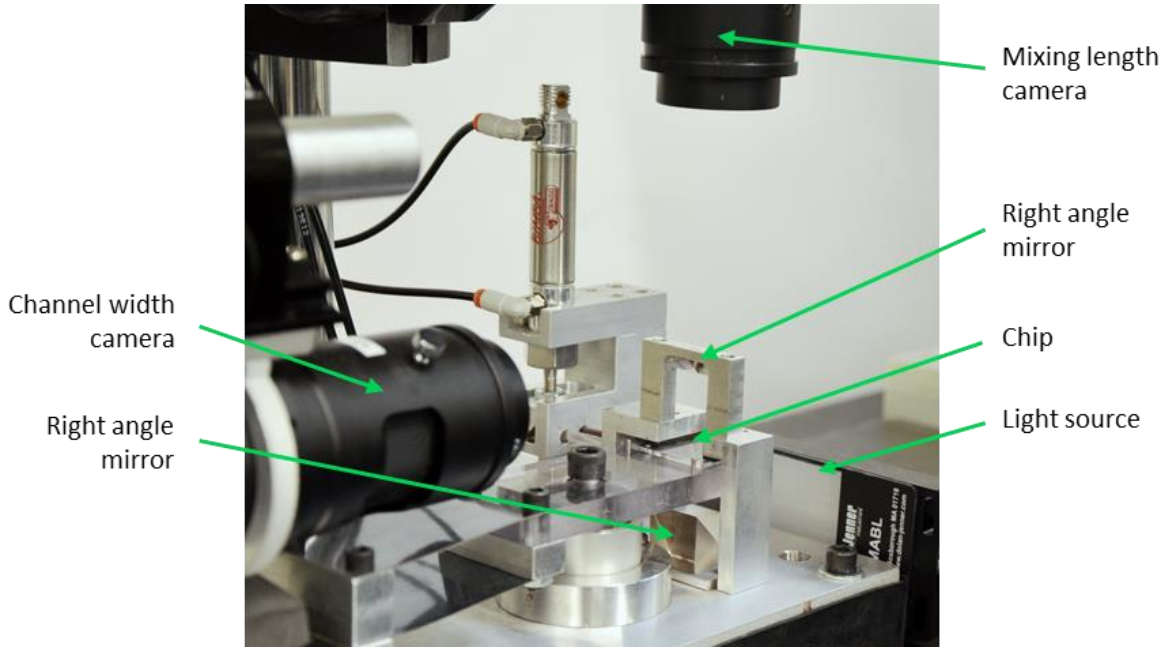

Figure 6-3: A photo of the new optical arrangement. The two cameras were placed perpendicular to each other and a right angle mirror was added to split the image of the chip. A right angle mirror below the stage redirects light into the optics.

Lastly, the optics were mounted to x-y linear stages from Edmund Optics for position adjustment[23]. They have 0.5 in. of travel in each direction, which is more than enough to correct for any misalignment. The optics are also mounted to z-stages for focal adjustment.

6.2.2 Chip Alignment

It is important for chips to be placed into the functional tester in a repeatable manner. If the chips are crooked, the inspection will be unable to take the necessary measurements. If the chips are extremely misaligned, the inlets of the chip will not cover the dye outlets of the testing machine, leading to potential leakage if the flow is turned on. Since the width measurement has a higher magnification and a smaller field of view (2.4 mm by 1.7 mm), it is more sensitive to differences in alignment and will control how repeatable the chip placement needs to be. In order to maximize the number of channels measured, there can be up to 0.5 mm of displacement in the x- and y-directions, seen in Figure 6-4. To keep the inlets aligned with the testing machine's dye outlets, there can be up to 4° of rotation in either direction.

[23] EdmundOptics.com Stock #66-387: 30 mm, Center drive, solid top, 1/2" travel, English micrometer

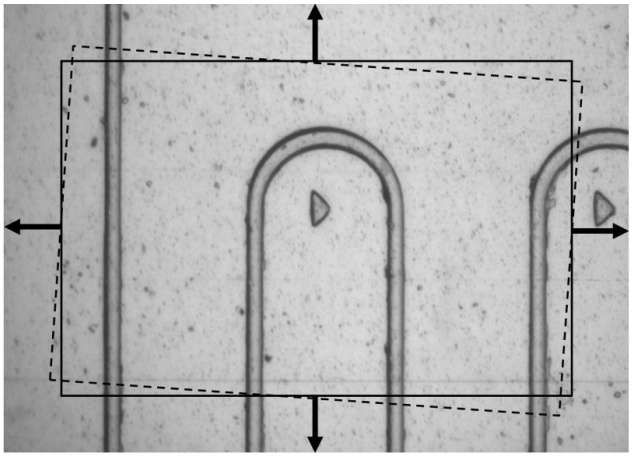

Figure 6-4: A sample image of the inspected channels. The measurement region is shown in the box, and the acceptable displacement and rotation are shown by the arrows and dashed box.

The robot arm has 25 μm repeatability in the horizontal plane [32]. The robot's repeatability can be reduced to 11.3 μm in the horizontal plane if the 3-pin alignment technique described in Section 3.1.3 is used [33]. Since the vacuum pressure of the robot is only 0.8 bar (80 kPa) in absolute pressure, and because the bottom surface of the end effectors are low friction, the chips are able to slide horizontally while still maintaining contact with the end effector heads. This allows the robot to overshoot during placement to ensure that the chip makes contact with each pin without damaging the machine. The 3 pins can also be placed such that they are located on the outer wings of the chip, as shown in Figure 6-5, and away from the embossing area, which is more likely to have bulk material deformation.

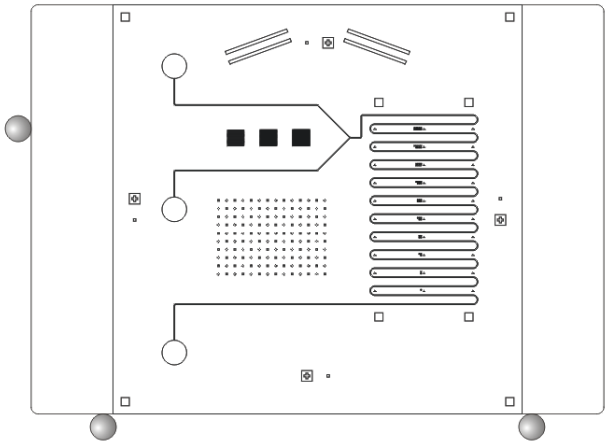

Figure 6-5: The locations of the 3 alignment pins along an embossed chip.

To prevent the chip from sliding out of alignment during the clamping process, a compact pancake air cylinder with a short (0.125 in.) stroke length was selected, which provides plenty of clearance for the robot to place the chips[24]. The air cylinder provides approximately 150 N of force when operated at 35 psi (241 kPa). The two fluid outlets of the testing machine have a total area of 16 mm^2. The maximum flow pressure for the current set-up is 30 psi (207 kPa). This corresponds to only 3.3 N of force caused by the flow. The rest of the clamping force is used to compress the o-rings for a tighter seal.

Since the optics are not mounted on motorized stages and do not have the ability to autofocus, it is very important that the channels are always at the same distance from lenses to stay in focus. Unfortunately, cast and extruded PMMA—from which the blanks were originally created—can have material thicknesses that vary by up to ±20%. This thickness difference of the chips alone is enough to cause the channels to appear out of focus. To solve this problem, the chips are placed on a stage that is attached to the air cylinder. When activated, the cylinder moves the stage upward to clamp the chip against a fixed hard stop as seen in Figure 6-6. Although the new blanks have a much higher thickness tolerance, this set-up allows the inspection microscopes to stay in focus from chip to chip regardless of changes in material thickness.

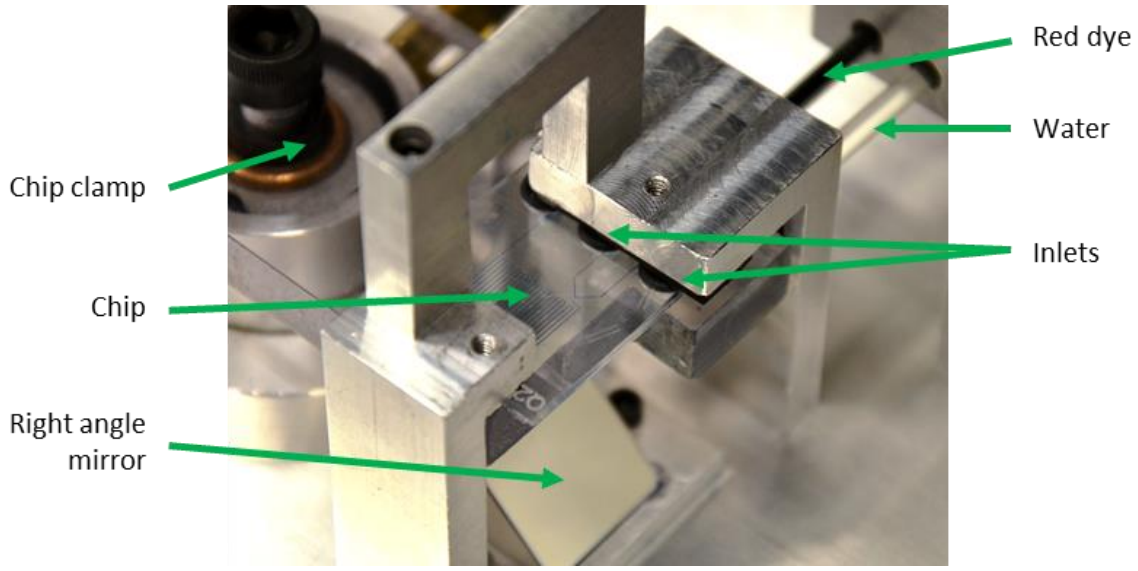

Figure 6-6: A chip that has been clamped in the functional testing machine.

[24] McMaster.com Part #6212K53: Super-flat pancake aluminum air cylinder, 1-1/8" bore, 1/8" stroke

6.2.3 Fluid Flow

Previous work on the microfactory project used a constant flow-driven functional test to measure the performance of the hot embossed serpentine micromixer channels [36]. However, high fluid capacitance in the tubing and pressure gauges made it difficult to test, since the fluid would spend a long time compressing any air trapped in the system before it got a chance to flow through the channels. To eliminate this problem, a constant pressure-driven functional test was used instead for this project.

Initially, blue and yellow food coloring were used as the two liquids, which would mix into green as shown in Figure 6-7. When the mixing images were analyzed, however, it was difficult to determine the extent of mixing using either RGB or grayscale intensities. The yellow dye was then replaced with water, seen in Figure 6-8, and grayscale intensity was used to determine mixing. This worked fairly well, but it was found that red food coloring shows up with higher contrast using the current lighting than blue food coloring, which helps with identifying a mixing location. The color CMOS microscope cameras were also replaced with monochrome CMOS microscope cameras, seen in Figure 6-9, because the RGB capability was not necessary anymore, and the monochrome cameras have higher effective resolutions.

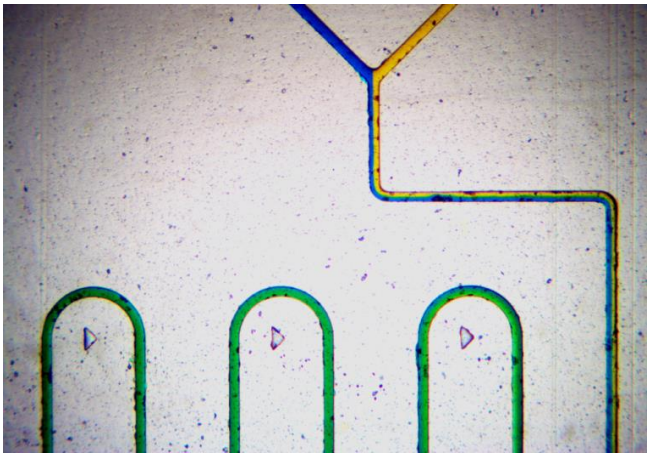

Figure 6-7: Blue and yellow dye mixing in a chip to form green.

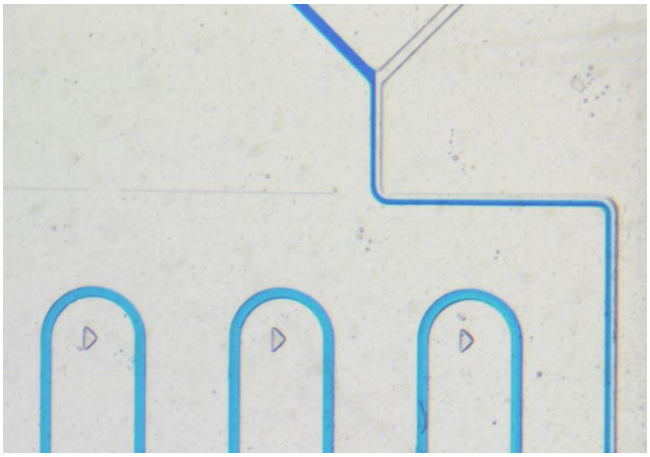

Figure 6-8: Blue dye and plain water help identify the mixing location.

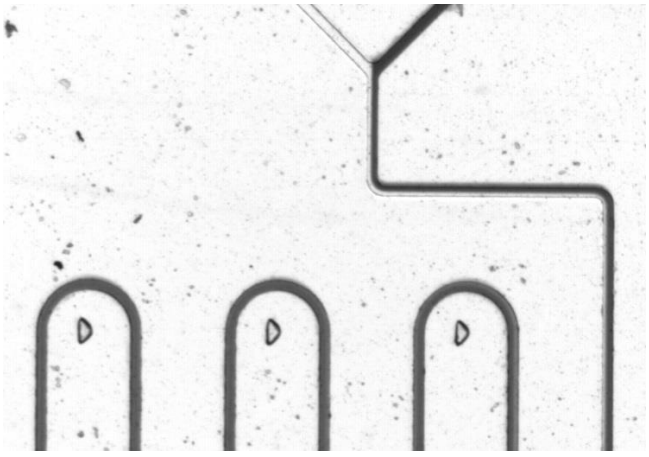

Figure 6-9: Red dye appears darker and improves the contrast for identifying mixing. A monochrome camera is used for its improved resolution.

Push-to-connect fittings were used to connect the outlets on the stage to 0.125 in. Tygon tubing, which connected to a dye reservoir. The reservoir needed to be easily refilled without introducing air bubbles into the tubing lines. The initial reservoir was made out of 1 in. polycarbonate that had been drilled through and tapped with NPT threads. Push-to-connect adapters could then be screwed into the top and bottom to connect to the 0.125" tubing. The top tubes could then be disconnected and a syringe could be inserted to refill the reservoirs. As long as the fluid level doesn't drop below the reservoir, then air could be kept out of the tubing. Unfortunately, the internal stresses from tapping the polycarbonate led to microfractures, and the dye leached into the surrounding plastic through the cracks over time. A new reservoir was designed to avoid tapping the plastic. Instead, two aluminum plates were drilled and tapped with the NPT threads. They were attached to the top and bottom of the reservoir using rubber gaskets and bolts.

Occasionally, air bubbles were accidentally introduced to the air lines. Sometimes the machine was sitting idle for too long and the dye evaporated from the outlets. Other times there was an incident that led to a large quantity of dye leaking. To reset the fluid lines efficiently, dye was added to the top of the reservoir until they were full. The flow pressure was then reduced to its minimum (0.1-0.2 psi), a sponge or towels were placed securely over the outlets, and the flow clamp was briefly opened until the air had been purged from the system. Bubbles also appeared when fluid was initially flowed through the chips. It helped to increase the pressure from 10 psi to 20 psi for at least 10 seconds to expel any bubbles that might have gotten trapped in the inlet channels.

Originally, the testing machine was built to include a drain hole that would connect to the outlet of the chips and catch the excess liquid. However, the flow rates are extremely low (approximately 3.3 μL/min at 10 psi) and there was not enough fluid after 30 seconds to exit the outlet port on the chip (approximately 4.7 μL).

6.3 Completed Hardware Design

The complete hardware with labeled key components is shown in Figure 6-10 and Figure 6-11.

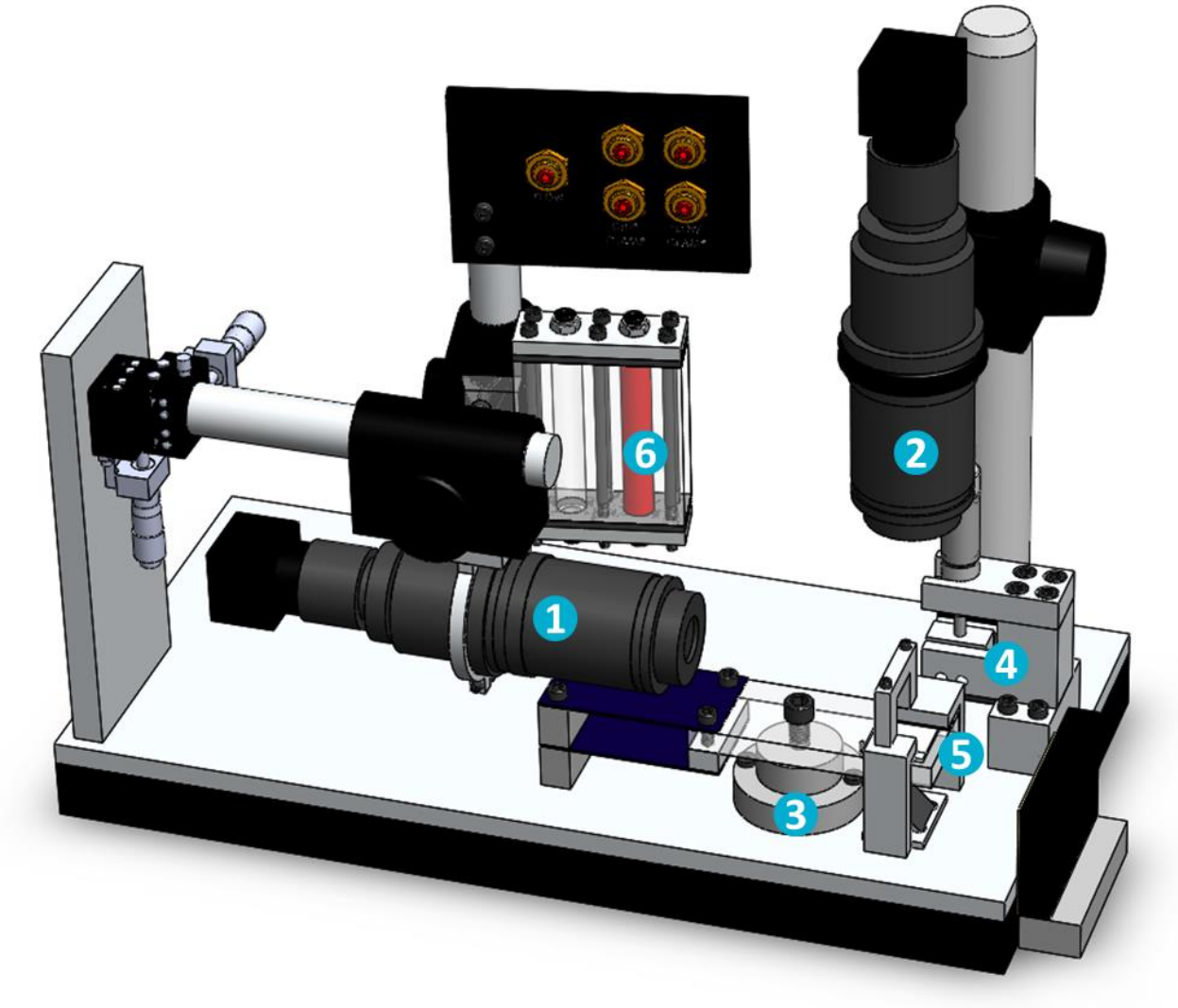

Figure 6-10: A solid model of the functional testing machine for clarity (tubing not shown). (1) Higher magnification optics with USB microscope camera for channel width measurement, (2) lower magnification optics with USB microscope camera for mixing location measurement, (3) air cylinder for chip clamp, (4) air cylinder for flow clamp, (5) dye outlets, (6) and dye reservoir.

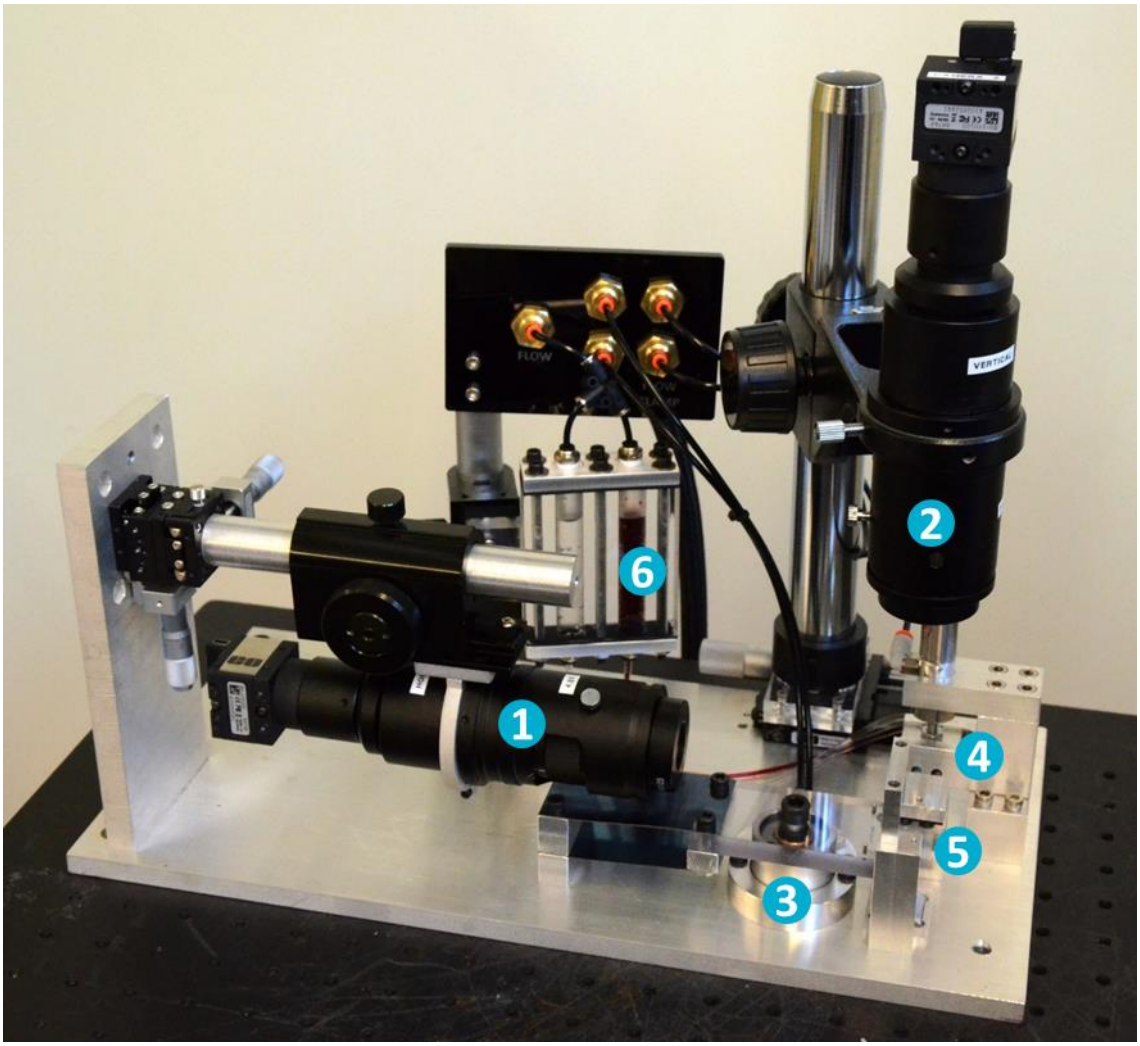

Figure 6-11: The final functional testing machine. (1) Higher magnification optics with USB microscope camera for channel width measurement, (2) lower magnification optics with USB microscope camera for mixing location measurement, (3) air cylinder for chip clamp, (4) air cylinder for flow clamp, (5) dye outlets, (6) and dye reservoir.

The horizontal optics with a 10.5 MP USB microscope camera mounted on the end is attached to a linear guide using custom adapters to allow the focus to be adjusted. The whole assembly is cantilevered off of a precision x-y stage to accommodate changes in position. A second set of optics with another 10.5 MP USB microscope camera is mounted vertically on another x-y stage. These microscopes have adjustable magnifications in case future changes need to be made.

A compact pancake double-acting air cylinder with a short 0.125” stroke length is mounted to the base. It is connected to the stage with two parallel spring steel flexures that keep the stage level and prevent unwanted bending when the clamp is turned on. The stage has 3 pins for

alignment and o-rings over the dye outlets to create a better seal. When a chip is in place, it can clamp upwards against two fixed hard stops that keep the chip features at a fixed focal length. A small bridge connects the hard stops and holds a 5 mm mirror suspended over half of the chip for the horizontal camera. Push-to-connect fittings connect the dye outlets to the dye reservoirs via flexible tubing. The dye reservoirs can be refilled by disconnecting the tubing from the top. Another double-acting air cylinder is used as a pinch valve to stop the flow of dye. This minimizes the length of tubing between the outlets and the pinch point. All of the tubing is connected to an adapter panel so that all of the air connections are organized in one location. The entire machine rests on a 1 in. thick piece of closed-cell foam to help dampen vibrations from the rest of the system during operation.

6.4 Control and Image Processing

Once the testing machine had been designed, built, and assembled, a method of controlling the inspection and analyzing the images to automate the process was needed. All of the valves and regulators that were used in the initial prototyping of the machine were manually controlled and needed to be switched over to automated valves. A 5-port, 2-position double solenoid was used on the double-acting chip clamp because it was better if the clamp remains in its last position if the power accidentally turns off[25].

The flow of the dye was originally controlled using another solenoid valve. However, when the flow was turned off, there was enough residual pressure in the rubber tubing (due to the compliance in the tubing) that dye would get pushed to the outlet when the chip was unclamped and pressure was returned to atmospheric. To minimize this problem, a custom pinch valve was placed as close as possible to the outlets to shorten the tubing length. This valve used a double-acting air cylinder with a 0.5 in. stroke length to pinch the 2 lines of tubing[26]. This clamp needs to close immediately if the power is accidentally cut for any reason. Therefore, a 5-port, 2-position single solenoid was used to control it[27].

Since the pressure needs to be modified within the testing cycle (to help expel any remaining air bubbles), the manual pressure regulator was replaced with an open-loop 550X electronic

[25] Automationdirect.com Part #AVS-05221-120A: Nitra double solenoid valve, 120VAC, 5-port, 2-position
[26] Bimba.com Part #020.5-DPK: double-acting air cylinder, pivot mount, 9/16” bore, 0.5” stroke
[27] Automationdirect.com Part #AVS-05211-120A: Nitra single solenoid valve, 120VAC, 5-port, 2-position

pressure transducer[28]. The calibration curve for the transducer is shown in Figure 6-12. The curve is very linear in the middle range, but starts to drop off at low pressures, so it never quite reaches 0 psi. A ProSense pressure transmitter was also added to monitor the flow pressure.

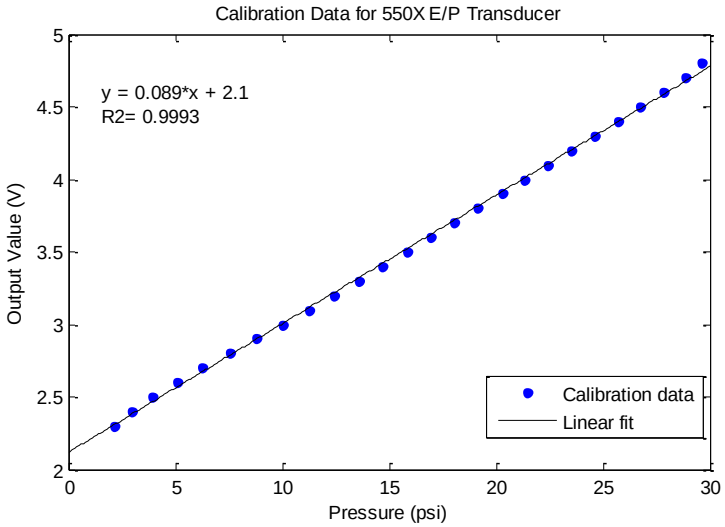

Figure 6-12: The calibration curve for the 550X electronic pressure transducer.

Since the hot embossing machine and the robot both use LabVIEW to operate, it made sense to use it to control the functional testing machine as well. This would greatly simplify software communication between the different machines. To communicate between the functional testing machine and LabVIEW, a low-cost data acquisition device from National Instruments (NI USB-6008) is used. The functional testing machine's LabVIEW code was modeled off of the code used to operate the hot embossing machine. It waits until it receives a "start" signal from the robot and then proceeds to clamp the chip, run the channel width inspection, open the flow valve, run the mixing location inspection, turn off the flow valve, unclamp the chip, and finally send a done signal to the robot.

Vision Builder, another National Instruments program that is designed specifically for part inspection, is used to perform the image processing and it can be compiled into LabVIEW code. For the channel width inspection, it first acquires and logs an image from the USB microscope camera and checks to see if there is a chip present by comparing the standard deviation and minimum intensity of a region of interest with certain thresholds. If either fails, it flags the chip as not present and the inspection ends, which triggers a network-published shared variable to end

[28] ControlAir.com Type 550X: Electronic pressure transducer, 0-5 VDC input

the functional testing machine's LabVIEW code. Otherwise, it searches for the template pattern in Figure 6-13 to locate the channels. If it can't find the pattern, it fails the inspection and flags the chip as not orientated, again triggering the end of the test. For a present and oriented chip, it scans the regions where it expects to find the channels relative to the pattern and uses an edge detection feature to measure the outer channel width at several locations along the channel. It averages the widths for each of the four channels and then averages all the widths for a final average. It records this data as well as an image such as Figure 6-13.

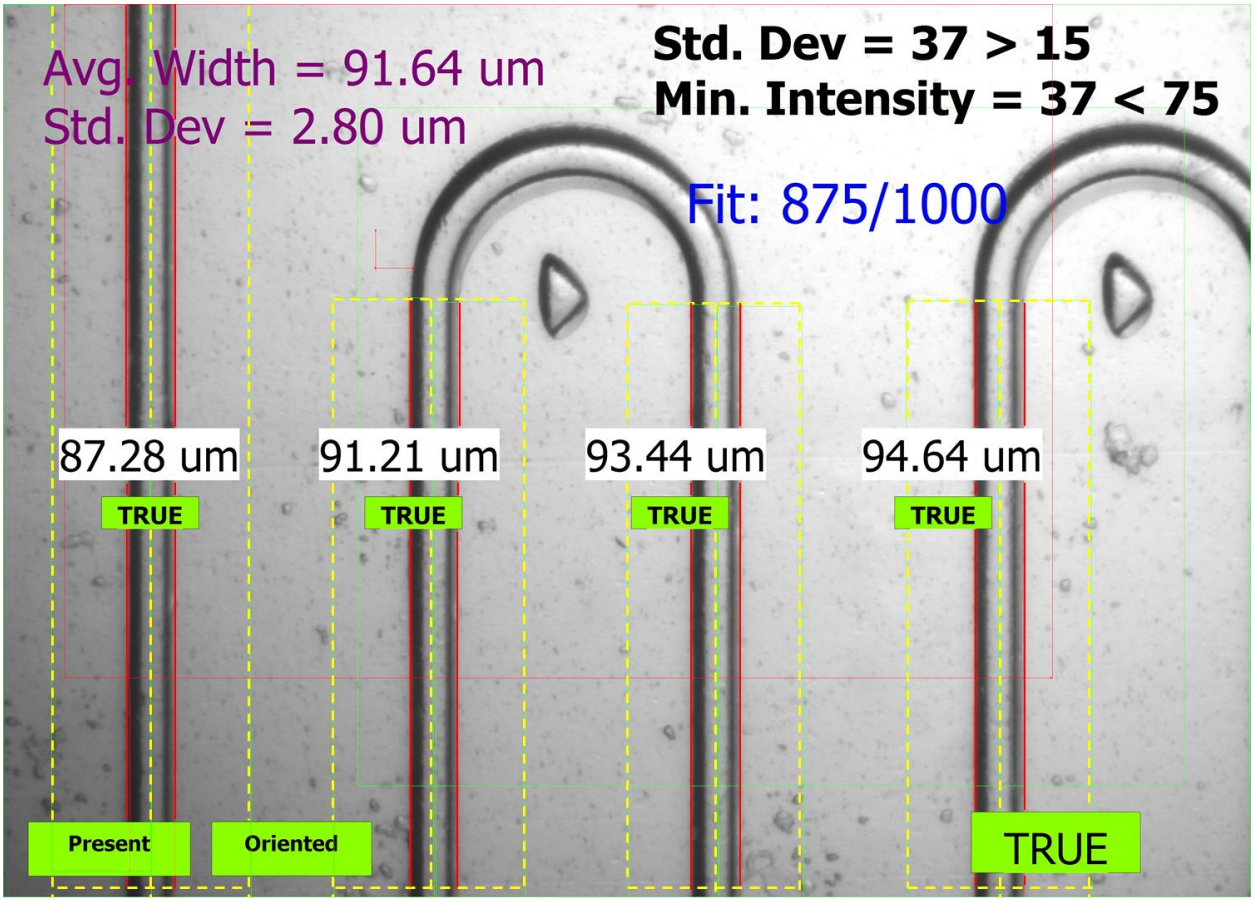

Figure 6-13: Sample recorded channel width image with measurement data overlay. Middle: The average width for each channel and the status of that measurement. Two lines (in red) were fit for each channel—one from each dotted yellow box. The average distance between these fitted lines were then calculated for the average width of that channel. Left: The final average of all 4 channel width measurements and their standard deviation. Top Right: The requirements for passing the test for chip presence and the fit quality of the pattern matching. Bottom Left: The status of the tests for chip presence and chip orientation. Bottom Right: The final status of the inspection.

For the mixing location inspection, Vision Builder is again set-up to acquire and log the image from the USB camera. It compares the image to another template pattern and tries to

locate the channels. If it fails to find a match, the inspection fails and the test ends. Otherwise, it begins to scan a series of 50 regions of interest along the first six channels that are 47.1 μm by 72.8 μm. It calculates the standard deviation of the pixels in each region and records them. Ideally, the inspection would also calculate the mixing location at this time. However, challenges with getting consistent lighting conditions have made this difficult to implement. Once it is finished, the inspection ends and an image such as Figure 6-14 is recorded along with the standard deviation data. The flow stops, the chip is unclamped, and the functional test is complete.

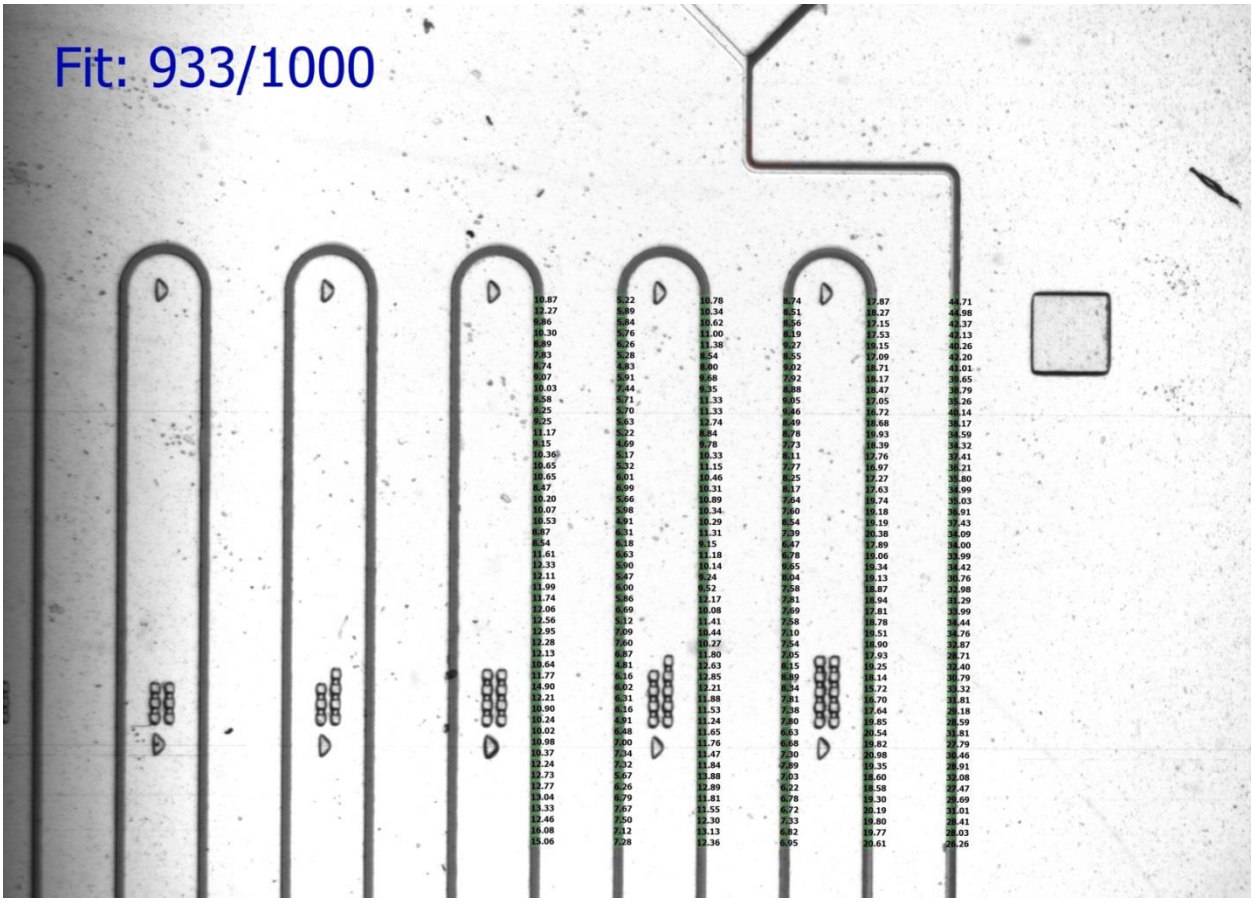

Figure 6-14: Sample recorded mixing location image with measurement data overlay. The fit quality of the pattern matching is shown in the top left. The standard deviations of intensity measurements are shown over each region of interest on the channels.

Close-up images of the mixing channels can be seen in Figure 6-15. Before mixing, the standard deviations of the pixel intensities in the channels are very high. After mixing, the

standard deviations reach a minimum. They never quite reach 0 due to natural variation in the camera sensor.

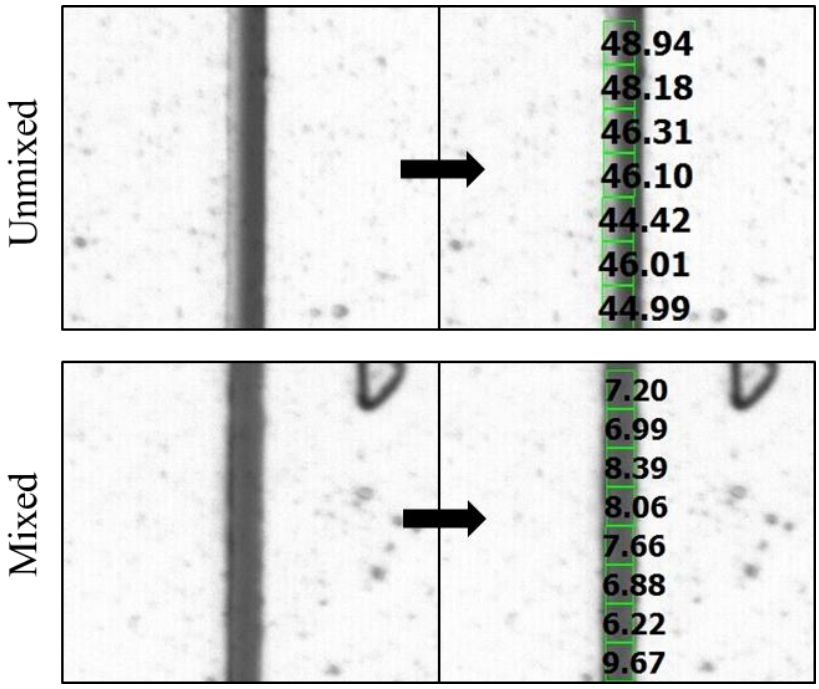

Figure 6-15: Close-up images of sample channels before and after measurement. The unmixed channel has a much higher standard deviation of pixel intensities than the mixed channel.

If the chips are aligned properly, then four images are logged per chip plus some additional data. At about 6.5 MB per image and up to a hundred chips in a run, the amount of storage required can add up quickly. The pre-measurement images are useful in case one of the codes needs to be modified and rerun on an old set of images, and the post-measurement images are useful to be able to understand a particular result. The master computer currently has 1 TB of hard drive space, so for now, it is not a problem to store all of the data.

6.5 Final Inspection Process

The inspection process requires the following steps:

1. The robot places an embossed and taped chip onto o-ring outlets that are connected to dye reservoirs in the functional testing machine.

2. The robot positions the chip by pushing it against 3 alignment pins. The pins contact the wings of the chip outside the embossed region where there is minimal bulk deformation from embossing.

3. The robot releases the chip, moves out of the testing machine, and triggers the inspection to begin.

4. The chip clamp moves upward to secure the chip against a fixed hard stop, which keeps the channels at a fixed focal distance despite variations in chip thickness.

5. A higher magnification image of the channels near the chip's outlet is recorded, and the image is compared to a template pattern. If there is no chip present or if the chip is not properly aligned, the inspection ends, and a signal is sent to the robot to remove the current chip and replace it with the next one.

6. If the chip is properly aligned, the inspection continues. The channel outer widths are measured, averaged, and recorded.

7. Dye and water are run through the channels at 20 psi for 15 seconds to purge any initial air bubbles. The flows are then reduced to 10 psi for 10 seconds.

8. A lower magnification image of the channels near the chip's inlets is recorded, and the image is compared to another template pattern to locate the channels.

9. If no flow is detected (due to poorly formed inlets, misaligned holes, etc.), the inspection fails and a signal is sent to the robot to remove the current chip and replace it with the next one.

10. If a pattern match is found, then a series of 50 regions of interest (47.1 μm by 72.8 μm) are scanned along each channel. The standard deviation of the pixel intensities within each region of interest is measured and recorded.

11. The flow is stopped and the chip is unclamped. A signal is sent to the robot to indicate the test has finished.

12. The robot removes the chip by pulling it out 4 mm with the hook on its end effector to break the surface tension on the inlets before turning the vacuum pressure on to pick up the chip. It drops it off in a container of tested chips.

The design requirements detailed in Section 6.1 have been met. Two sets of cameras and optics were used to achieve both a high resolution image and a large field of view image. The first image has a resolution of 1.6 pixels per μm over a region of 2.4 mm by 1.7 mm. The second image has a resolution of 0.5 pixels per μm over a region of 8.2 mm by 5.9 mm, which includes both the inlets and the first 12 channels. A 3-pin alignment system that has been shown to have 11.3 μm of repeatability (as detailed in Section 3.1.3) was used. Two reservoirs are filled with plain water and red dye. They are connected to the inlets of the embossed devices to flow fluid through the mixing channels. An inspection program was written to analyze the test images and identify two measures of quality—the outer channel width of the embossed chips and the mixing location. The entire test is fully automated and has been integrated with the rest of the system. It takes 85 seconds to run.

CHAPTER 7 RESULTS AND DISCUSSION

The taping machine and the functional testing machine were integrated with the current hot embossing machine and the robotic arm to complete the microfactory. The system is now fully running and can autonomously produce completed microfluidic devices. The final system can be seen in Figure 7-1.

Figure 7-1: The complete microfactory system with labeled stations. (1) Spring-loaded dispenser with blank chips. (2) Hot embossing machine. (3) Taping machine. (4) Cutting station. (5) Functional testing machine. (6) Tray for collecting tested chips.

When the machines were first integrated, several unanticipated problems were identified that had not been present with the machines running separately. For example, all of the machines communicated with the main desktop computer via one or more USB cables. A USB hub was used originally until it was discovered that the devices connected to the hub were disconnecting frequently and randomly. Extra webcams had been used to monitor the different stations, but these were removed to allow the critical components to plug directly into the computer. Several of the robot's paths had to be optimized to prevent it from accidentally running into any of the other machines, especially if it had been shut down in the middle of a previous cycle. The functional test was found to be sensitive to vibrations. To minimize this, the entire machine was placed on a 1 in. thick piece of foam to help absorb the vibrations caused by the rest of the system. It was also discovered that if the robot picks up a chip from the hot embosser immediately after a cycle has finished (and the chip is still warm), then the chip tends to adhere to the end effector slightly. This is just enough that it will not release when the vacuum is turned off. To solve this problem without adding extra time for the chip to cool, two tabs were placed above the belt on the sides of the taping machine to act as demolding tabs similar to those on the hot embosser.

Once the system was functioning, tests could be run to characterize the machines. The tests were generally 20 to 50 cycles long, depending on what was being measured and if there were any major machine failures during the run. The first 5 buffered chips out of the taping machine were generally logged separately each day since they had been embossed on a previous day. Similarly, the last 5 embossed chips of a run could not be tested, since they were needed to fill the taping machine buffer.

7.1 Machine Performance

7.1.1 Taping Machine

The taping machine takes approximately 15 seconds to tape and cut a chip. It spends 5 seconds running the chips under the tape rollers, 5 seconds waiting, and 5 seconds to cut the chips. It is currently the fastest machine in the system, and it is highly unlikely that it will ever become the bottleneck for the current system.

The taping machine currently has a success rate of about 93%. However, most of its failure modes require halting production to repair. Because of its chip-aligning belt guides, the machine

can handle a large amount of variation in chip placement by the robot. As long as the chips are placed in front of the next belt spacer, the plastic guides will push the chips into alignment. Occasionally, the chips get pushed up over their designated spacer, leading to one of the machine's failure modes. If the chips are not spaced correctly when they reach the cutting block, the alignment fork that positions the chips for cutting will jam against the displaced chips and will be unable to finish its cut. This leads to a failure mode that the machine cannot recover from and intervention is needed. This type of failure occurs for ~4% of the chips. The other common taping failure is the tape between chips occasionally sticking to the belt spacers. Most of the time, the tape comes unstuck, but for ~2% of the cycles, the tape will get pulled underneath belt instead of continuing to the cutting block. This type of failure can sometimes be resolved fairly quickly if the error is caught and the machine is stopped before the cutting cycle triggers. Other times, it requires removing the previous 3 chips by hand.

7.1.2 Functional Testing Machine

The functional testing machine takes approximately 72 seconds to run. It waits 5 seconds after clamping the chip, spends 11 seconds capturing and processing the first image, 25 seconds to flow the dye, 21 seconds to capture and process the second image, and then spends 10 seconds to unclamp and reset. This is currently much faster than the current hot embossing machine's cycle time (110 seconds). However, if a shorter testing cycle is desired, it is possible to reduce the cycle time to less than 60 seconds by simply removing some of the overly-conservative wait times. If an even shorter cycle time is desired, it is possible to optimize the image inspections to run even faster. Alternatively, the images can be taken first and then processed by the computer while the chip is unclamped and removed by the robot.

The functional testing machine has a success rate of about 89%. Fortunately, most of the failure modes do not require production to stop. Unlike the taping machine, the functional testing machine requires a fair amount of precision when loading chips to be inspected. If the chips are misaligned by 0.5 mm, the machine will be unable to detect and measure the channels. More importantly, it is possible that the inlets on the chip might not be aligned with the outlets of the machine, which could lead to no flow (in the best case) or severe leaks that drain the dye reservoirs (in the worst case). The machine's 3-pin alignment system typically prevents any problems with positioning. However, occasionally a chip will not contact all 3 pins correctly.

Sometimes there is a small tab of tape sticking out over the edge of the chip after it has been cut that interferes with the alignment. This will lead to a failed inspection of the chip, and no data will be collected. Fortunately, this does not cause any problems with the rest of the system and the robot can remove the chip as usual. The other common failure mode is when the machine does not properly identify chip features during its inspection. This can lead to over- or underestimating the channel dimensions or not measuring them at all. This is usually caused by the inspection's sensitivity to the lighting conditions. Again, the chip can be cleared by the robot as usual after this happens and does not require any additional intervention. On very rare occasions (< 1%), the robot has trouble removing a chip from the functional testing machine and then will try to place a second chip on top of the first. This results in a jam that needs to be removed manually.

The outer width measurements taken during the first inspection have proved to be very useful in predicting channel geometry. They might not be able to provide detailed information about the embossed features, but they can still detect small changes in forming quality. Figure 7-2 and Figure 7-3 show data from a sample well-formed chip and a sample under-formed chip that were taken on the Zygo. The measurements from the functional testing machine are added for comparison.

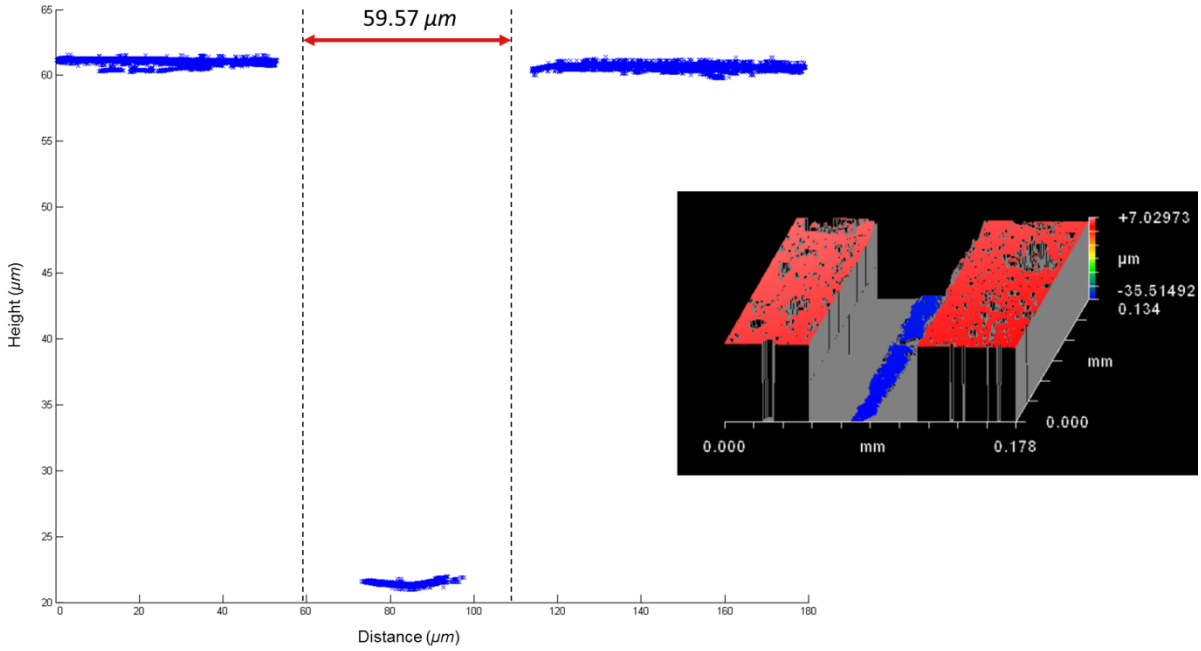

Figure 7-2: Channel geometry data for a well-formed chip taken on the Zygo. The functional testing machine's width measurement is labeled on the 2D graph for comparison.

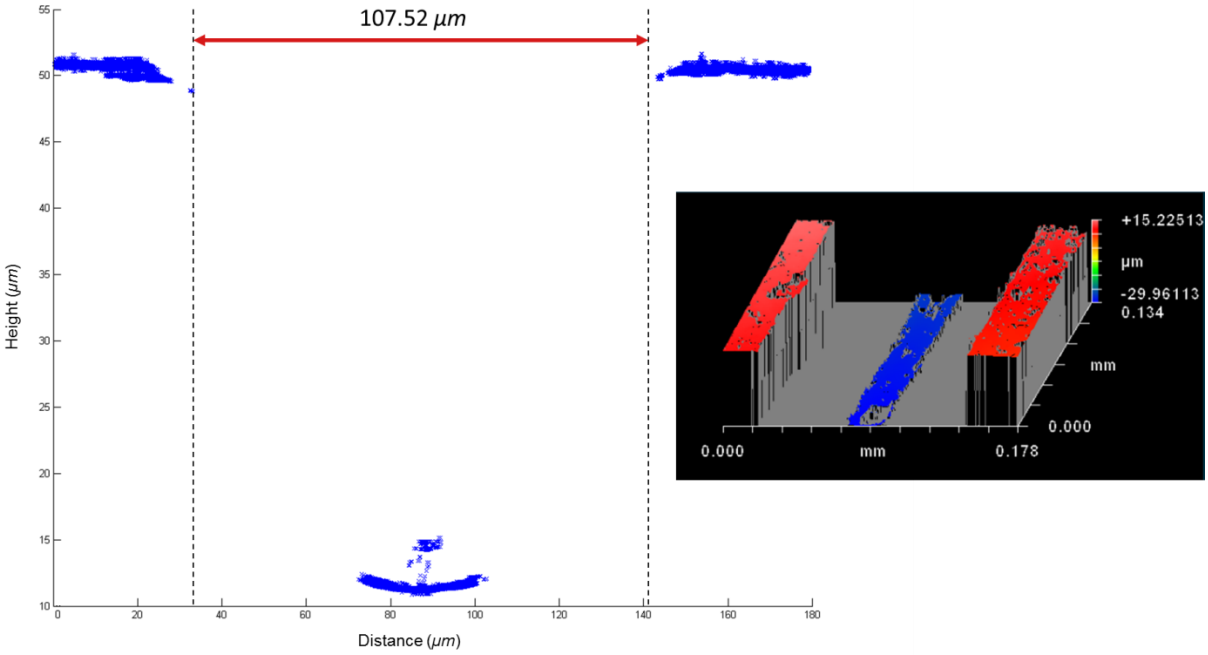

Figure 7-3: Channel geometry data for an under-formed chip taken on the Zygo. The functional testing machine's width measurement is labeled on the 2D graph for comparison.

The mixing length measurements, on the other hand, have been much more difficult to acquire. Any gradients in the lighting on the image (top to bottom or side to side) will alter the amount of contrast in the channels. This changes the standard deviations of the pixels measured, so the measurement is extremely sensitive to lighting. Originally, a battery-operated LED light covered with a diffuser was being used to illuminate the chips. However, over the course of a run, the battery would slowly drain and the images could be seen to get darker and darker. This was remedied by using a new plug-in light source[29]. Unfortunately, the new light source has a warmer color, which washes out the red dye, making it even more difficult to identify mixing. To improve the contrast, a green lighting gel was used over the light. This still needs to be tested more thoroughly, though. Additionally, having the bulk of the lighting shining from the side—despite the right angle mirror to redirect the light to below the chip—adds some glare along one side of each channel, which can also change the measurement. Because of this, it would be more effective to cut a hole in the machine's base below the chip area and place the light underneath it.

[29] EdmundOptics.com Stock #54-228: Fiber optic backlight, 1.86" x 1.63"

Now that the machine is sitting on a 1 in. thick piece of foam, there is space below the base to fit a light.

The USB microscope cameras have been successful in communicating with LabVIEW and in capturing images. However, the camera parameters can be difficult to change. They need to be altered in the camera files themselves rather than in the LabVIEW program. Since the two cameras have the same light source, yet one of them is at a lower magnification (causing it to receive more light), the mixing location image can often appear too washed out or overexposed. This can be improved by adjusting the camera parameters. Alternatively, a neutral density filter can be added to the optics, which might be an easier solution.

Because of these difficulties, it has been challenging to automate the mixing location inspection. Most of the collected data focused on the outer width measurement. The "average outer channel width" presented in the following sections refers to an average of the four channel widths in the frame of the first image. These channels are measured by fitting lines to the outermost edges and measuring the distance between them. A sample image and the measurements can be seen in Figure 6-13.

7.1.3 Microfactory

The microfactory has a total cycle time of 170 seconds when it reaches steady state. The additional time is from loading/unloading the chips as well as the robot's travel time. The system currently has a success rate (embossed, taped, and tested chips) of about 85%. For some of the runs, this number is higher since some manual intervention occurred to keep the system running. A run chart of 41 chips was performed to check if the process was random and to measure the variation in the system. The chips were formed using the same temperature, pressure, and hold times. They were then taped and tested. The resulting width measurements can be seen in Figure 7-4. It appears to have an increasing trend, so the process is not quite stationary yet. An x-bar chart of the data with sample size of n=3 is shown in Figure 7-5 and an s-bar chart of n=3 is shown in Figure 7-6. It appears that in addition to the increasing mean, the variance is also slightly increasing throughout the duration of the test.

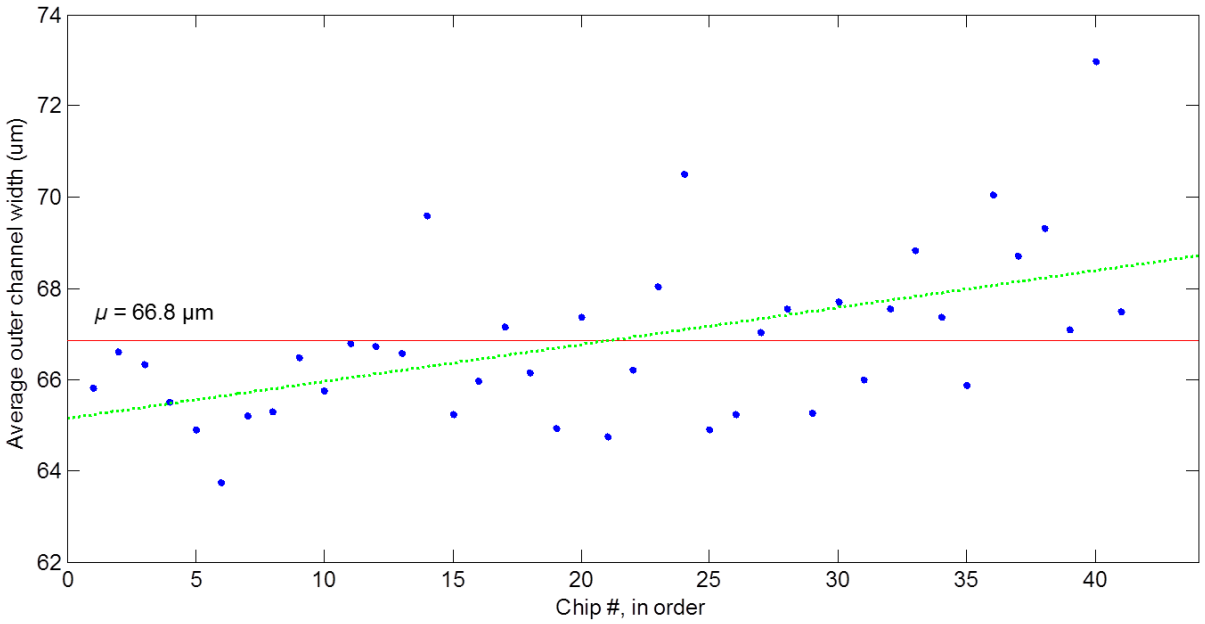

Figure 7-4: A run chart of the entire system using data from the functional testing machine. The hot embossing machine's parameters were held constant at 1000N forming force and 115°C forming temperature. There is a slight upward trend of approximately 3.5 μm in the data (shown by the linear fit in green), which means that the process is not quite stationary yet.

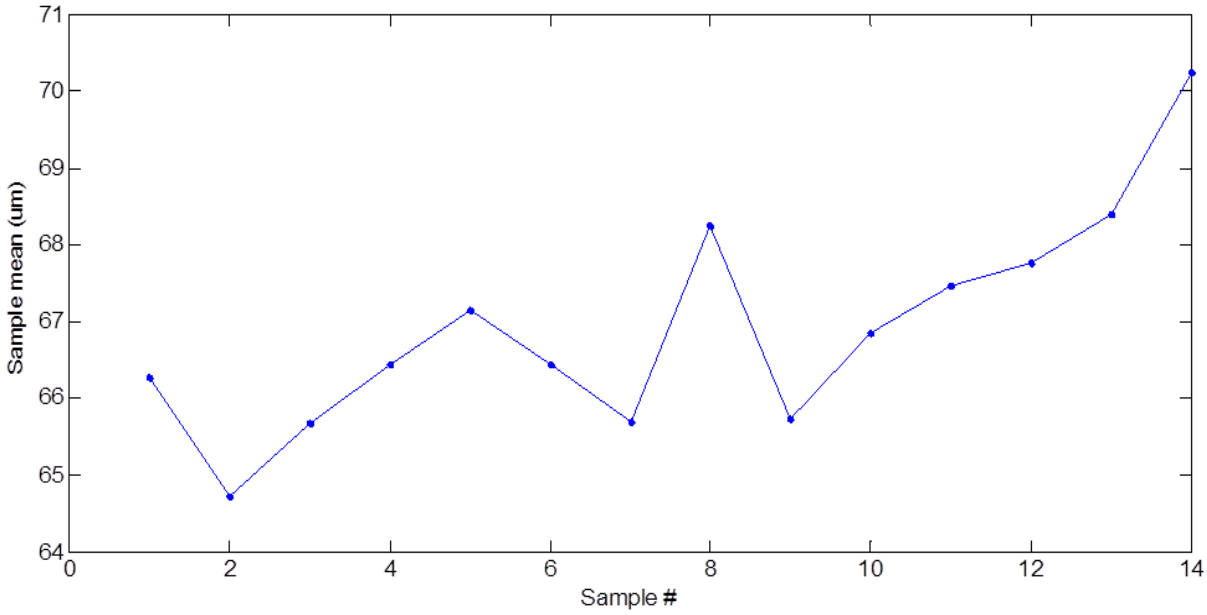

Figure 7-5: An x-bar chart of the data in Figure 7-4 for sample size of n=3. There is still a slight upward trend in the sample means.

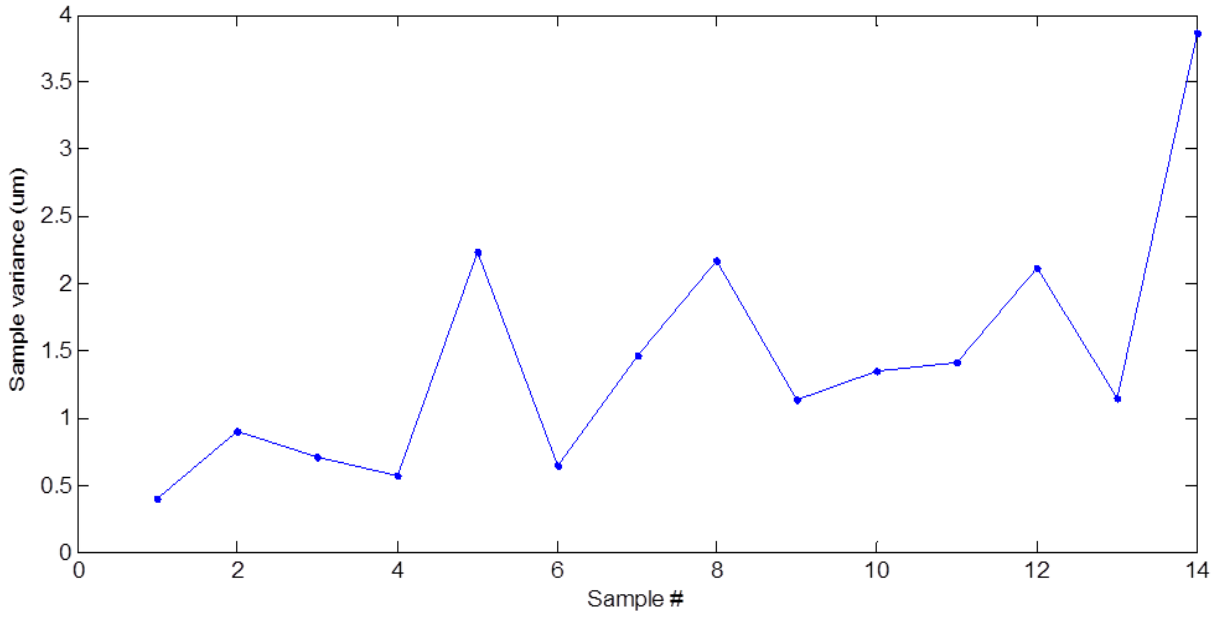

Figure 7-6: An s-bar chart of the data in Figure 7-4 for sample size of n=3. There is also a slight upward trend in the sample variances.

7.2 Sources of Variation

Given, the variability in the run chart, the measurement systems were analyzed to determine the sources of variation. First, one chip was taped and placed in the functional testing machine by the robot. When the measurement was complete, the chip was returned to the end of the taping machine. This would then characterize the variation in the functional testing machine as well as the effects of slight alignment variations from the robot. The fluid could not be run during this test because the width measurement can no longer be taken when the channels have been filled with fluid. Because the test was quick to run, it was repeated 50 times. The results can be seen in Figure 7-7 and Figure 7-8. The functional testing machine was shown to have a sub-micron standard deviation, and the data appears to be fairly normally distributed. This test was also repeated for the other port on the robot, and no significant difference was detected.

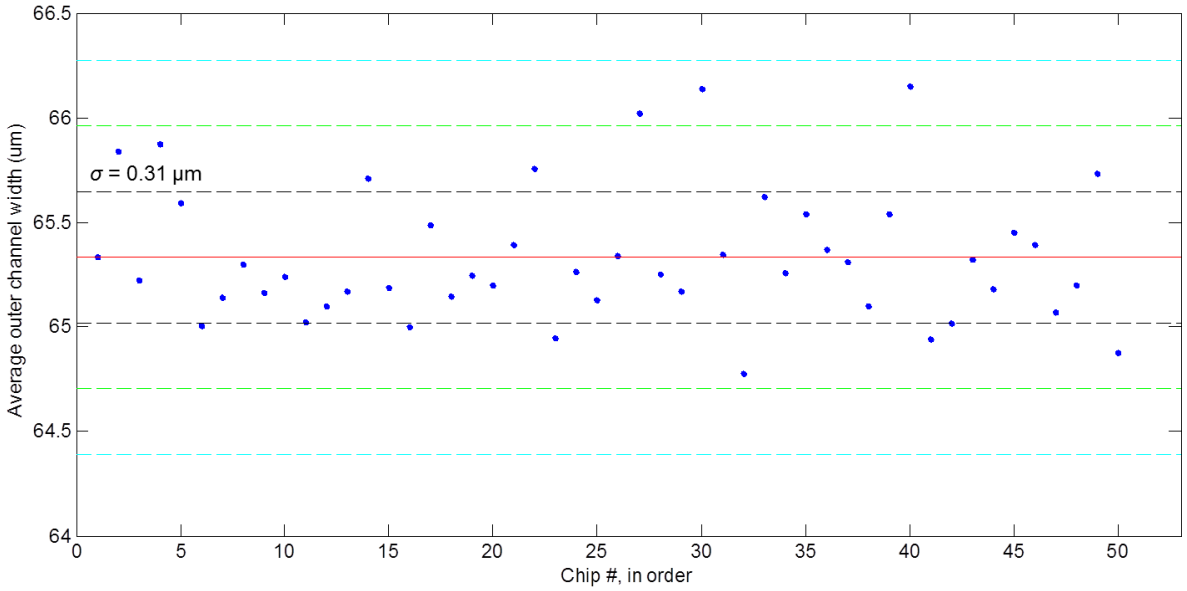

Figure 7-7: A run chart to test the variation in the functional testing machine. The same taped chip was positioned and inspected multiple times. The test is shown to have a standard deviation of 0.31 µm.

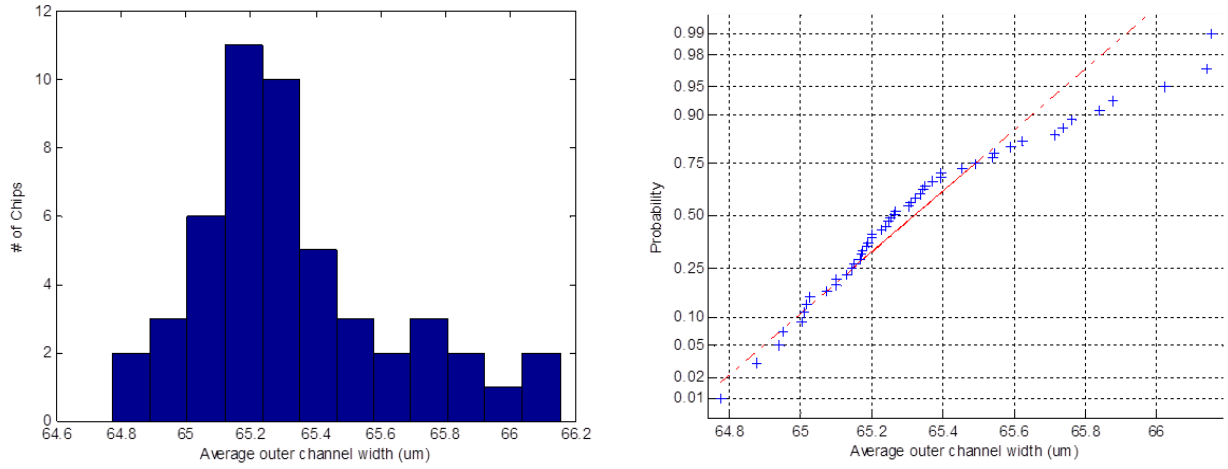

Figure 7-8: A histogram and normal probability plot for the data in Figure 7-7.

Next, the same 6 chips were fed through the taping machine and then tested multiple times to test the variation in the taping machine. Multiple chips were used due to the buffer of 5 chips in the taping machine. Only 10 runs were performed since this experiment required a much longer time to run. The results can be seen in Figure 7-9. The functional testing machine and the taping machine were shown to still have sub-micron standard deviations.

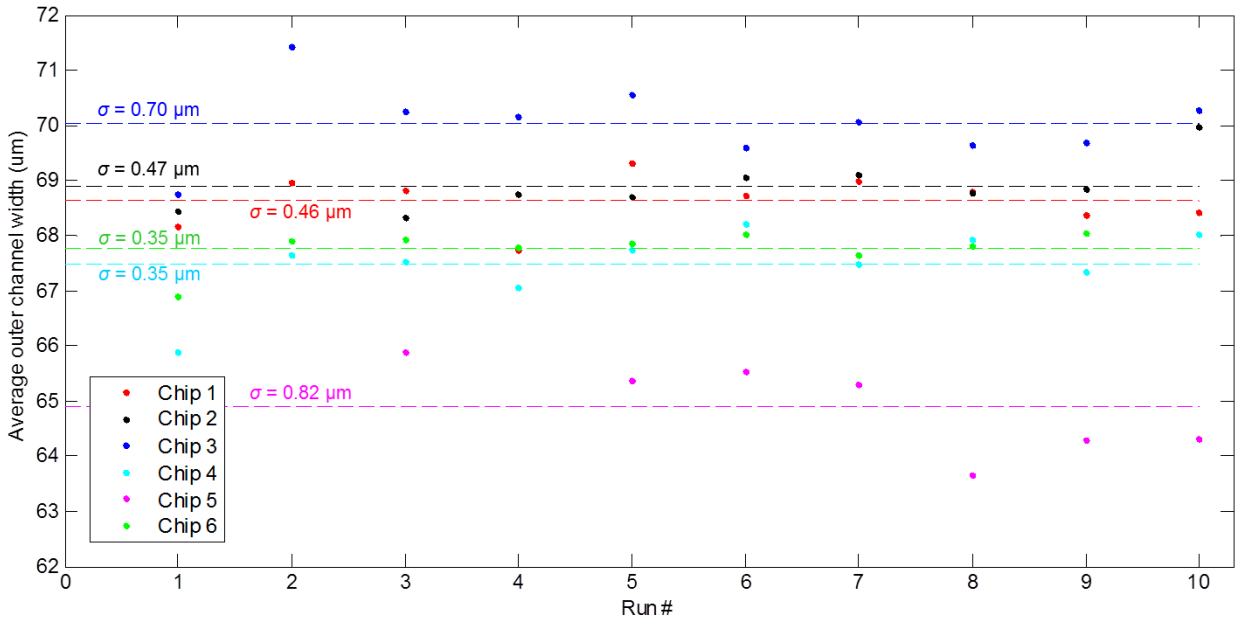

Figure 7-9: Run charts to test the combined variation in the taping and testing machines. The same 6 embossed chips were taped and tested multiple times. The standard deviation ranges from 0.35 µm to 0.82µm.

Table 7-1 summarizes the variation in the two machines. In addition to these, there is additional variation in the hot embossing machine that could be caused by a number of reasons. The temperature profiles of the embossing machine might be slightly different from run to run. The PMMA blanks might have slightly different residual stresses caused by injection molding that cause the material to flow differently. A build-up of dirt and plastic on the tool over time could also cause defects along the channels, which affect the width measurement. After a few hundred runs, or whenever the tool appears to be especially dirty, the tool is removed from the hot embossing machine for cleaning. The tool is soaked in an acetone bath overnight to loosen the PMMA particles that have accumulated along the features of the tool. It is then rinsed with a small amount of soap because thermal grease—used to improve thermal conduction between the heater and the tool—can sometimes contaminate the surface of the tool. Since this is usually not enough to remove plastic particles from the tight corners of the features, additional agitation is required. The features are covered with acetone, and a Dremel rotary tool with a soft nylon brush attachment is used at medium speed to clean the tool. Even after scrubbing and rinsing multiple times, it is difficult to remove all of the particles. Instead, the tool was remounted into the hot embossing machine and an embossing cycle was run. This cycle served as a "cleaning cycle" to

remove the remaining loose particles from the tool. Figure 7-10 shows an image of the tool taken on a scanning electron microscope (SEM) after scrubbing and rinsing the tool but before running a cleaning cycle. It also shows test image of the first embossed chip after cleaning, which picked up most of the loose particles from the tool. The subsequent chips looked much cleaner and did not show signs of additional particles.

	Standard Deviation, σ [μm]
Functional Test	0.31
Functional Test + Taping	0.35 - 0.82

Table 7-1: Standard deviations from measuring variability in the two machines after the embossing step.

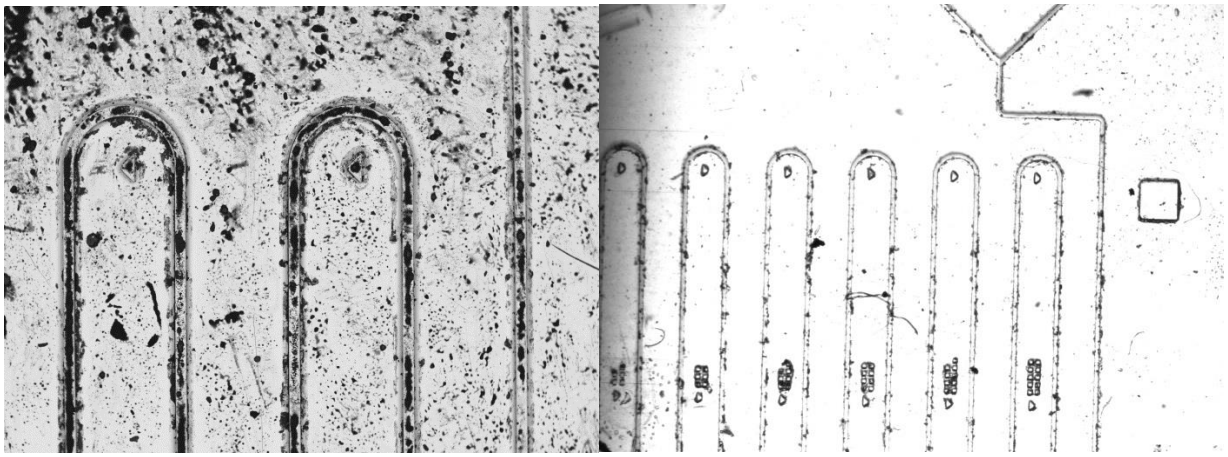

Figure 7-10: Some of the variation could be caused by a build-up of dirt and plastic on the tool. Left: Image of the tool (near the outlets) taken on the SEM at 60x. Right: Image taken on the functional testing machine of the first embossed part after cleaning. The part appears to pick up most of the loose particles on the dirty tool after scrubbing.

7.3 Effects of Temperature on Channel Width

The purpose of the functional testing machine is to be able to detect changes in the embossing quality. These changes could be caused by temperature or force changes, or by changes in the blank material. An experiment was run to test the machine's ability to detect changes in geometry and to see the effect of parameter changes on the final product. The system was set to produce a series of chips with different embossing settings. For this experiment, the force was held constant at 1000 N and the temperature was varied between 110°C, 115°C and 120°C. Figure 7-11 shows the average outer channel width measurements recorded during this test. There is a clear distinction between the measurements for different embossing temperatures. The nominal channel size is 50 µm. Due to shadow effects as well as slight rounding at the edges of even over-formed channels, the outer width measurement tends to saturate around 57 µm. There is a slight difference in width that can be detected between 115°C and 120°C. However, when the temperature is dropped to 110°C, there was a drastic increase in width. This is likely because the temperature is just below the glass transition temperature of this grade of PMMA (~115°C).

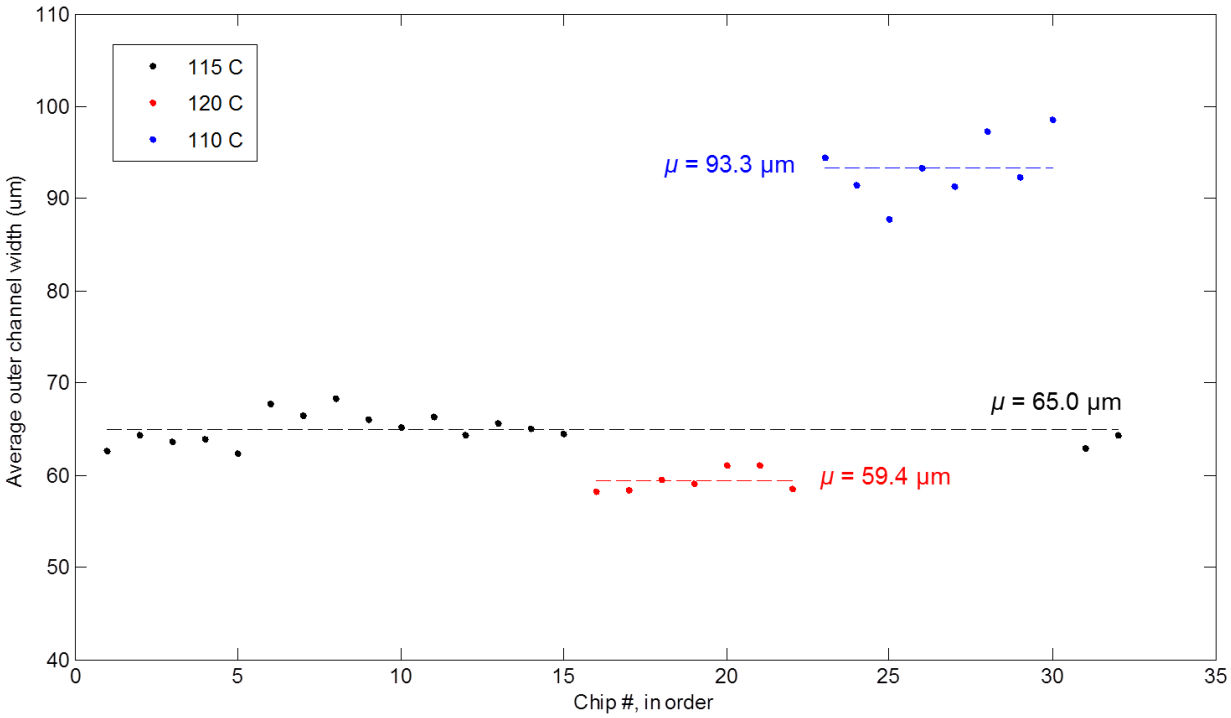

Figure 7-11: The effect of embossing temperature on average channel width. Embossing force was held constant at 1000 N.

By doing a Student-t test on the data, the mean shift between 115°C and 120°C was shown to be statistically significant. Using the sample means and sample standard deviations, it was determined to 95% confidence that the range for the true mean of 115°C is between 64.1-65.9 μm and the range for the true mean of 120°C is between 58.3-60.5 μm. These ranges do not overlap, so it is likely that the temperature increase had a significant effect on the embossing quality. It can also be noted that the last two points on the plot were embossed at 115°C and appear to agree with the previous measurements at that temperature. This suggests that there is no history in the system and that the previous settings do not affect the result of the current settings.

7.4 Mixing Location

In addition to the difficulties automating the mixing location inspection (Section 7.1.2), the observed mixing lengths appear to be much shorter than the predicted mixing lengths for the given channel geometries and pressure setting. Since the mixing length is very sensitive to changes in the channel width, the tool was inspected for possible damage. The current tool has been used for over two thousand cycles, which is far longer than most aluminum, silicon, or epoxy tools typically last. It was measured using the Zygo profilometer to verify the channel dimensions. The images taken by the Zygo can be seen in Figure 7-12. Since the Zygo can only measure flat surfaces, it cannot provide data for any surfaces that are at an angle. The Zygo shows that there is a width of at least 35 μm at the top of the tool and a width at the bottom of 62 μm. From this data, it is unclear what the profile looks like in between. The walls could be vertical with rounded corners at the top and/or bottom, the walls could be angled, or it could be a mix of the two.

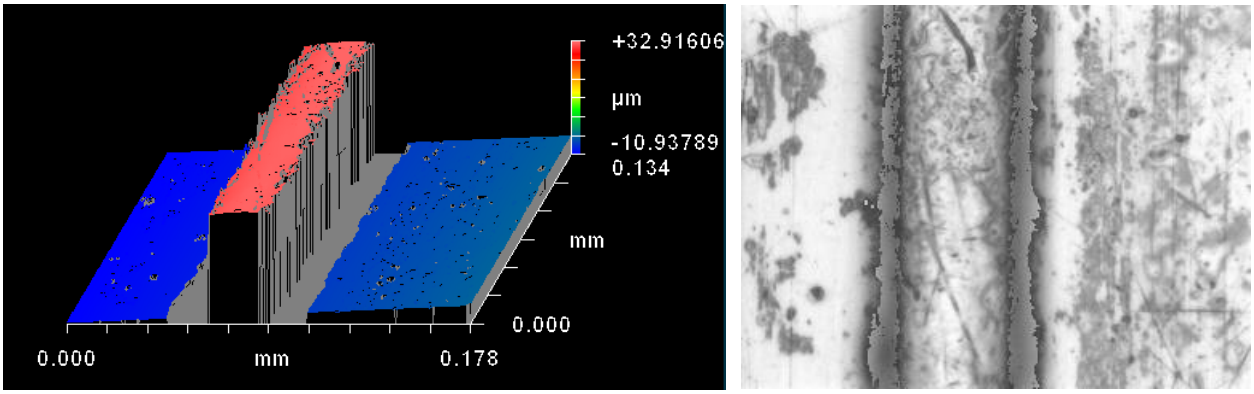

Figure 7-12: Images taken of a channel on the tool using the Zygo profilometer. Left: 3D scan. Right: Image from above.

Since the mixing length was so much shorter, it was possible that the flow velocity was much lower than predicted. A mass flow rate test was performed to confirm the flow velocity. Since the flow rates are extremely low, the pressure was increased to 30 psi for this test to be able to collect more fluid in the same amount of time and minimize measurement error. A taped well-formed chip was placed in the functional testing machine, and fluid was run just until the channels were filled. This would ensure that all of the following fluid would appear in the outlet and not remain in the channels. Even at 30 psi, the flow rate is low enough that it is difficult to capture the liquid in a container for measuring. Instead, a syringe was used to collect droplets as they formed. This also helped reduce evaporation of the fluid. The initial mass of the empty syringe was measured before the test. At the end of the test, the syringe was used to remove any fluid left in the outlet reservoir on the chip, and the mass of the full syringe was measured. The average flow velocity could be calculated using

$$\bar{u} = \frac{\dot{m}}{\rho A} = \frac{m}{t\rho wh} \tag{7.1}$$

where ρ is the fluid density (approximated as 997.86 kg/m^3 for water at 22°C), w is the channel width (50 µm), and h is the channel height (40 µm). The results of the experiment and calculations are shown in Table 7-2. The velocity calculated from the mass flow rate was within the range of the expected flow velocity calculated from (5.8) at 30 psi, assuming a variation of ± 0.5 psi in flow pressure. This means that the channel geometries of a well-formed chip are likely quite close to the nominal dimensions.

Mass [g]	0.631 ± 0.004
Time [min]	62.5
Mass Flow Rate [g/min]	0.010 ± 0.0001
Calculated Average Velocity, $\bar{u}$ [m/s]	0.084 ± 0.001
Expected Average Velocity, $\bar{u}$ [m/s]	0.082 ± 0.002

Table 7-2: The results of the mass flow rate experiment for a chip at 30 psi. The calculated velocity from this test was within the range of the expected flow velocity from Eqn. (5.8) at 30 psi.

The tool was also brought to a scanning electron microscope (SEM) to verify that the channels were the correct dimensions and not damaged. A close up of a channel at a slight angle from above can be seen in Figure 7-13. The same scratch mark at the top of the Zygo image in Figure 7-12 can be seen in the middle of the channel under the SEM. The channels are, in fact, still 50 μm wide. The edges appear to be fairly sharp, both at the top and bottom surfaces. It is possible that there is just enough curvature at the sides of the top surface for the Zygo to be unable to measure them, but they don't appear to be severely rounded.

The rest of the tool was scanned for defects. Besides the excess dirt and plastic and a few minor cavities, the tool is still in fairly good condition. The only major defect is an approximately 300 μm length of one of the middle channels that appears to have collapsed slightly, shown in Figure 7-14. This section was measured under the Zygo and the channel height appears to be decreased by only a few microns. Since the measured velocity is close to the predicted velocity, the defect does not appear to have much of an effect on the chip performance.

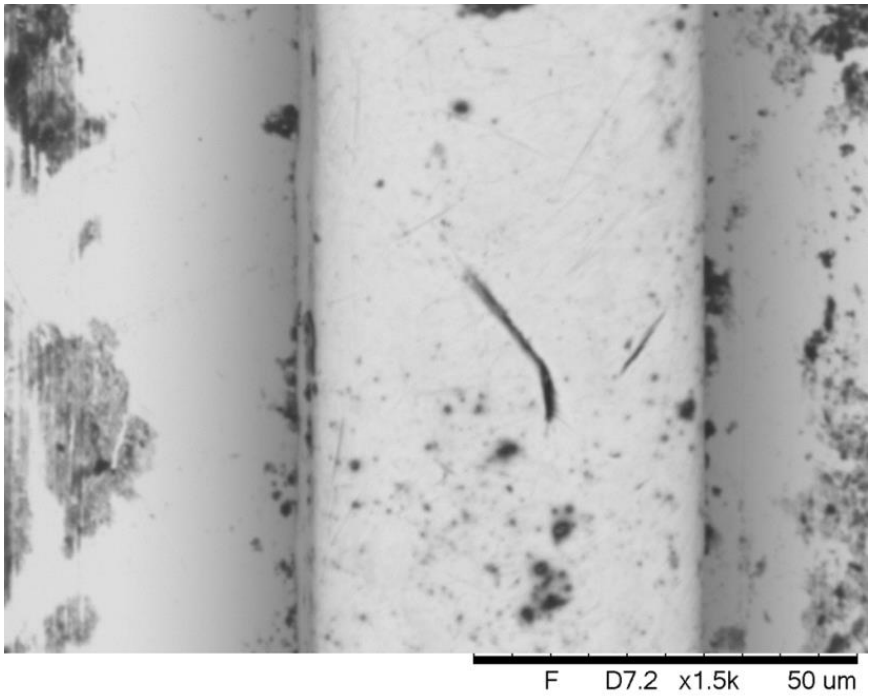

Figure 7-13: A 1500x SEM image of a section of a channel on the tool. The scale on the image confirms that the channels are still 50 μm wide. The tool is at a very slight downward angle to the right, so a sliver of the side of the channel can be seen on the left. The edges do not appear to have any significant rounding.

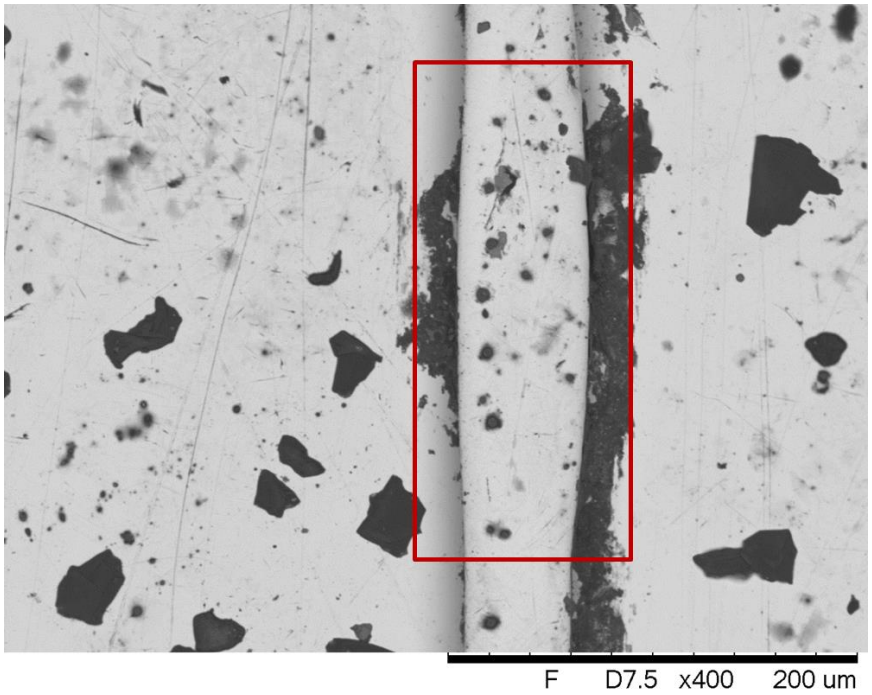

Figure 7-14: A 400x SEM image of defect in a channel on the tool. The channel bulges out slightly (highlighted in red), indicating that it has been compressed. When measured under the Zygo, it did not appear to be collapsed by more than a few microns.

Therefore, the difference in mixing length must be caused by something else. It is possible that the diffusion constant of the food dye being used is higher than expected. It is also possible that that the pixels on the camera are saturating before the flow is fully mixed. If that camera cannot distinguish between pure dye and dye that is mixed in ratios of 1:1 with water, then it is possible that the true mixing length is longer than the observed length. This suggests that in addition to optimizing the camera and lighting conditions, more experiments should be performed to characterize the dye for the mixing length measurement.

CHAPTER 8 CONCLUSION

Machines for sealing, cutting, inspecting, and testing hot embossed microfluidic chips were designed, built, and tested. These machines were integrated with a novel hot embossing machine and a robotic arm to create a working desktop manufacturing cell that is capable of automatically producing functional microfluidic devices. This is the first time since the start of the microfactory project that the entire system has been integrated and running together. The system is controlled by a series of LabVIEW programs, and it runs with a total cycle time of 170 seconds.

The functional testing machine is able to make a reliable measure of the embossed channel quality to a resolution of 0.63 μm and can detect changes in embossing parameters. The machine is also capable of functionally testing the chips by flowing two fluids through the inlet ports at set pressures. It has proved that it is feasible to take quick in-line measurements to monitor embossing quality without the use of advanced metrology-grade equipment. The inspection takes 85 seconds. The taping machine is able to reliably seal the embossed chips and cut them into individual devices. The tape creates a strong seal, does not clog the channels, and has good optical clarity. The taping process takes 15 seconds per cycle. The taping and width measurement processes have a standard deviation of 0.82 μm. Preliminary tests demonstrated credible run data, and the effect of embossing temperature on channel width was detected to a resolution of 2 μm.

8.1 Future Work

The system is close to being used for a wide-range of tests that can be performed to help understand the microfluidic hot embossing process. First, the process needs to be stabilized. External sources of variation need to be reduced to bring the process in control. Once a run chart has shown that the process is stationary, a more thorough design of experiments can be used to

study the effects of forming temperature, forming pressure, heating time, forming time, and cooling time on the channel geometry of the embossed chips. Once these effects are understood, the parameters can be optimized to produce well-formed chips. Closed-loop cycle-to-cycle process control can then be implemented by sending the results of the functional test measurements to the hot embossing machine. This would allow the system to recover from disturbances, such as a change of material, and continue producing high quality of chips under a variety of conditions.

There are some improvements that could be made to the microfactory system that would allow it to be more robust and reliable. The mixing length measurement would still be a valuable measurement to describe the overall performance of each chip. Too many difficulties were encountered to be able to implement it in this version of the functional testing machine, but with a few changes, it should be possible to make this measurement using the current system with an accuracy of 72.8 μm. Mainly, the lighting needs to be improved so that it is much more uniform and has the correct exposure time. Once the lighting has been improved, the mixing location inspection can be re-implemented and tested. Ideally, the standard deviation of the pixel intensity across the channels should decrease along the length of the serpentine channels. The measurement should also be similar before and after each turn rather than having any significant jumps. The measurement can then be tested to make sure it is working properly by varying the flow pressure. For lower pressures and slower flow rates, the mixing length should be shorter. For higher pressures and faster flow rate, the mixing length should be longer.

Also, there currently is not a lot of feedback regarding chip locations in the system other than what is recorded based on the actions of the robot. However, this does not take into account chips that have been incorrectly loaded or unloaded and chips that have accidentally dropped. If each of the machines had the capability to monitor chip presence, it would avoid possible jams and unnecessary system repair time. There is also currently a buffer of 5 chips in the taping machine, which causes a long delay before a problem can be detected in the embossing quality. If this can be eliminated, then a true cycle-to-cycle control strategy can be implemented. The buffer of the current design can definitely be reduced by removing the second compliant upper roller, since it is not currently needed. While it is difficult to remove the buffer completely, it should be possible to reduce the buffer to only 1 chip by implementing a new cutting mechanism with a smaller profile such that it can fit closer to the taping roller.

Finally, the current system is only designed to emboss and test a simple micro-mixer chip pattern that has no real application outside of the microfactory. If the system can be adapted to produce chips with different patterns—possibly with higher aspect ratios and smaller features—it could address a larger range of challenges faced by the microfluidic manufacturing industry today.

APPENDIX

A MEASUREMENT DATA

System Run Chart
(All chips formed at 1000 N and 115°C)

Mean, μ (μm): 66.85

Std. Dev., σ (μm): 1.82

Chip #	Width (μm)	Chip #	Width (μm)
1	65.84	22	66.21
2	66.62	23	68.04
3	66.33	24	70.52
4	65.51	25	64.91
5	64.92	26	65.26
6	63.74	27	67.03
7	65.21	28	67.55
8	65.32	29	65.29
9	66.49	30	67.70
10	65.78	31	66.01
11	66.80	32	67.54
12	66.73	33	68.84
13	66.58	34	67.36
14	69.60	35	65.88
15	65.24	36	70.06
16	65.98	37	68.71
17	67.18	38	69.34
18	66.14	39	67.12
19	64.95	40	72.97
20	67.38	41	67.51
21	64.76		

Functional Testing Machine Variation

(Same chip formed at 1000 N and 115°C, taped once)

Mean, μ (μm): 65.33

Std. Dev., σ (μm): 0.31

Run #	Width (μm)	Run #	Width (μm)
1	65.34	26	65.34
2	65.84	27	66.02
3	65.23	28	65.25
4	65.88	29	65.17
5	65.59	30	66.14
6	65.01	31	65.35
7	65.14	32	64.78
8	65.30	33	65.62
9	65.17	34	65.26
10	65.24	35	65.54
11	65.03	36	65.37
12	65.10	37	65.31
13	65.17	38	65.10
14	65.71	39	65.54
15	65.19	40	66.15
16	65.00	41	64.94
17	65.49	42	65.02
18	65.15	43	65.32
19	65.25	44	65.19
20	65.20	45	65.45
21	65.39	46	65.39
22	65.76	47	65.07
23	64.95	48	65.20
24	65.27	49	65.74
25	65.13	50	64.88

Taping Machine and Functional Testing Machine Variation

(Same 6 chips formed at 1000 N and 115°C, taped multiple times)

Chip 1		Chip 2		Chip 3	
Mean, μ (µm):	68.63	Mean, μ (µm):	68.88	Mean, μ (µm):	70.04
Std. Dev., σ (µm):	0.46	Std. Dev., σ (µm):	0.47	Std. Dev., σ (µm):	0.70

Run #	Width (µm)	Run #	Width (µm)	Run #	Width (µm)
1	68.16	1	68.44	1	68.76
2	68.96	2	N/A	2	71.42
3	68.82	3	68.34	3	70.25
4	67.73	4	68.75	4	70.16
5	69.31	5	68.69	5	70.55
6	68.72	6	69.05	6	69.58
7	68.98	7	69.10	7	70.05
8	68.81	8	68.77	8	69.64
9	68.36	9	68.85	9	69.70
10	68.41	10	69.96	10	70.26

Chip 4		Chip 5		Chip 6	
Mean, μ (µm):	67.49	Mean, μ (µm):	64.91	Mean, μ (µm):	67.77
Std. Dev., σ (µm):	0.65	Std. Dev., σ (µm):	0.82	Std. Dev., σ (µm):	0.35

Run #	Width (µm)	Run #	Width (µm)	Run #	Width (µm)
1	65.90	1	N/A	1	66.90
2	67.65	2	N/A	2	67.90
3	67.53	3	65.89	3	67.92
4	67.05	4	N/A	4	67.79
5	67.75	5	65.36	5	67.86
6	68.22	6	65.53	6	68.02
7	67.48	7	65.30	7	67.65
8	67.94	8	63.67	8	67.80
9	67.35	9	64.28	9	68.05
10	68.01	10	64.31	10	N/A

Effect of Embossing Temperature

(Chips formed at 1000 N and 110°C, 115°C, and 120°C)

110°C		115°C		120°C	
Mean, μ (μm):	93.31	Mean, μ (μm):	64.96	Mean, μ (μm):	59.43
Std. Dev., σ (μm):	3.46	Std. Dev., σ (μm):	1.67	Std. Dev., σ (μm):	1.22

Run #	Width (μm)	Run #	Width (μm)	Run #	Width (μm)
1	94.46	1	62.71	1	58.19
2	91.49	2	64.41	2	58.40
3	87.76	3	63.68	3	59.52
4	93.29	4	63.92	4	59.14
5	91.27	5	62.39	5	61.04
6	97.33	6	67.75	6	61.14
7	92.36	7	66.49	7	58.60
8	98.50	8	68.27		
		9	66.11		
		10	65.25		
		11	66.35		
		12	64.32		
		13	65.70		
		14	65.11		
		15	64.51		
		16	62.91		
		17	64.42		

APPENDIX

B PART DRAWINGS

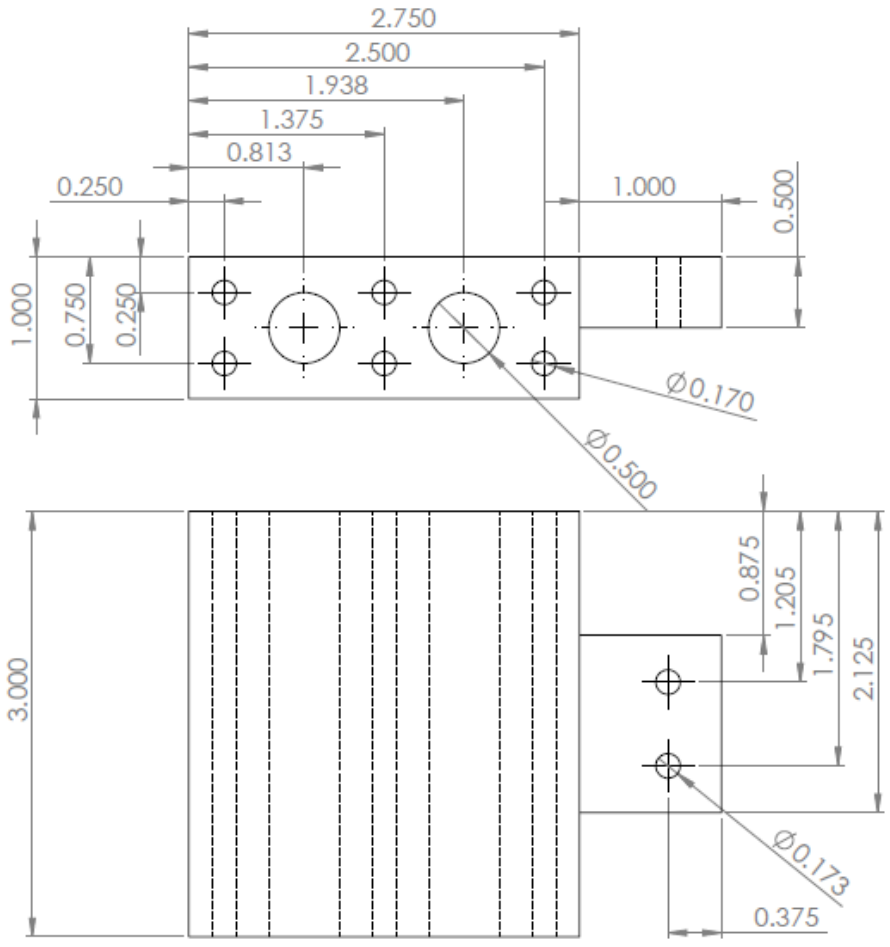

Functional Test: Reservoir_v1

Material: PMMA

Dimensions: Inches

Tolerance: +/- 0.005"

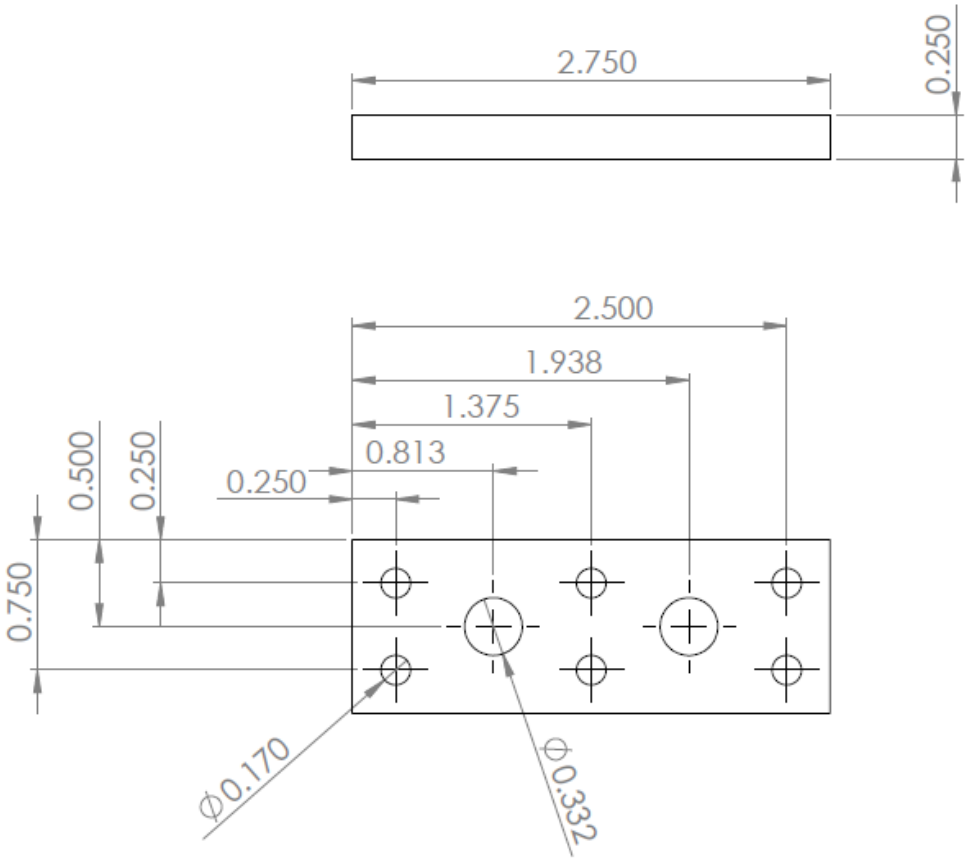

Functional Test: Reservoir caps v1

Material: 6061-T6 Aluminum

Dimensions: Inches

Tolerance: +/- 0.005"

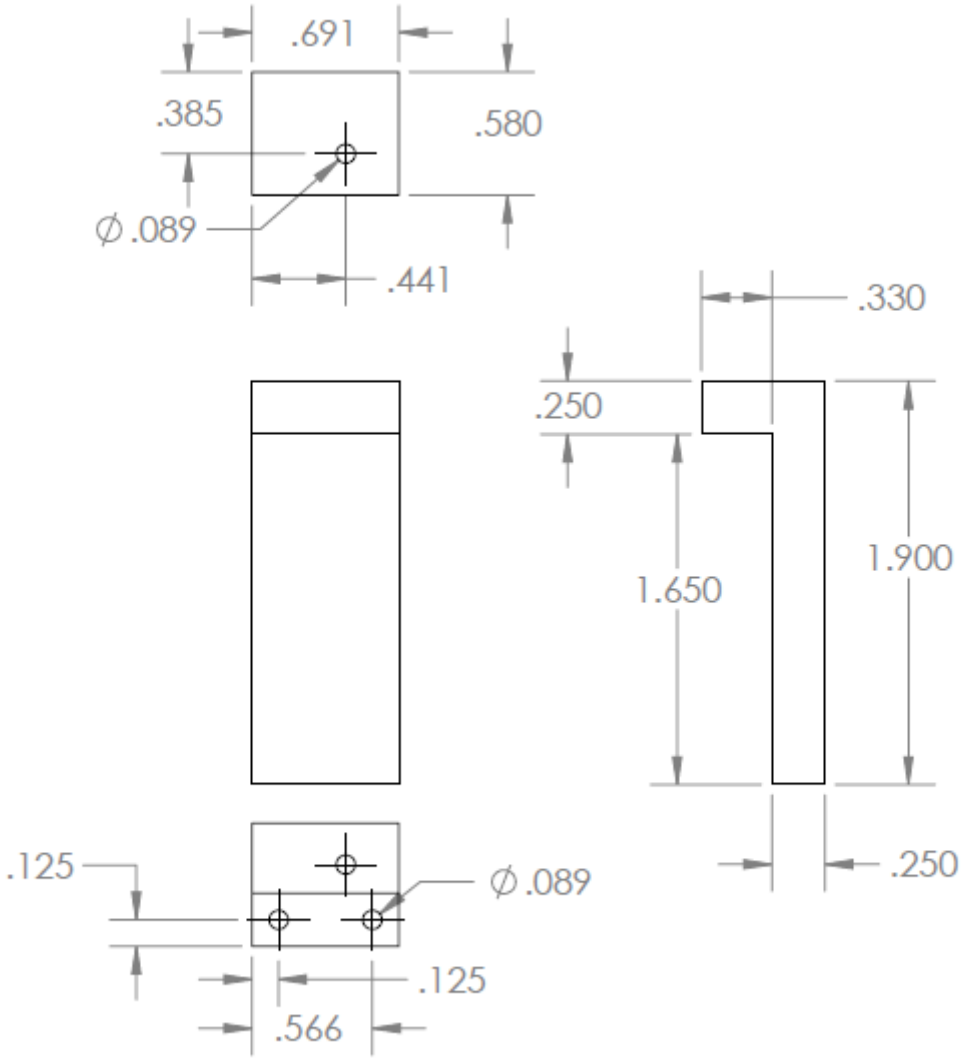

Functional Test: hardstop_bottom_v1

Material: 6061-T6 Aluminum

Dimensions: Inches

Tolerance: +/- 0.005"

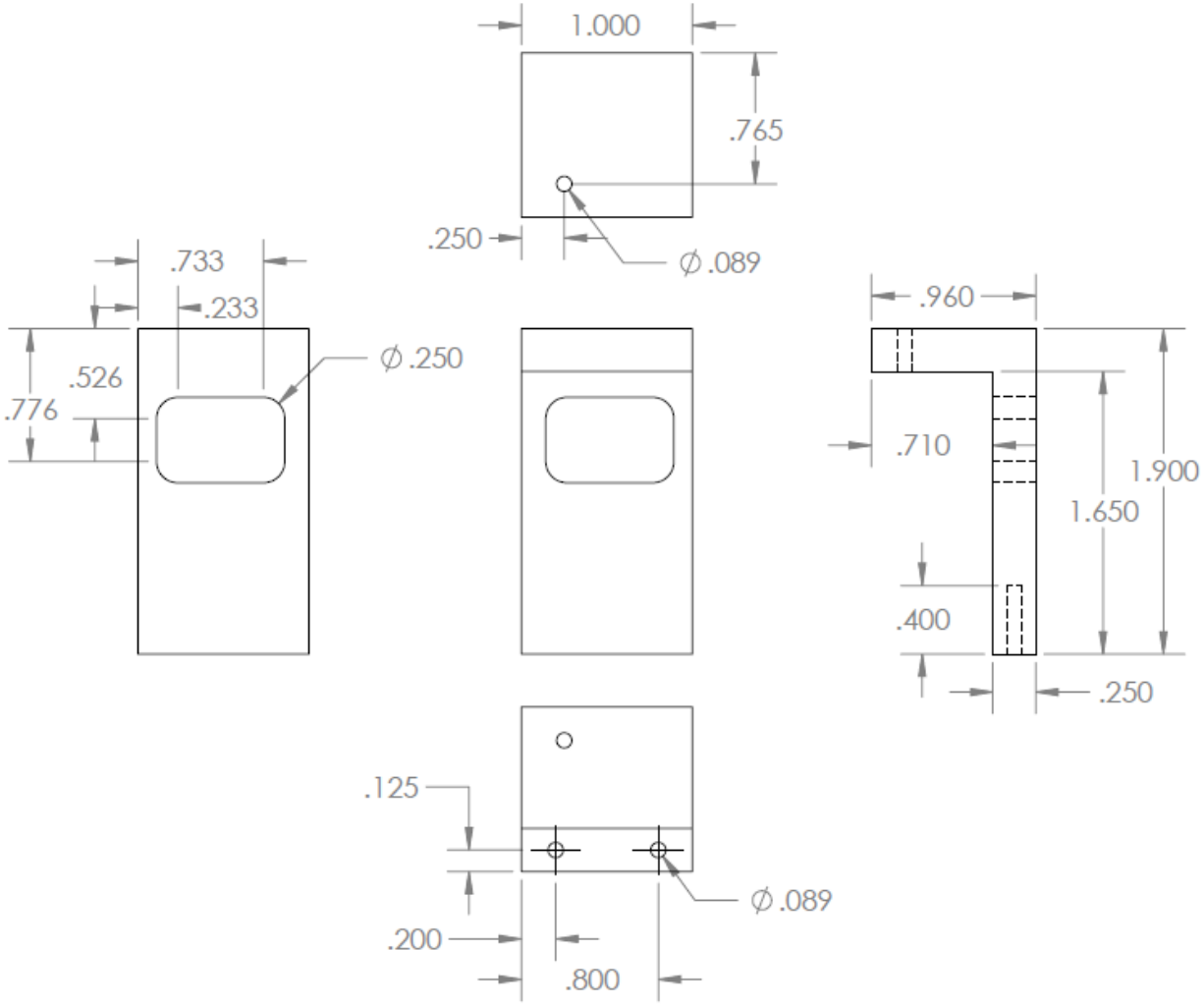

Functional Test: hardstop_outlets_v1

Material: 6061-T6 Aluminum

Dimensions: Inches

Tolerance: +/- 0.005"

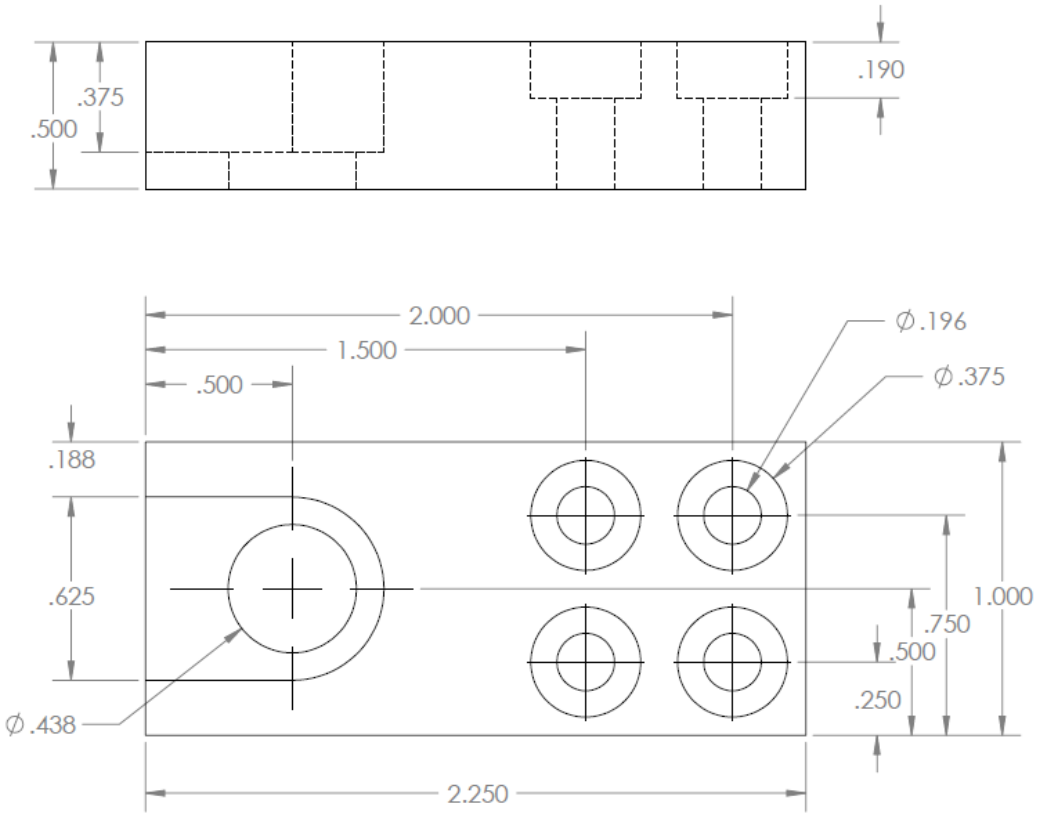

Functional Test: CylinderMount

Material: 6061-T6 Aluminum

Dimensions: Inches

Tolerance: +/- 0.005"

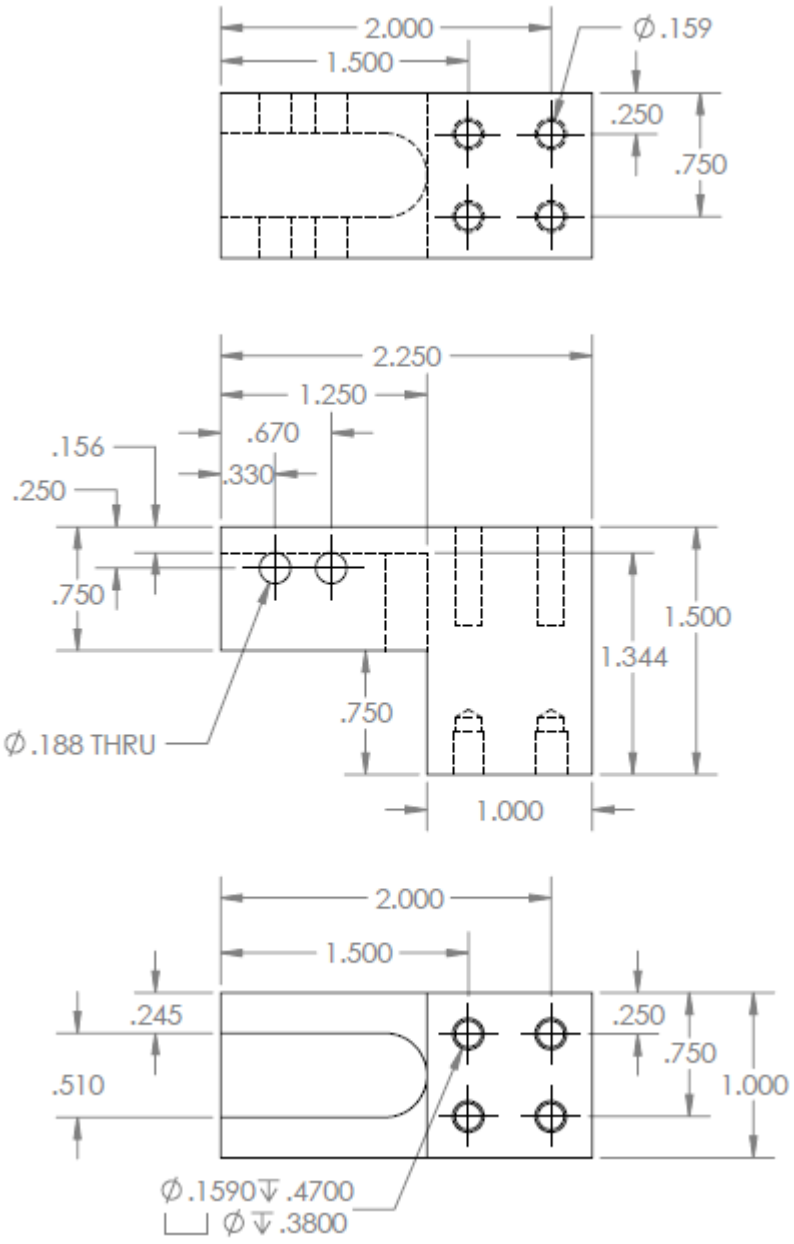

Functional Test: RodMount

Material: 6061-T6 Aluminum

Dimensions: Inches

Tolerance: +/- 0.005"

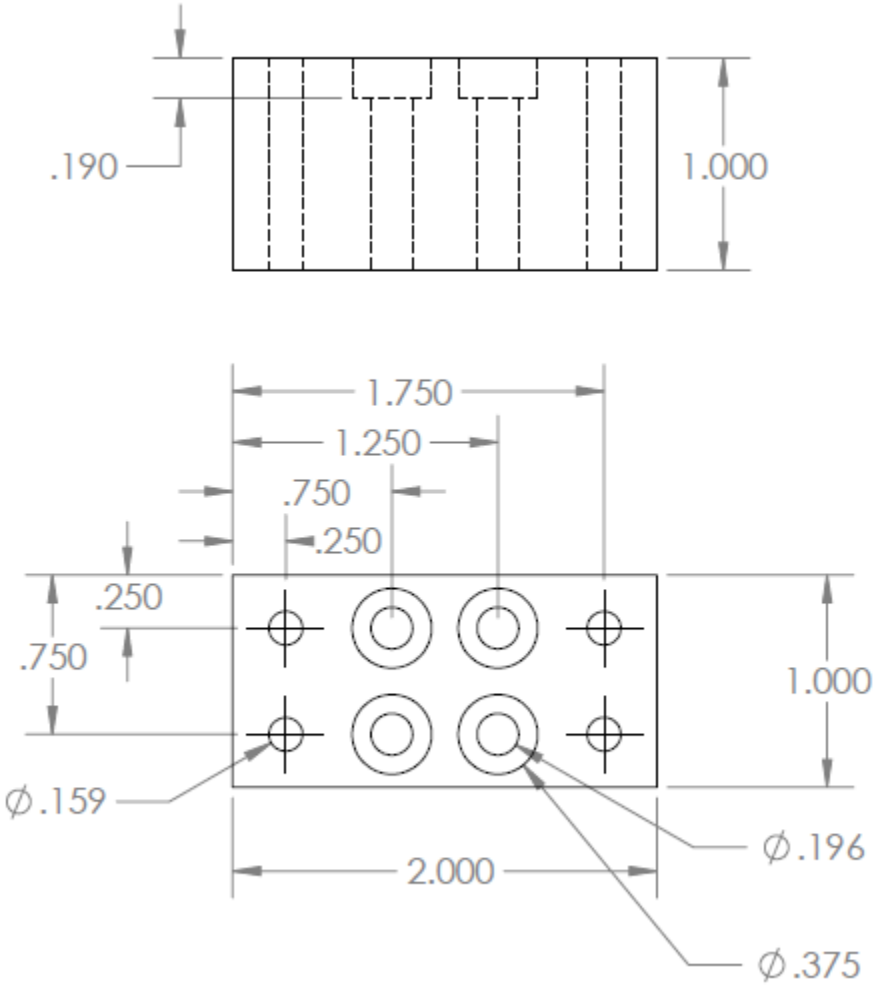

Functional Test: PinchValveBase

Material: 6061-T6 Aluminum

Dimensions: Inches

Tolerance: +/- 0.005"

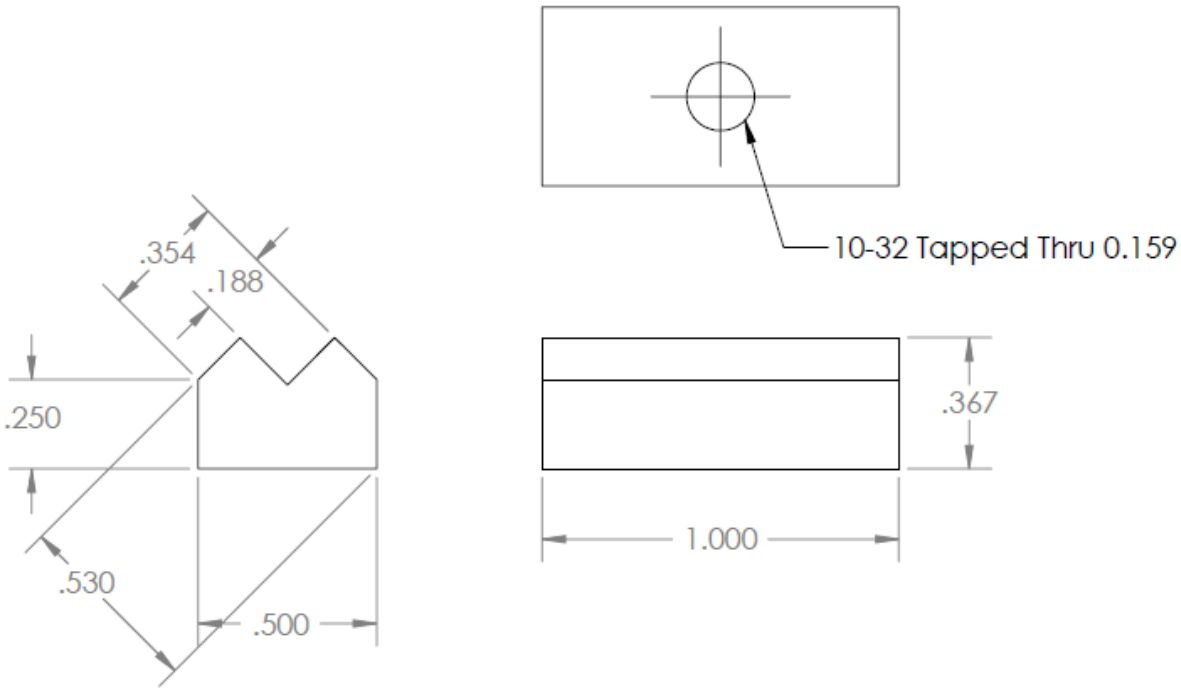

Functional Test: MovingStop

Material: 6061-T6 Aluminum

Dimensions: Inches

Tolerance: +/- 0.005"

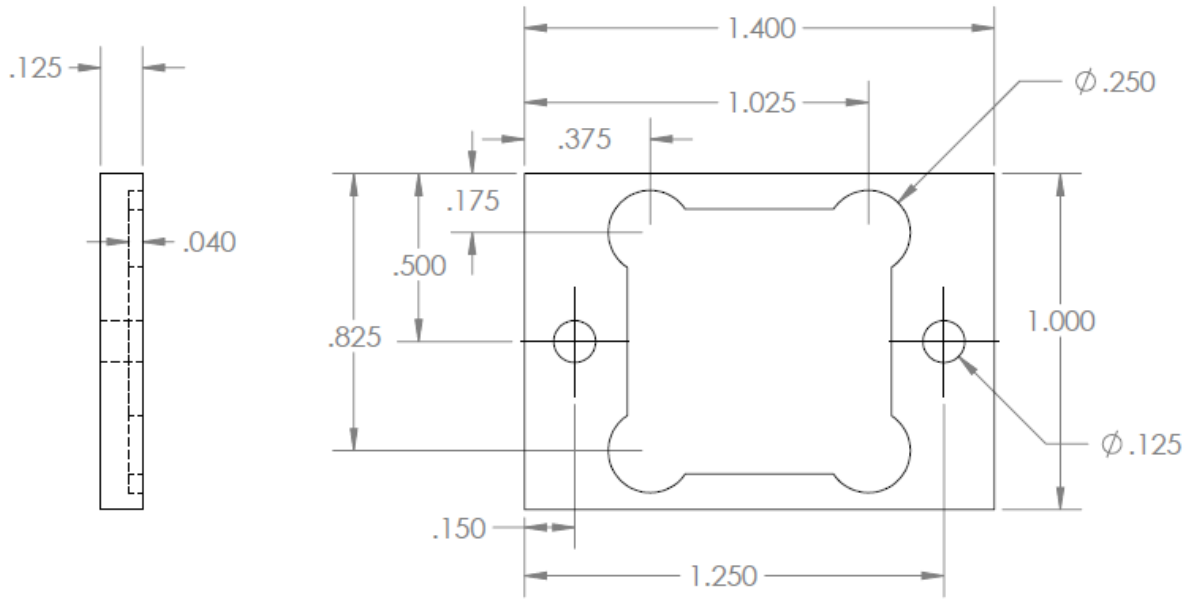

Functional Test: Mirror base 20mm

Material: 6061-T6 Aluminum

Dimensions: Inches

Tolerance: +/- 0.005"

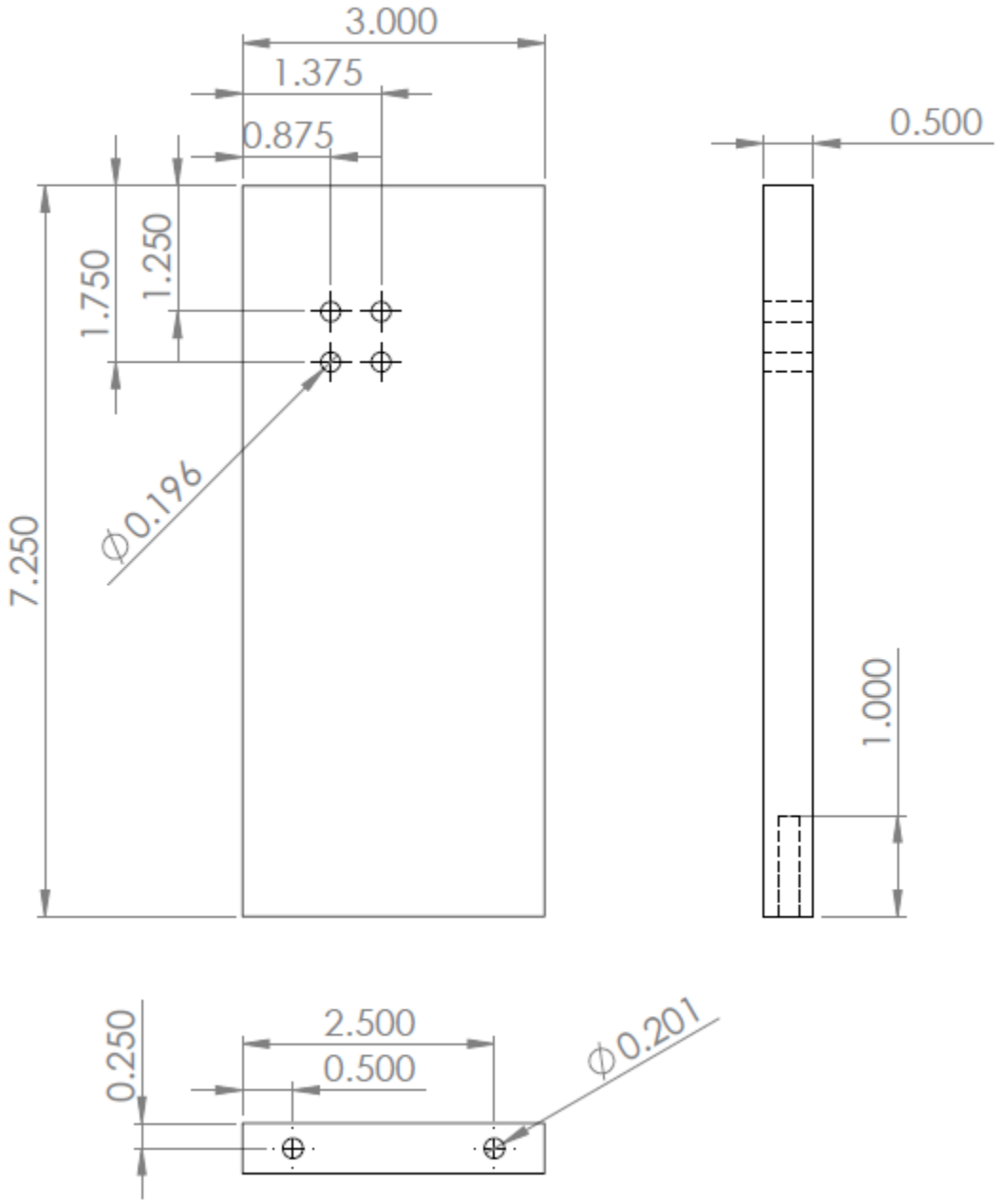

Functional Test: Z bracket v1

Material: 6061-T6 Aluminum

Dimensions: Inches

Tolerance: +/- 0.005"

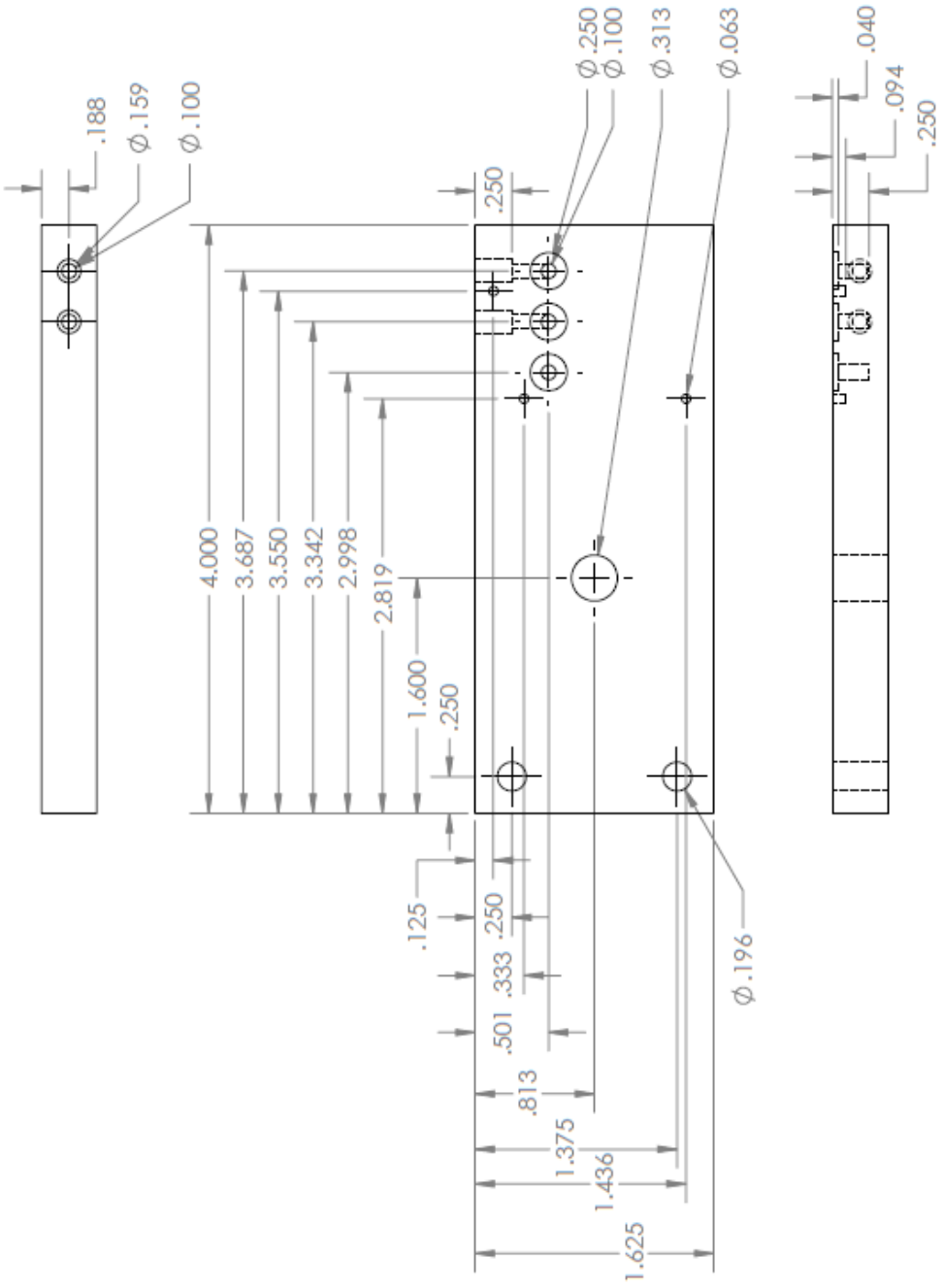

Functional Test: outlets_v2

Material: Polycarbonate

Dimensions: Inches

Tolerance: +/- 0.005"

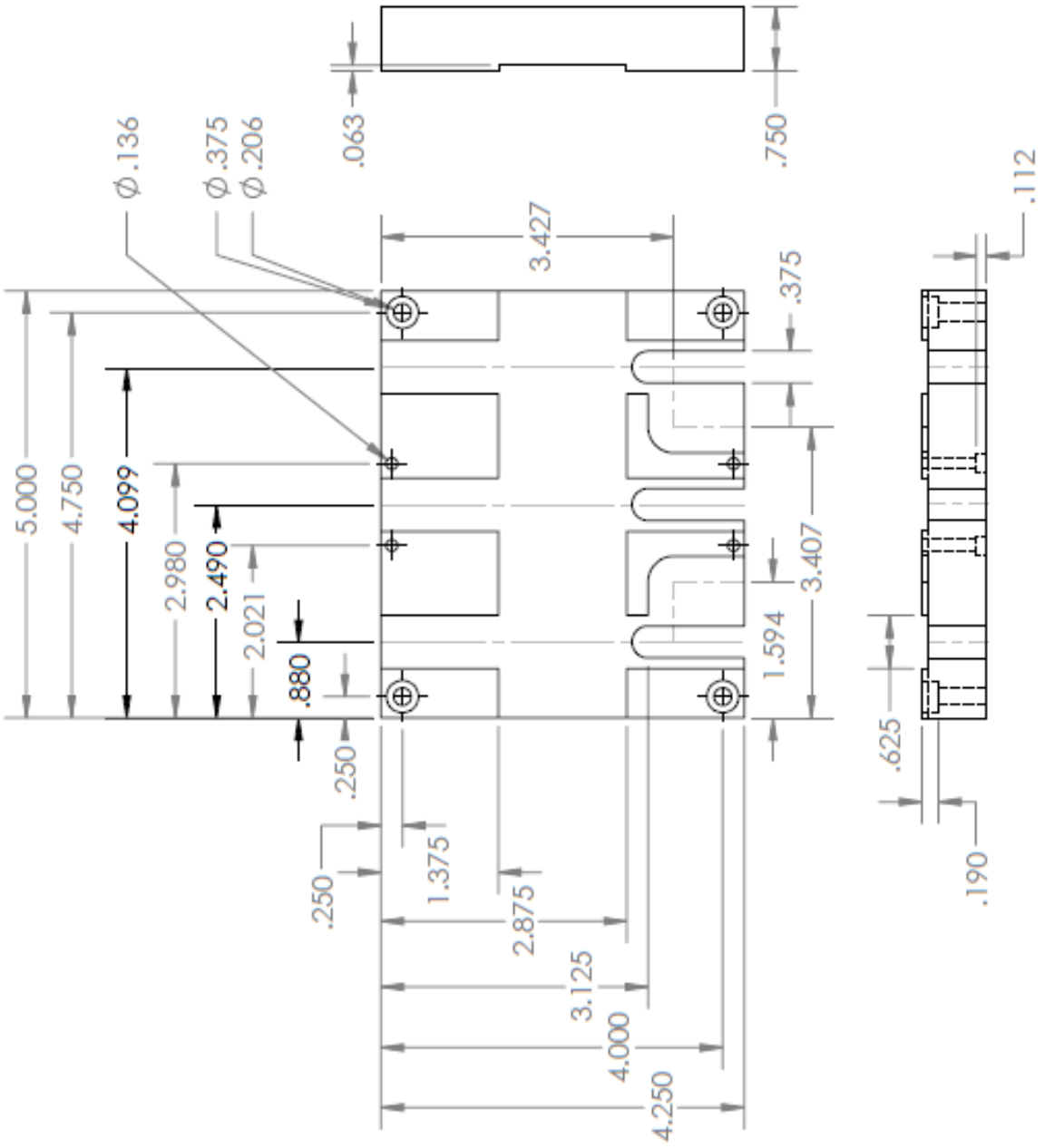

Taping Machine: chopping block v5

Material: Delrin

Dimensions: Inches

Tolerance: +/- 0.005"

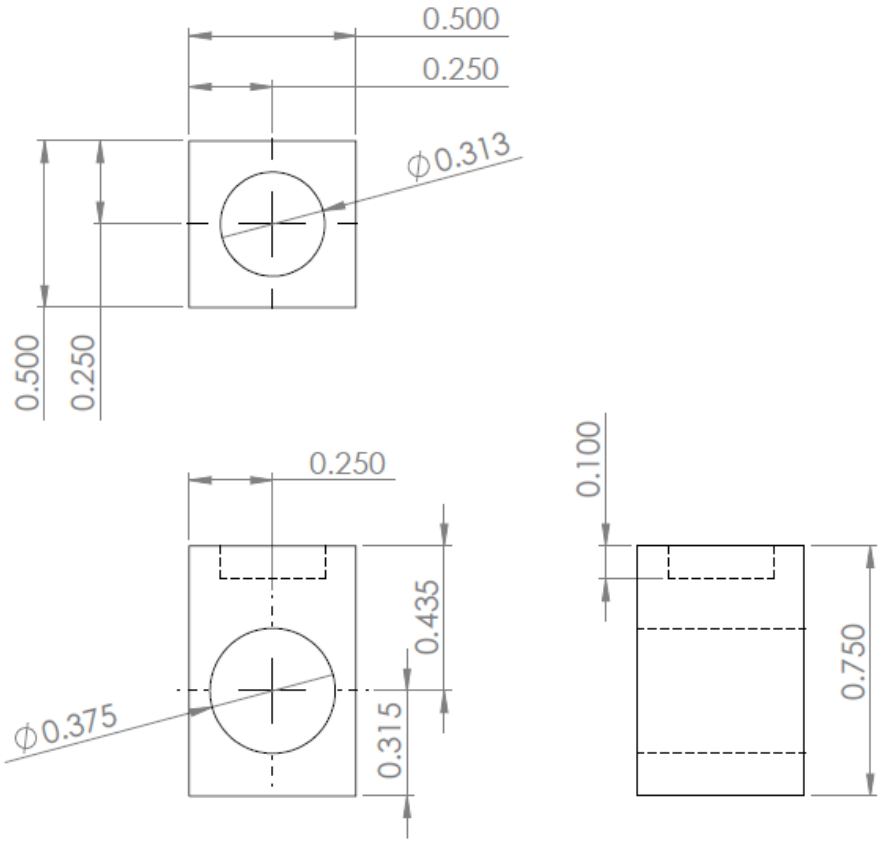

Taping Machine: Spring connector lower v1

Material: 6061-T6 Aluminum

Dimensions: Inches

Tolerance: +/- 0.005"

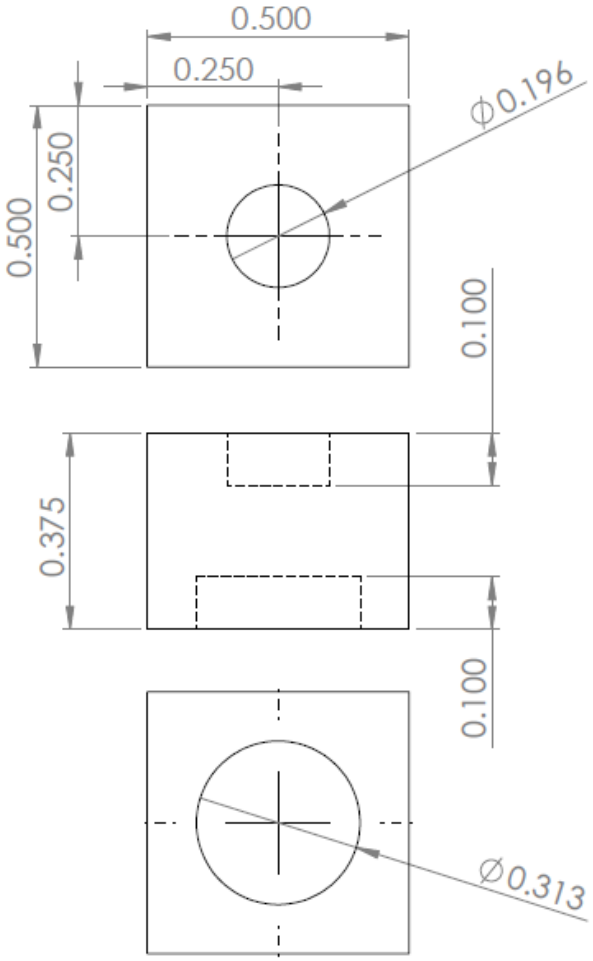

Taping Machine: Spring connector upper v1

Material: 6061-T6 Aluminum

Dimensions: Inches

Tolerance: +/- 0.005"

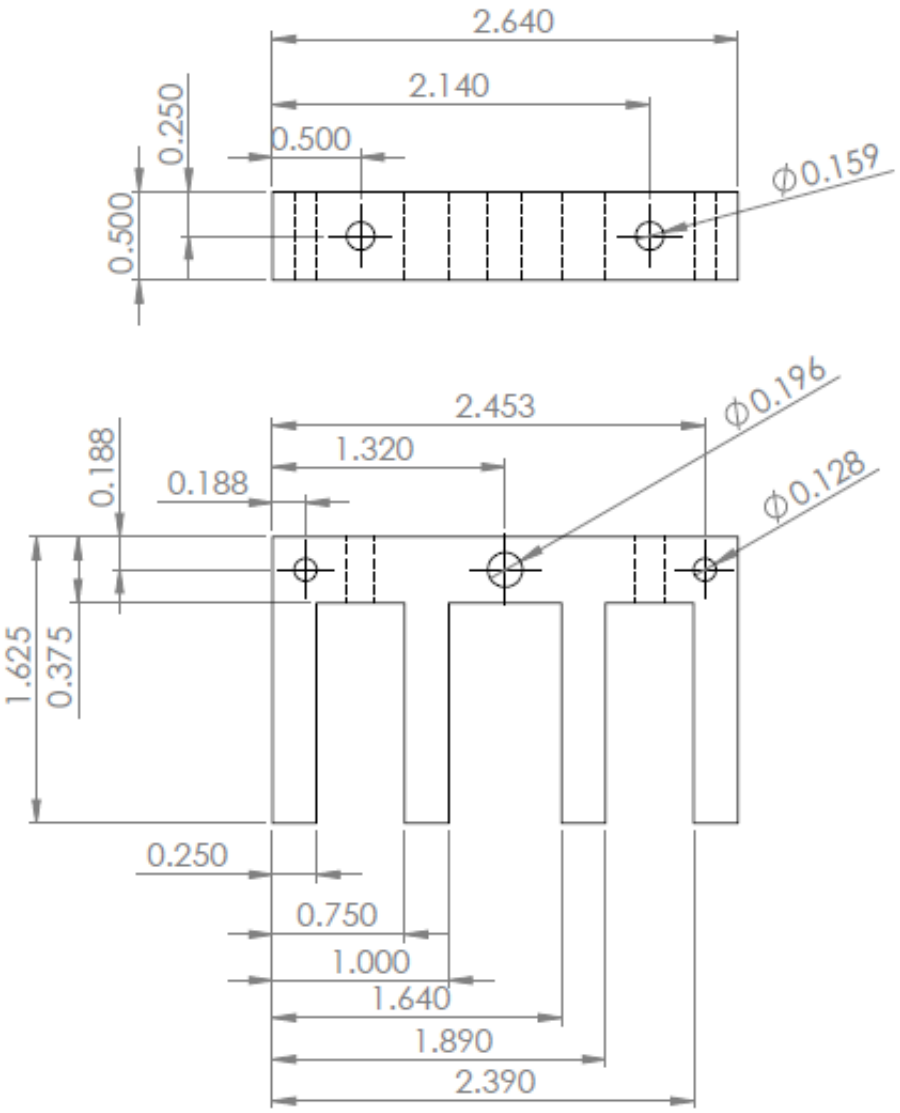

Taping Machine: spring guide v1

Material: 6061-T6 Aluminum

Dimensions: Inches

Tolerance: +/- 0.005"

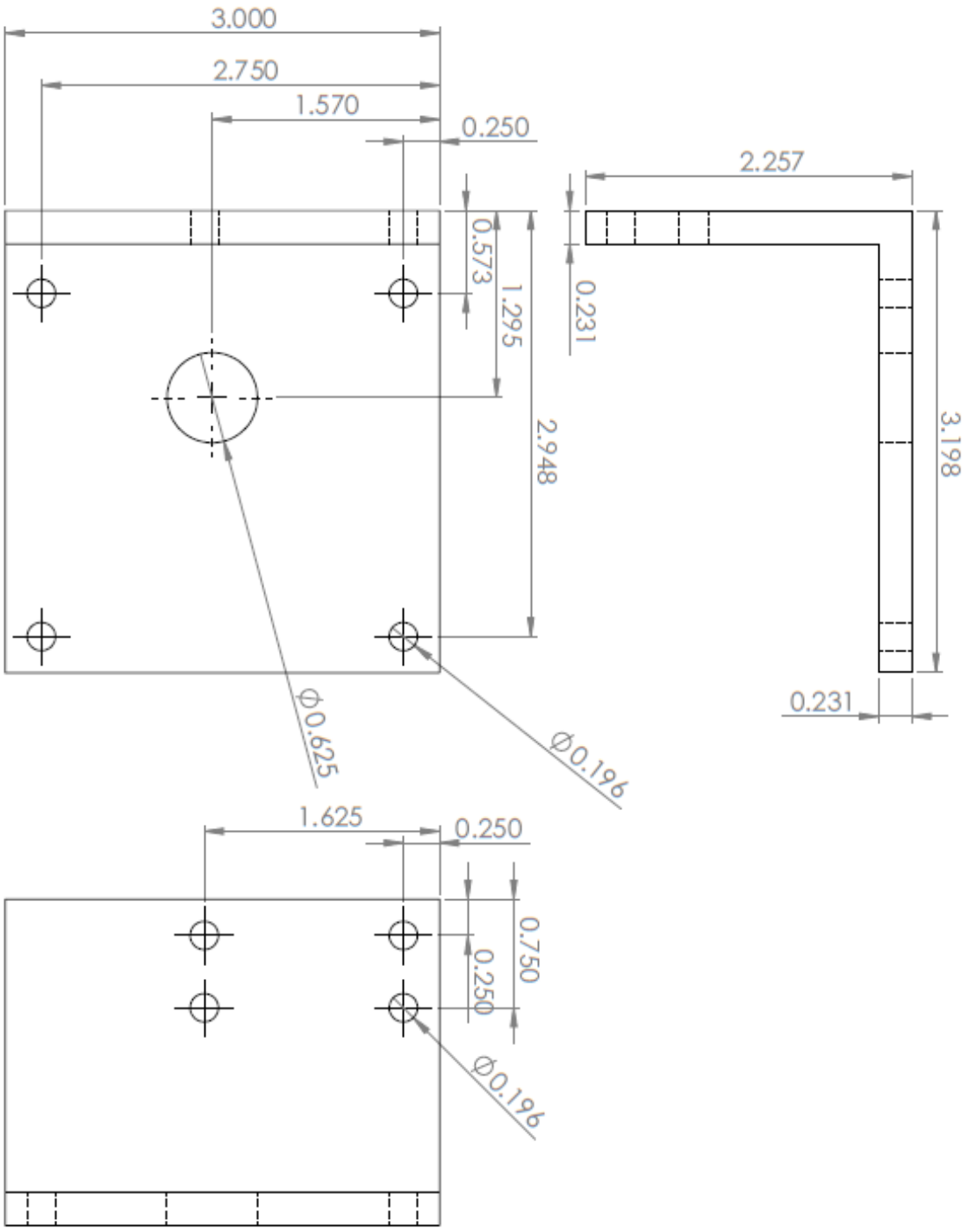

Taping Machine: motor mount face plate v2

Material: 6061-T6 Aluminum

Dimensions: Inches

Tolerance: +/- 0.005"

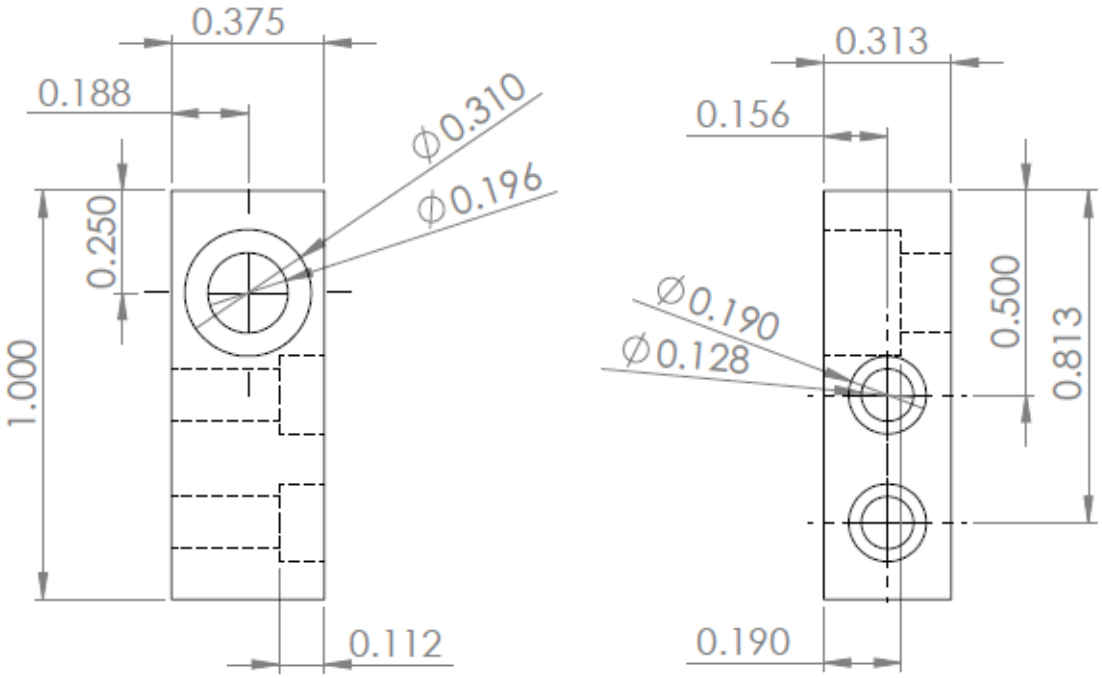

Taping Machine: belt tension anchor v1

Material: 6061-T6 Aluminum

Dimensions: Inches

Tolerance: +/- 0.005"

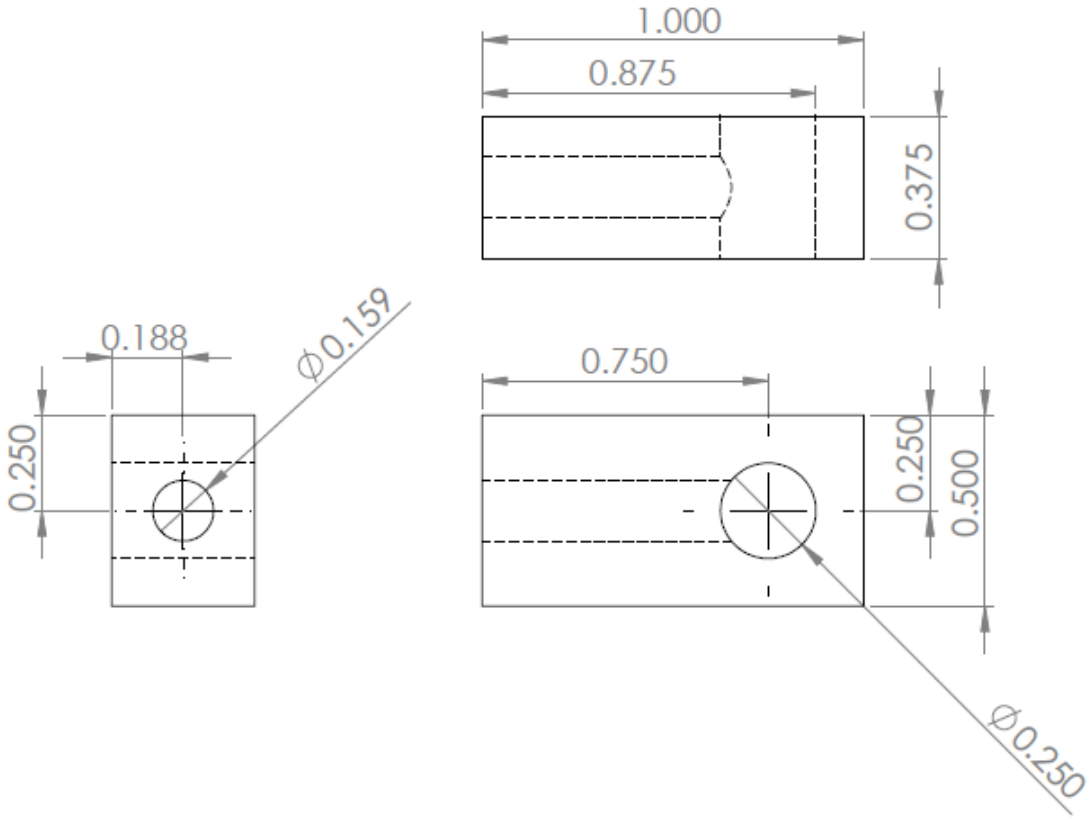

Taping Machine: belt tension connector v1

Material: 6061-T6 Aluminum

Dimensions: Inches

Tolerance: +/- 0.005"

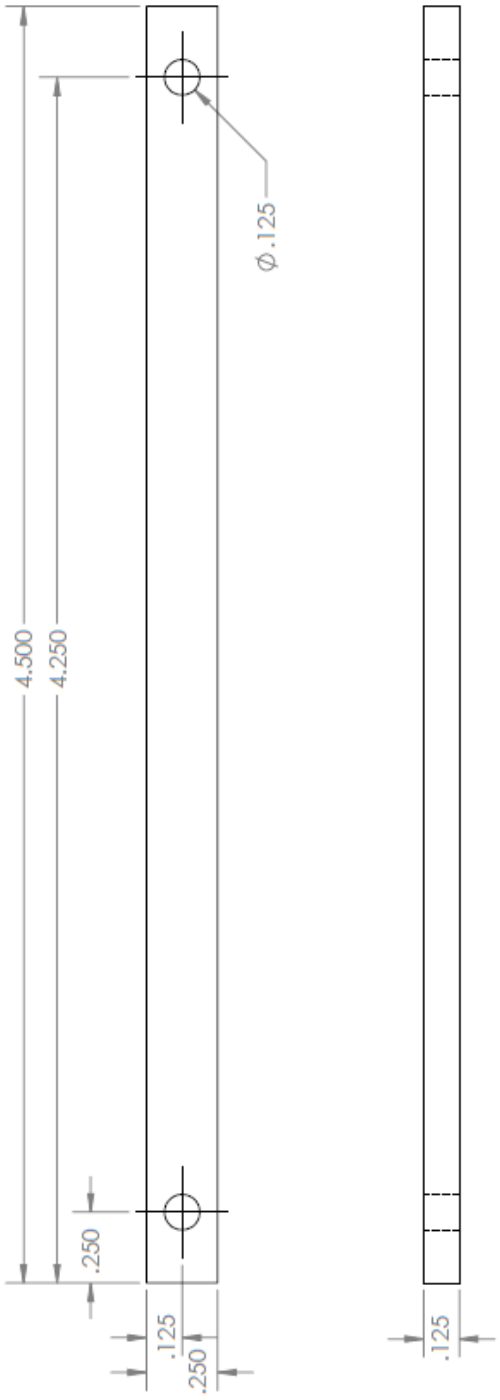

Taping Machine: blade guides v1

Material: 6061-T6 Aluminum

Dimensions: Inches

Tolerance: +/- 0.005"

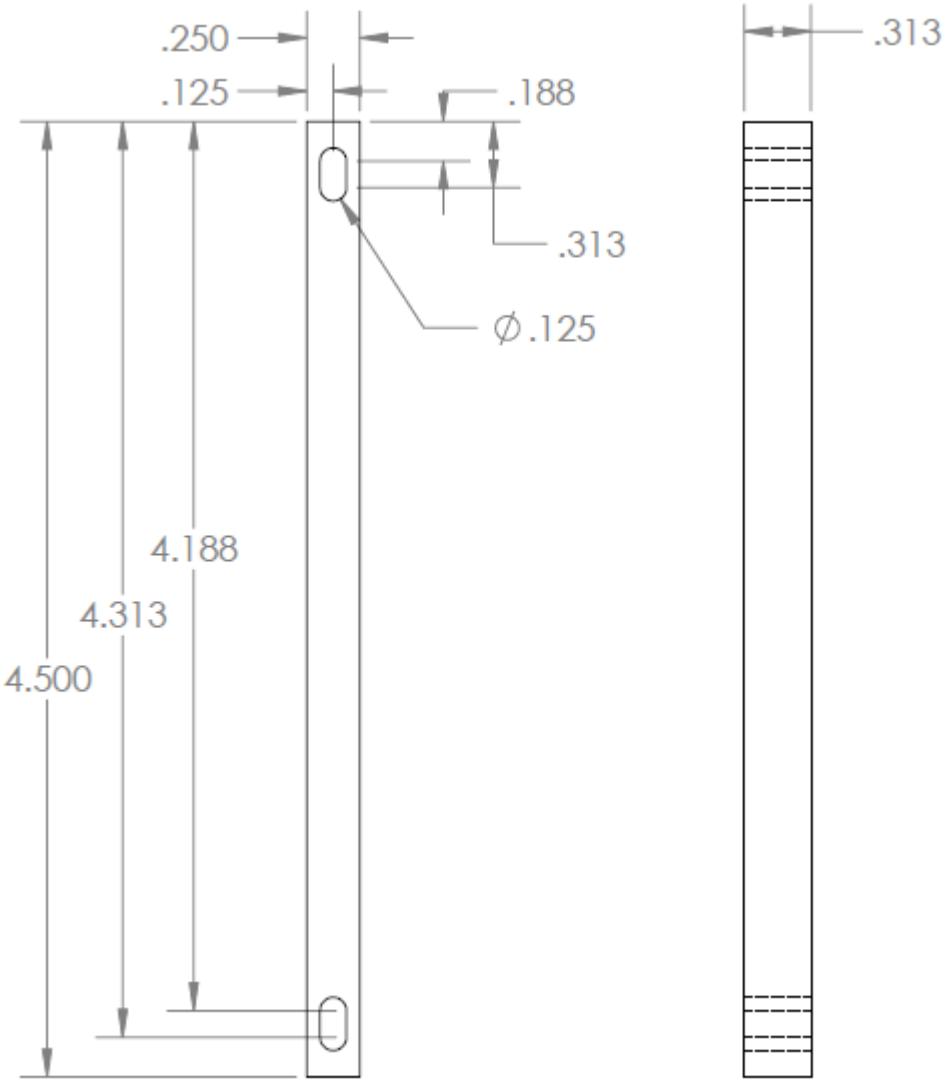

Taping Machine: guide rails v1

Material: 6061-T6 Aluminum

Dimensions: Inches

Tolerance: +/- 0.005"

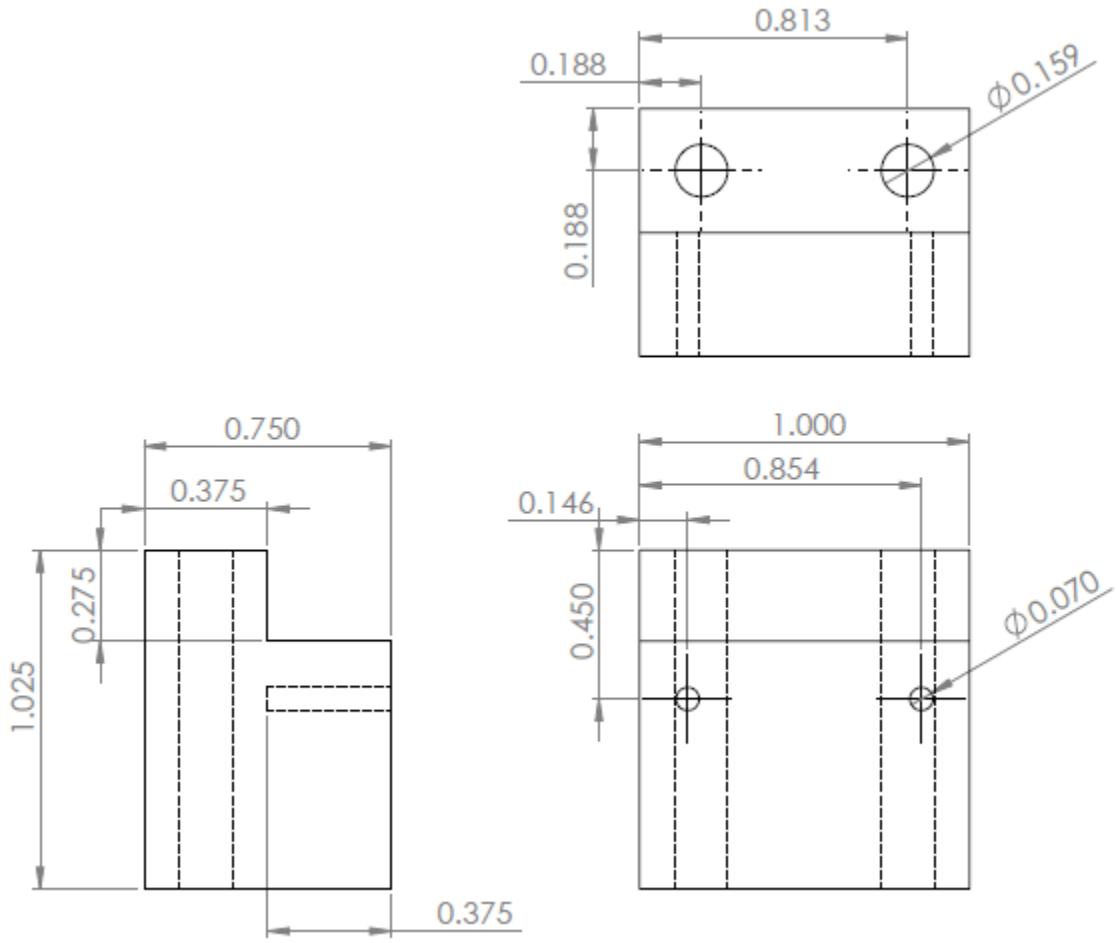

Taping Machine: micromotor bracket mount v1

Material: 6061-T6 Aluminum

Dimensions: Inches

Tolerance: +/- 0.005"

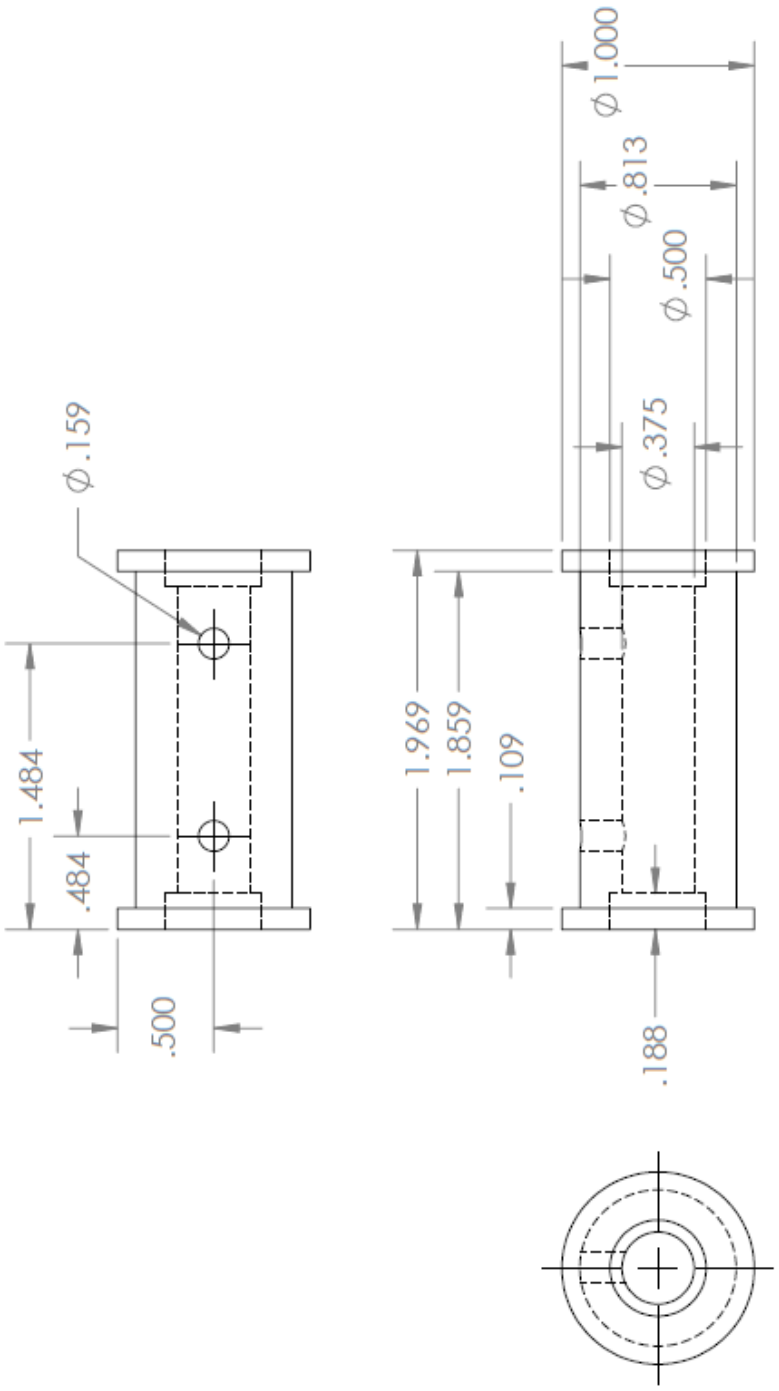

Taping Machine: lower roller large drive v1

Material: Delrin

Dimensions: Inches

Tolerance: +/- 0.005"

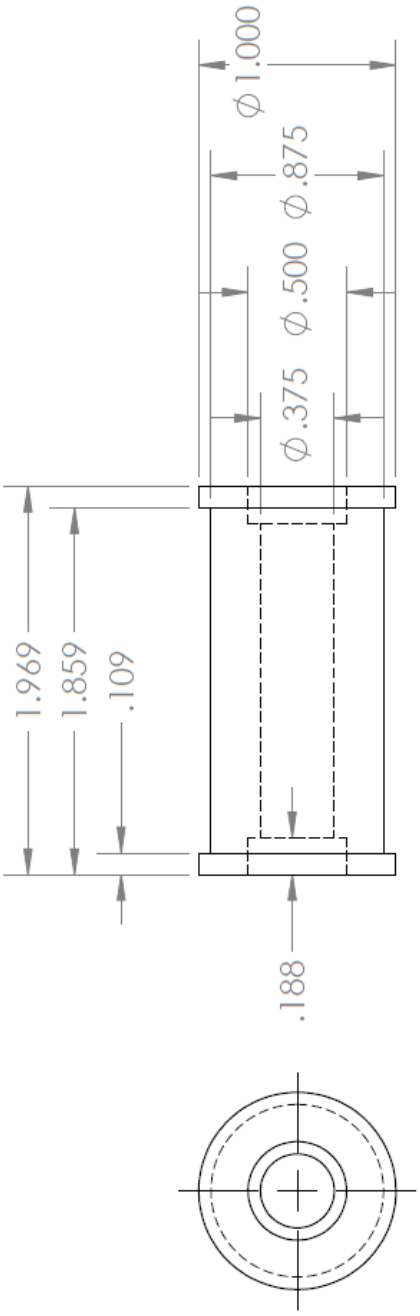

Taping Machine: lower roller large tension v1

Material: Delrin

Dimensions: Inches

Tolerance: +/- 0.005"

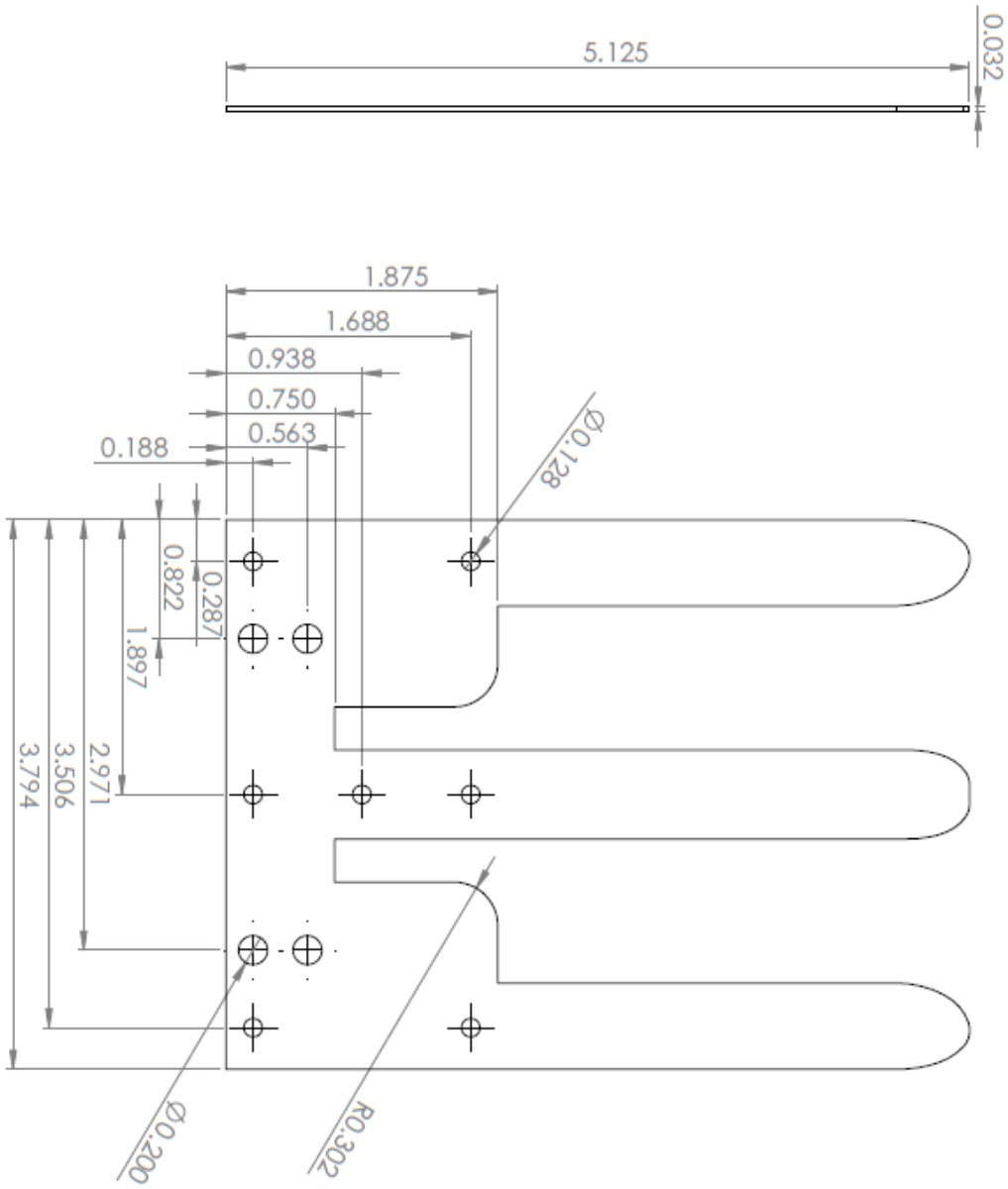

Taping Machine: fork v4

Material: Steel

Dimensions: Inches

Tolerance: +/- 0.005"

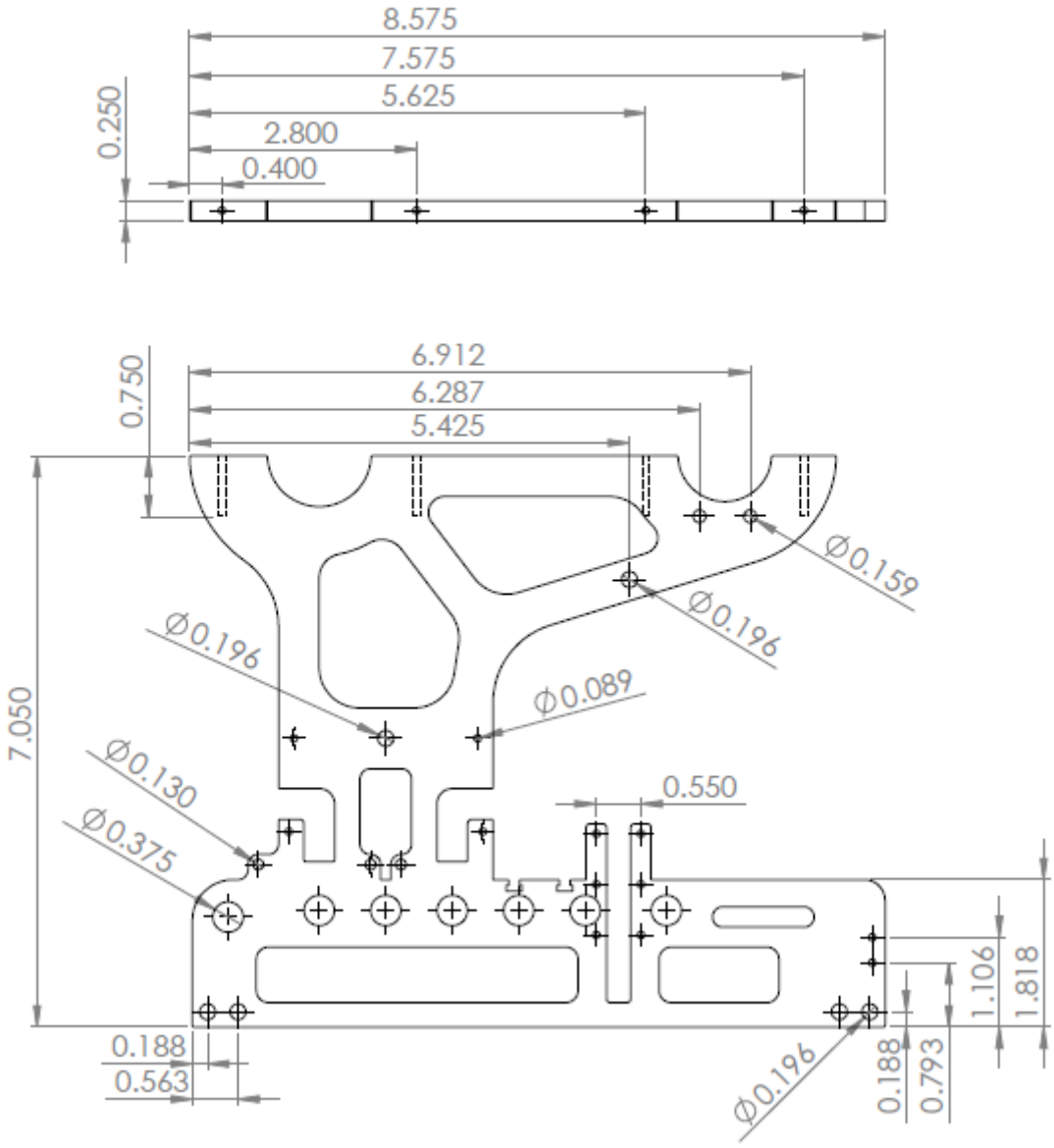

Taping Machine: side wall v1

Material: 6061-T6 Aluminum

Dimensions: Inches

Tolerance: +/- 0.005"

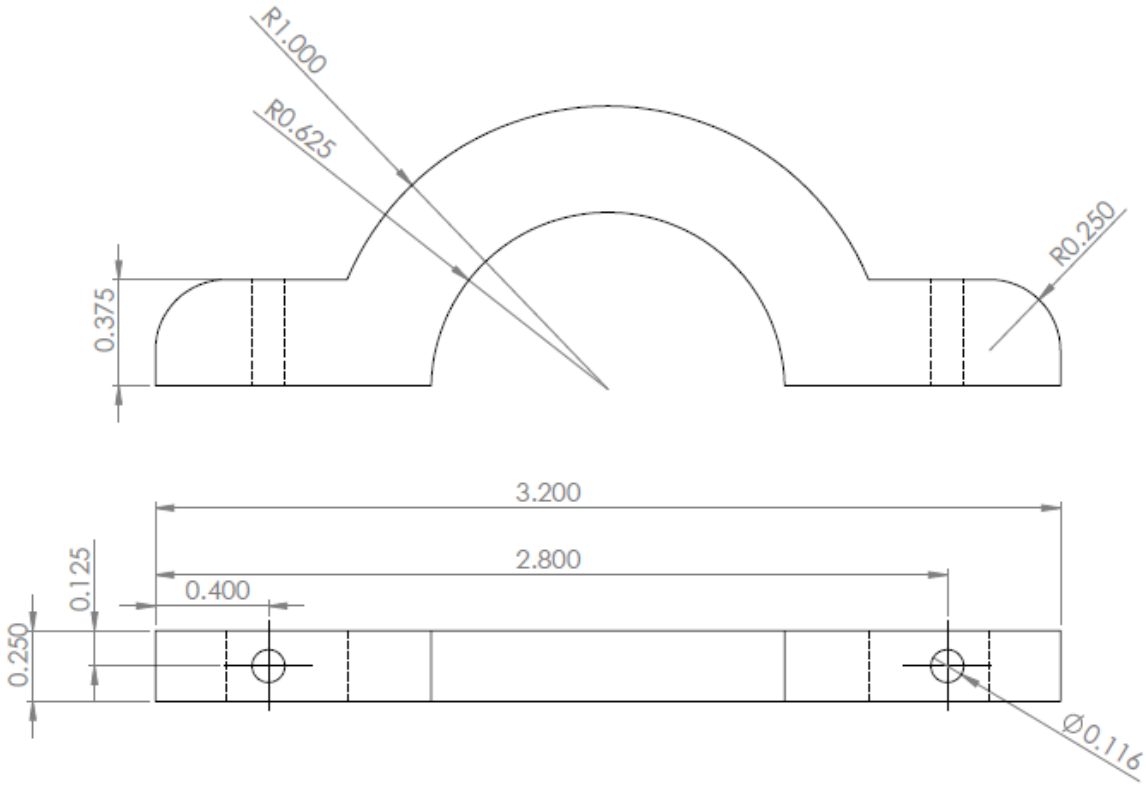

Taping Machine: side wall clamp v1

Material: 6061-T6 Aluminum

Dimensions: Inches

Tolerance: +/- 0.005"

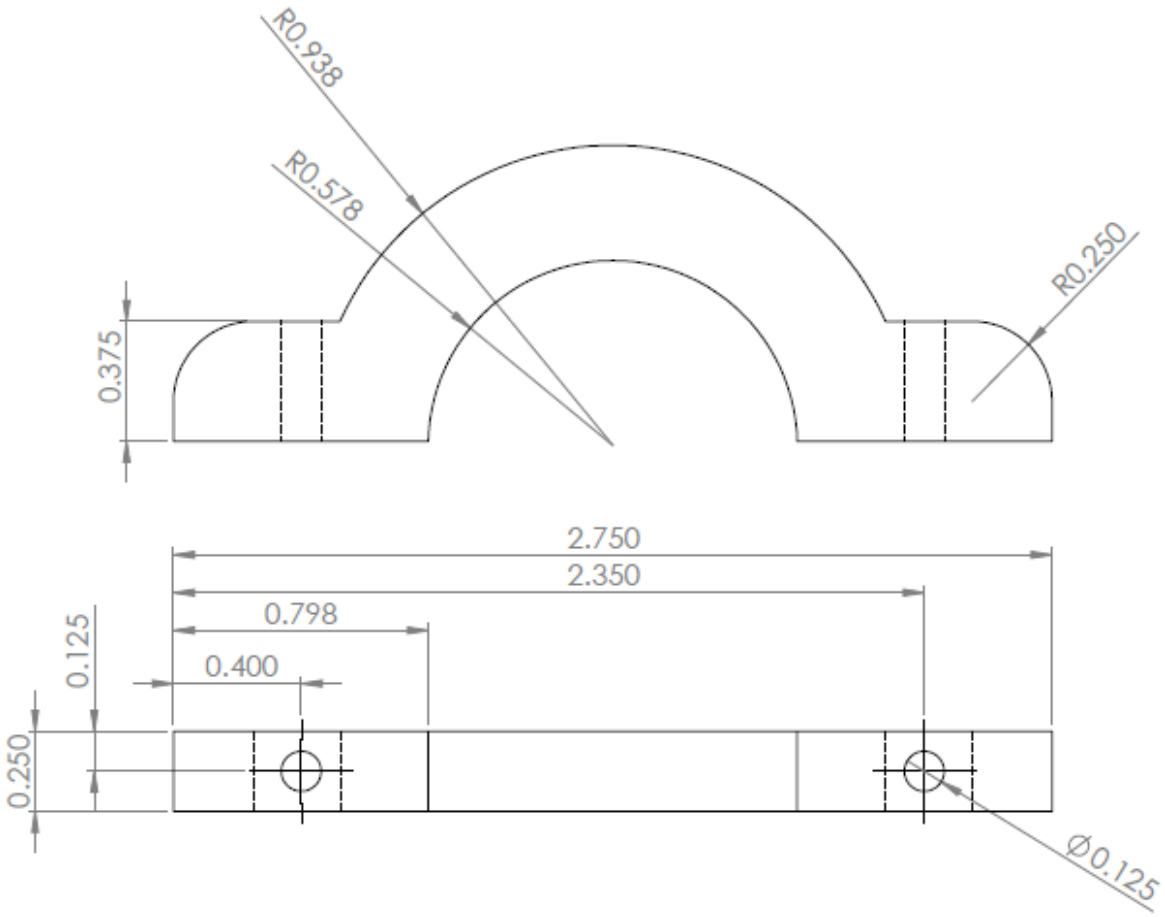

Taping Machine: side wall liner clamp v1

Material: 6061-T6 Aluminum

Dimensions: Inches

Tolerance: +/- 0.005"

APPENDIX

C SYSTEM DIAGRAMS

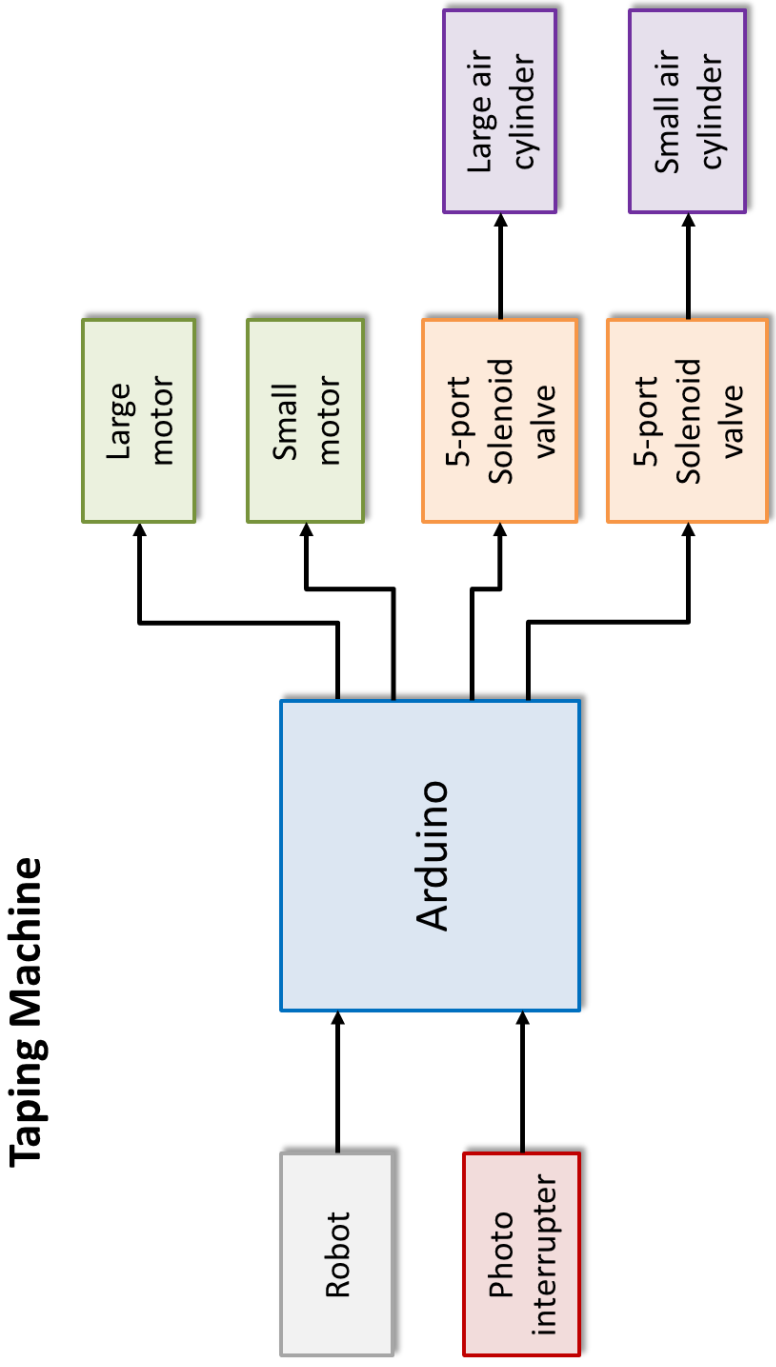

Functional Testing Machine

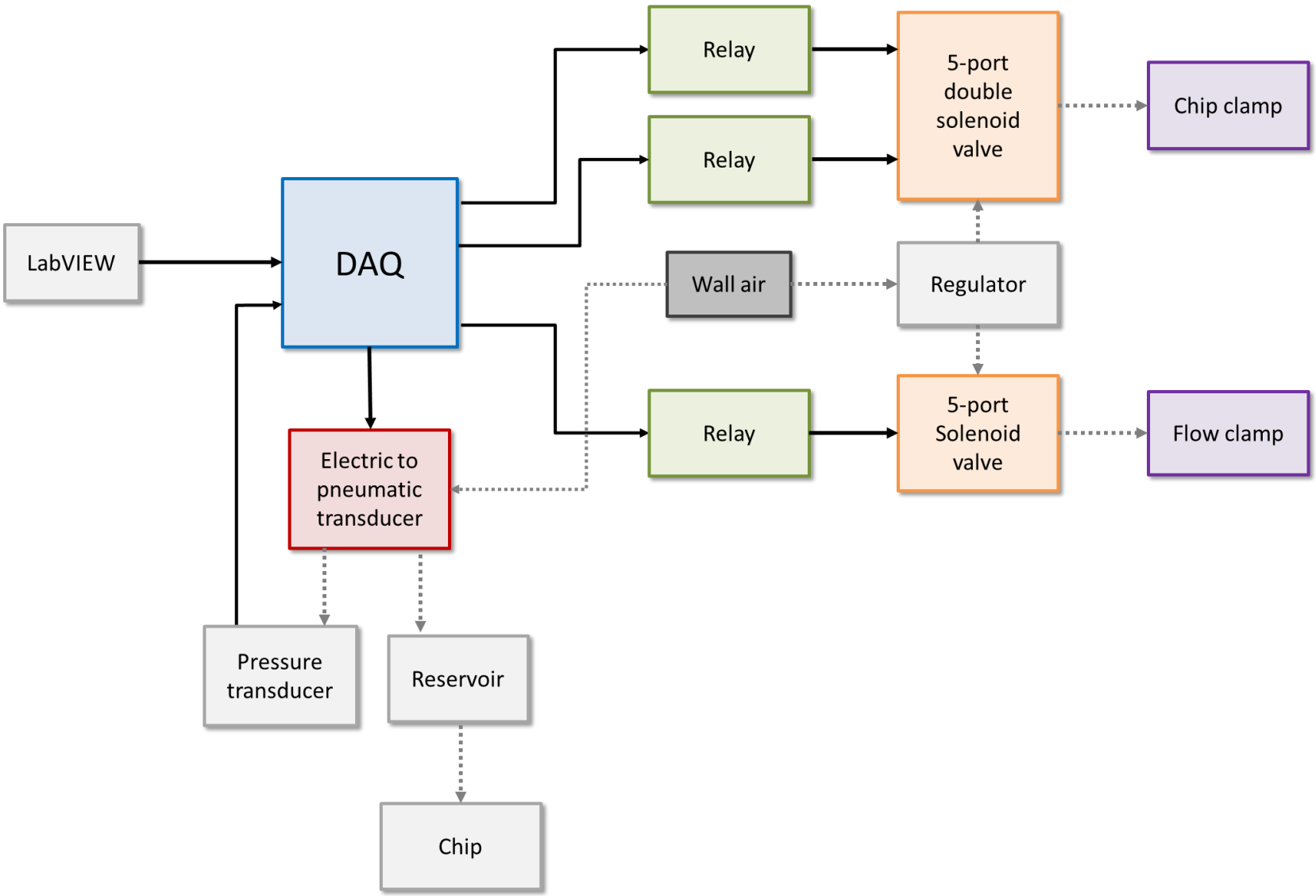

CHAPTER 9 REFERENCES

[1] G.M. Whitesides. "The origins and the future of microfluidics." *Nature*. 442: 368-373, 2006.

[2] K. Regehr, et. al. "Biological implications of polydimethylsiloxane-based microfluidic cell culture." *Lab on a Chip*. 9: 2132-2139, 2009.

[3] M. Heckele and W. K. Schomburg. "Review on micro molding of thermoplastic polymers." *Journal of Micromechanics and Microengineering*. 14: R1-R14, 2004.

[4] S. Kang. *Micro/Nano Replication: Processes and Applications*. New Jersey: John Wiley & Sons, Inc., 2012.

[5] GnuBio. "Embossing microfluidic features." Personal communication to the author. Email, 28 June 2012.

[6] D. Hardt and T. Siu. "Cycle to cycle manufacturing process control." *Innovation in Manufacturing Systems and Technology*. Singapore-MIT Alliance, 2002.

[7] M. Bageant. "Development of a precision hot embossing machine with in-process sensing." S.M. Thesis. MIT, 2013.

[8] Q. Wang. "Process window and variation characterization of the micro embossing process." S.M. Thesis. MIT, 2006.

[9] M. Dirckx. "Demolding of hot embossed polymer microstructures." Ph.D. Thesis. MIT, 2010.

[10] G. Vladisavljević, et. al. "Industrial lab-on-a-chip: design, applications and scale-up for drug discovery and delivery." *Advanced Drug Delivery Reviews*. 65: 1626-1663, 2013.

[11] C. Tsao and D. DeVoe. "Bonding of thermoplastic polymer microfluidics." *Microfluidics and Nanofluidics*. 6: 1-16, 2009.

[12] F. Huang, et. al. "CE chips fabricated by injection molding and polyethylene/thermoplastic elastomer film packaging methods." *Electrophoresis Journal*. 28: 1130-1137, 2007.

[13] C. Lu, et. al. "Packaging of microfluidic chips via interstitial bonding technique." *Electrophoresis Journal*. 29: 1407-1414, 2008.

[14] M. Arroyo, et. al. “Novel all-polymer microfluidic devices monolithically integrated within metallic electrodes for SDS-CGE of proteins.” *Journal of Micromechanics and Microengineering*. 17: 1289-1298, 2007.

[15] R. Kelly and A. Woolley. “Thermal bonding of polymeric capillary electrophoresis microdevices in water.” *Analytical Chemistry*. 75: 1941-1945, 2003.

[16] Y. Sun, et. al. “Low-pressure, high-temperature thermal bonding of polymeric microfluidic devices and their applications for electrophoretic separation.” *Journal of Micromechanics and Microengineering*. 16: 1681-1688, 2006.

[17] L. Yao, et. al. “Micro flow-through PCR in a PMMA chip fabricated by KrF excimer laser.” *Biomedical Microdevices*. 7: 253-257, 2005.

[18] X. Zhu, et. al. “Study of PMMA thermal bonding.” *Microsystem Technologies*. 13: 403-407, 2007.

[19] M. Koesdjojo, et. al. “Fabrication of a microfluidic system for capillary electrophoresis using a two-stage embossing technique and solvent welding on poly(methylmethacrylate) with water as a sacrificial layer.” *Analytical Chemistry*. 80: 2311-2318, 2008.

[20] R. Truckenmüller, et. al. “An ultrasonic welding based process for building up a new class of inert fluidic microsensors and -actuators from polymers.” *Sensors and Actuators A: Physical.* 132: 385-392, 2006.

[21] Z. Zhang, et. al. “Ultrasonic bonding of polymer microfluidic chips.” *IEEE International Conference on Electronic Packaging Technology & High Density Packaging*. 1-5, 2008.

[22] J. Moyne, et. al. *Run-to-Run Control in Semiconductor Manufacturing*. Florida: CRC Press, LLC, 2001.

[23] Hitachi High-Tech. “Ultra-high resolution scanning electron microscope.” Product brochure. Accessed January 2014.

[24] Zygo. “NewView 5000 Optical Surface Profilometer.” Product manual. Accessed January 2014.

[25] B. Anthony, et. al. “A research factory for polymer microdevices: muFac.” Proceedings of SPIE. 7593: 75930A, 2010.

[26] V. Srivastava, et. al. “Design of a microfluidic device containing a micro-mixer.” 1-6, 2008.

[27] D. Henann. “A constitutive theory for the mechanical response of amorphous metals at high temperatures spanning the glass transition temperature: application to microscale thermoplastic forming of $Zr_{41.2}Ti_{13.8}Cu_{12.5}Ni_{10}Be_{22.5}$.” S.M. Thesis. MIT, 2008.

[28] B. Ganesan. “Process control for micro embossing: initial variability study.” S.M. Thesis. MIT, 2004.

[29] M. Dirckx. “Design of a fast cycle time hot micro-embossing machine.” S.M. Thesis. MIT, 2005.

[30] M. Hale. “Development of a low-cost, rapid-cycle hot embossing system for microscale parts.” S.M. Thesis. MIT, 2009.

[31] N. Zarrouati, 2010.

[32] Epson. “SCARA robot G10/G20 series manipulator.” Product manual. Revision 12, 2012.

[33] N. Zarrouati. “A precision manipulation system for polymer microdevice production.” S.M. Thesis. MIT, 2010.

[34] M. Lustrino. “The development of an innovative bonding method for microfluidic applications.” S.M. Thesis. MIT, 2011.

[35] D. Ljubicic. “High speed instrumentation for inspection of transparent parts.” Ph.D. Thesis. MIT, 2013.

[36] K. Thaker. “Design of a micro-fluidic functional testing system for process characterization of a hot micro-embossing machine.” S.M. Thesis. MIT, 2003.

[37] E. Maurel. “Microfactory: testing machine and sealing methods.” Summer Internship Final Report. MIT, 2011.

[38] C. Lim. “Bonding apparatus for microfluidic devices.” Final year project (B490), NTU School of mechanical and aerospace engineering, 2012.

[39] W. Sim. “Semi-automated tape bonding apparatus for microfluidic devices.” Final year project (A256), NTU School of mechanical and aerospace engineering, 2013.

[40] V. Mengeaud, et. al. “Mixing processes in a zigzag microchannel: finite element simulations and optical study.” *Analytical Chemistry*. 74: 4279-4286, 2002.

[41] K. Sharp, et. al. “Liquid flows in microchannels.” *MEMS: Introduction and Fundamentals*. Florida: CRC Press, LLC, 2005.

[42] R. Shah. “Laminar flow friction and forced convection heat transfer in ducts of arbitrary geometry.” *International Journal of Heat and Mass Transfer*. 18: 849-862, 1975.

[43] M. Werts. “Quantitative full-colour transmitted light microscopy and dyes for concentration mapping and measurement of diffusion coefficients in microfluidic architectures.” *Lab on a Chip*. 12: 808-820, 2012.